ANP-10286NP
Revision 0

U.S. EPR Rod Ejection Accident Methodology Topical Report

November 2007

AREVA NP Inc.

Nature of Changes

Item	Section(s) or Page(s)	Description and Justification
Original Issue	NA	NA

Contents

List of Tables

List of Figures

Nomenclature

Acronym	Definition
β_{eff}	Beta effective (effective total delayed neutron fraction)
BOC	Beginning Of Cycle
BOL	Beginning Of Life (of a fuel rod)
cal/g	Calories per gram
CG/CP	Constant Gap/Constant Properties
CG/TDP	Constant Gap/Temperature Dependent Properties
CHF	Critical Heat Flux
DNBR	Departure From Nucleate Boiling Ratio
DTC	Doppler Temperature Coefficient
EOC	End Of Cycle
EOL	End Of Life (of a fuel rod)
FGR	Fission Gas Release
FGRF	Fission Gas Release Failures
FOP	Fraction Of Power
$F_{\Delta H}$	Peak rod power (in the core)
F_Q	Peak local power (in the core)
Gd_2O_3	Gadolinium Oxide
GWD/MTU	GigaWatt Days per Metric Ton Uranium
HCF	Hot Channel Factor
HFP	Hot Full Power
HZP	Hot Zero Power
IR	Importance Ratios
KN	Knowledge Ratios
LOCA	Loss-Of-Coolant Accident
MDNBR	Minimum Departure from Nucleate Boiling Ratio
MTC	Moderator Temperature Coefficient
NEACRP	Nuclear Energy Agency Committee on Reactor Physics
pcm/°F	PerCent Milli-rho per degree Fahrenheit
PCMI	Pellet Cladding Mechanical Interaction
PIRT	Phenomena Importance Ranking Tables
REA	Rod Ejection Accident
RIA	Reactivity Initiated Accident

Acronym	Definition
SA	Safety Analysis
SAFDL	Specified Acceptable Fuel Design Limit
SRSS	Square Root Sum of the Squares
TFGR	Transient Fission Gas Release
T-H	Thermal Hydraulics
TS	Technical Specifications
μm	Micrometers
UO_2	Uranium Dioxide
VG/TDP	Variable Gap/Temperature Dependent Properties
w/o	Weight percent
3-D	Three Dimensional

1.0 INTRODUCTION

The methodology to analyze the rod ejection accident (REA) for the U.S. EPR is presented. The methodology includes the use of a nodal 3-D kinetics solution with both thermal-hydraulic (T-H) and fuel temperature feedback and a separate peak rod thermal evaluation with an open channel T-H and fuel thermal model. These models provide more precise localized neutronic and thermal conditions than previous methods to show compliance with the interim Reactivity Initiated Accident (RIA) criteria in the SRP Section 4.2 (Reference 1). The boundary conditions and uncertainty values are defined for the REA methodology. The overall REA sample problem results for the U.S. EPR are well within the limiting criteria for this REA methodology, with maximum Δcal/g less than 14 and failures less than 8 percent of the rods in the core. This report presents the REA regulatory requirements, followed by the code and model requirements, U.S. EPR methodology, computer codes, application of boundary conditions and uncertainties, sample problem results, and conclusions.

2.0 REA REGULATORY REQUIREMENTS

The first step of the methodology is to use the appropriate regulatory requirements to define the specific criteria that the REA analysis will meet. This methodology addresses the requirements in Reference 1 for cladding failure, core coolability, and radiological consequences. The requirements for radiological assessment and the maximum pressure are not addressed by this methodology.

2.1 Cladding Failure

Reference 1 contains several criteria to determine whether the cladding is assumed failed. The failure criteria to be assumed for the U.S. EPR are provided for pellet cladding mechanical interaction (PCMI), total energy deposition, and departure from nucleate boiling ratio (DNBR). Each rod is examined to determine whether it has exceeded any of these criteria and is considered failed if it does.

2.1.1 PCMI Criteria for M5™ Cladding

The prompt PCMI cladding failure criteria for M5™ Cladding is based on Figure B-1 from Reference 1. The maximum corrosion expected for U.S. EPR fuel cladding with M5™ at end of life is less than 35 μm. This oxide thickness is based on a conservative COPERNIC (Reference 2) analysis for a limiting rod using a bounding rod power history at burnups in excess of 62 GWD/MTU. The corresponding oxide to wall thickness ratio is 0.061, which leads to a conservative PCMI failure limit of 110 cal/g.

The maximum prompt energy deposition in the RIA simulations is shown to be less than 110 cal/g for all burnups. Hence, no cladding failures occur based on the PCMI criteria for all initial power levels from hot zero power (HZP) to hot full power (HFP).

In order to calculate the fuel enthalpy rise to assess PCMI failures, the prompt fuel enthalpy rise is defined as the radial average fuel enthalpy increase from the initial conditions to the time corresponding to one pulse width after the peak of the prompt pulse.

2.1.2 Cladding Failure Due to Total Energy Deposition

The maximum total enthalpies are shown as less than 150 cal/g, which precludes failures in fuel rods below and above system pressure. This is demonstrated for powers from HZP to HFP.

2.1.3 DNBR

For powers greater than 5 percent rated thermal power, fuel cladding failure is assumed if the cladding surface heat flux exceeds the thermal design limits for MDNBR.

2.2 Coolability

The coolability requirements from Reference 1 are as follows:

1. Peak radial average fuel enthalpy must remain below 230 cal/g.

2. Peak fuel temperature must remain below incipient fuel melting conditions.

3. Mechanical energy generated as a result of (1) non-molten fuel-to-coolant interaction and (2) fuel rod burst must be addressed with respect to reactor pressure boundary, reactor internals, and fuel assembly structural integrity.

4. No loss of coolable geometry due to (1) fuel pellet and cladding fragmentation and dispersal and (2) fuel rod ballooning.

From conditions set forth in Sections 2.1.1 and 2.1.2, energetic ejection of fuel into the coolant is prevented by preserving the cladding integrity during high energy deposition pulses by staying below the cladding and fuel cal/g limits and below the fuel melt temperature.

Coolability for fuel rods undergoing DNB (DNBR failures) is established by limiting rod heatup during post critical heat flux (CHF). If the rod does not heatup enough to rupture, there are no coolability issues. Rupture and significant ballooning are unlikely if the maximum cladding temperature is below **[ ]**, and there is no significant exothermic oxidation of the cladding. Therefore, coolability is maintained by precluding

PCMI failures, maximum total enthalpies above 150 cal/g, fuel melt, and maximum cladding temperatures greater than **[ ]**.

2.3 Radiological Consequences

The radiological consequence evaluation associated with the postulated REA is based on the guidance in SRP Section 15.0.3 and RG 1.183, Appendix H. Consideration is also given to the fission-product gap inventory for RIA, and the interim acceptance criteria and guidance provided in Reference 3. One of the objectives of the evaluation is to determine the maximum cladding failure for an REA without exceeding 90 percent of the dose acceptance criterion at any receptor. The acceptable fuel cladding percent failure (DNBR) that meets this objective is approximately 30 percent of the rods in the core dictated by the dose at the exclusion area boundary (EAB).

The radiological consequences could be more severe for failed pins that experience high local energy depositions during an REA causing transient fission gas release. The formula in Section D of Reference 1 is used to increase the fission product gap activity for those rods that fail and is shown below.

$$TFGR = (0.2286 \times \Delta H) - 7.1419$$

where:

TFGR = Transient Fission Gas Release, percent (must be ≥ 0)

ΔH = Increase in prompt fuel enthalpy, Δcal/g

The gap activity of the axial node rod segments experiencing delta prompt fuel enthalpies greater than 31.2 cal/g ($\Delta H = 31.2$ when TFGR = 0) will increase by the above equation. The radiological consequences will incorporate two relative source terms for rods that fail due to DNBR during the REA event. The radiological consequences can be simplified to a function of the equivalent number of rods failed and can be represented by the following equation.

$$EQP = F + FGRF \leq A$$

where:

EQP = The equivalent number of rods failed

F = Total number of rods failed due to DNBR or fuel melt

FGRF = Equivalent number of additional rods failed due to Transient Fission Gas Released from high Δcal/g

A = The maximum allowed number of rods that could fail due to only DNBR failures and stay within the dose limits.

TFGR will be calculated for every rod that failed using the relationship with delta cal/g and converted to FGRF. The total effective number of rods failed will be reported when failed rods are counted for radiological consequences. The radiological assessment remains valid when the equivalent number of pins failed due to REA yields less than 30 percent of the core due to DNBR failures.

2.4 Licensing Criteria for the U.S. EPR

The conditions in Table 2-1 define the limits to be met for the U.S. EPR.

Table 2-1 REA Limits for U.S. EPR

Criterion Description	Limit
Maximum enthalpy of the fuel	≤150 cal/g
Maximum energy deposition during prompt power pulse for core powers <5%	≤110 cal/g
Fuel Melt	0%
Maximum Cladding Temperature	[ ]
After power pulse, number of equivalent rods failed due to DNBR or fuel melt	≤30% *

Notes:

* For sample problem.

3.0 COMPUTER CODE REQUIREMENTS

The use of a nodal 3-D kinetics solution with both T-H and fuel temperature feedback and a peak rod thermal evaluation model with an open channel T-H and fuel thermal model are required. The requirement for the computational codes is that they are qualified and approved by the U.S. NRC for time-dependent solutions.

In general, the 3-D neutronic solution will calculate the core power and the local power distribution response to an ejected rod. This information will then be used by an open channel T-H and fuel thermal code to calculate the fuel enthalpy, the temperature distributions, and the DNBR for the peak rod in the core. If the peak rod fails due to DNBR, the open channel T-H and fuel thermal code is also used to establish the power conditions at which a rod will not fail. The boundary conditions and uncertainties used in the codes for the REA simulation are addressed in Section 4.0.

4.0 MODEL BOUNDARY CONDITIONS AND UNCERTAINTIES REQUIREMENTS

This section addresses the boundary conditions and uncertainties considered for the REA. The analysis can be divided into two parts, the plant transient analysis and the fuel rod transient analysis as defined in the Phenomenon Identification and Ranking Tables (PIRT) in Reference 4. A list of the phenomena, their importance ratio and knowledge ratio is presented in Table 4-1 for the plant transient analysis.

A similar list is presented in Table 4-2 for fuel and cladding temperatures. Many of the items included in Table 3-3 in Reference 4 are not included in Table 4-2 because they are captured by a cal/g limit or have little relevance to a DNBR limit. The items that are categorized relative to “PCMI loading to cladding” effects are captured by the cal/g failure limit. The gap size, gas pressure, gas composition, gas distribution, fuel-cladding gap friction coefficient and rod volume are essentially captured in the context of gap conductance. The hydrogen concentration, hydrogen distribution, and spallation effects on the cladding are captured in the cal/g failure limit. Fast fluence, porosity, rim size, bubble size, and bubble distribution are captured by the fuel pellet conductivity and/or the cal/g limit. Therefore, these items are not included in Table 4-2.

Reference 4 states that the phenomena with importance ratios above 75 are important and those with knowledge ratios above 75 are well known. It also warns that parameters near the threshold should not necessarily be ignored. Additional parameters address impacts on DNBR since the scope of Reference 6 was primarily concerned with PCMI type failures and not DNBR. Each of the parameters are addressed with respect to the requirements for modeling relative to the need to bound, apply uncertainty, or to demonstrate a negligible consequence.

4.1 Plant Transient Analysis

The plant transient analysis is dominated during the first 5-10 seconds (less than the loop time) by the core kinetics, nodal fuel temperatures and nodal T-H conditions. Inlet

temperature, core pressure, and flow are relatively constant during an REA so that the 3-D core kinetics can be used with, or independently of, a system T-H code. The results and dependencies of a 3-D kinetics solution are identical to a point kinetics solution for uniform changes to a core. The difference in the two solutions is the local weighting of the changes that occur, which become very important during an REA. Therefore, many of the dependencies of the parameters from the point kinetics models remain applicable to 3-D kinetics. Since a static reactivity calculation provides a 3-D weighting of the core effects, standard static methods to calculate reactivity coefficients, delayed neutron fractions, and rod worths can be used to evaluate the initial conditions for the sensitivities. This section is a review of the parameters listed in Table 4-1 relative to 3-D kinetics and other effects that could impact the results.

4.1.1 Maximum Ejected Rod Worth

The maximum ejected rod worth is a limiting parameter and is the driver for the event. It is integral to the neutronic nodal simulator solution through the input of the initial insertion of the rod bank(s) and the control rod cross sections. The worth is not a direct input and is calculated using standard static methods with moderator temperature and fuel temperature held constant. The worth depends on fuel cycle design, cycle lifetime, and initial xenon conditions. The initial conditions are required to be a reasonable representation of the limiting conditions allowed by Technical Specifications that maximize the worth. In addition, an uncertainty is applied that is equal or greater than the approved uncertainty value. Additional conservatisms can be applied to bound future fuel cycle designs.

4.1.2 Rate of Reactivity Insertion

Rate of reactivity insertion is not rated as an important parameter for prompt critical rod ejections. A sensitivity study is performed to confirm the impact for the range of conditions analyzed.

4.1.3 Moderator Feedback

Moderator feedback (i.e., Moderator Temperature Coefficient, (MTC)) is not rated as an important parameter relative to the power pulse. However, the MTC does affect the power after the pulse, which can affect DNBR. The MTC is not a direct input to the neutronics computer code and is required to be adjusted to represent an uncertainty.

4.1.4 Fuel Temperature Feedback

The fuel temperature feedback (i.e., Doppler Temperature Coefficient, (DTC)) terminates a prompt critical power excursion and is an important parameter. The DTC is calculated using standard static methods with moderator temperature held constant. The DTC is dependent upon core design and cycle lifetime. The magnitude of DTC is conservatively reduced by the uncertainty.

4.1.5 Delayed Neutron Fraction

For a given reactivity insertion, the sensitivity of total delayed neutron fraction (β_{eff}) is addressed from a point kinetics viewpoint. The β_{eff} determines the rate of neutron flux change from an initial static condition. The higher the reactivity relative to β_{eff}, the faster the flux increases. For reactivity insertions less than β_{eff}, a higher reactivity will increase the prompt jump and decrease the subsequent doubling time. When the reactivity insertion exceeds β_{eff}, the core becomes critical on prompt neutrons and the doubling time can decrease by more than an order of magnitude. For step reactivity insertions as with an REA, a low β_{eff} results in higher core powers. Therefore, the β_{eff} is lowered by the uncertainty for the cases where fast increases are limiting.

4.1.6 Reactor Trip Reactivity

For prompt critical excursions, the power excursion is terminated by DTC and the core returns to a much lower power level. Also, the excore flux or flux rate trip is reached shortly after the rod is ejected. After the DTC terminates the pulse, the core power flattens with time until the rods are inserted from the reactor trip. The reactor trip reactivity reduces the core power to shutdown conditions. The trip reactivity sensitivity

is most important for the “at power” cases where a trip limits the amount of time the core is at elevated powers and can limit the core damage due to potential DNBR failures. The timing of the trip is also important relative to the excore response of the detectors to the asymmetric flux caused by the ejected rod. As with the ejected rod worth, the trip reactivity is not an input quantity to the 3-D kinetics calculations. It can be adjusted by changing the amount of banks inserted prior to the accident, the control rod cross sections, and the trip time parameters. The sensitivity of the trip reactivity to the “at power” events is used to determine the level of conservatisms required.

4.1.7 Fuel Cycle Design

Most of the fuel cycle design dependencies are captured by examining the beginning of cycle (BOC) and end of cycle (EOC) behavior on ejected rod worth, β_{eff}, DTC, MTC, and peaking. The fuel cycle design can also influence the proximity of the high burnup rods to the ejected rod location. When burnup dependent limits are used, a lower ejected rod worth in a high burnup assembly could be more limiting than a higher worth rod. More than the maximum ejected rod location is evaluated for burnup dependent limits if they are used. These fuel cycle design elements are addressed in Section 7.1.5.

4.1.8 Heat Resistances and Transient Cladding to Coolant Heat Transfer

The heat resistances and transient cladding to coolant heat transfer are not viewed as sensitive parameters to the ejected rod event and sensitivity calculations are used to confirm their use. The heat resistances comprise the thermal conductivity of the fuel and cladding, and the gap conductance. Nominal gap conductance values can vary by more than a factor of ten for an open gap between the fuel pellet and cladding versus a closed gap.

4.1.9 Heat Capacities

The heat capacity is rated as an important parameter in Reference 4. The heat capacity determines how much the fuel temperature increases as the energy is deposited into the fuel; therefore, the energy deposited is proportional to the heat capacity. For prompt

critical power excursions, the point kinetics equations can be approximated by the following analytical equation representing the energy deposition:

$$ED = \frac{2(\rho - \beta) \cdot C_p}{DTC}$$

where:

ED = Energy Deposition

ρ = Step Reactivity Change

β = Beta Effective

C_p = Heat Capacity of the Fuel

DTC = Doppler Temperature Coefficient

This equation shows the dependence of the energy deposition on heat capacity. If the temperature is the parameter of interest, then the delta temperature reached from an energy deposition with no heat loss can be represented as follows:

$$\Delta T = ED / C_p$$

where:

ΔT = Temperature rise

Substituting the first equation yields:

$$\Delta T = \frac{2 \cdot (\rho - \beta)}{DTC}$$

The temperature increase from the power excursion with a step change in reactivity is not a function of heat capacity of the fuel. For slow transients near static conditions, the

fuel temperature is dominated by the heat resistance of the rods. Therefore, for fuel temperature predictions, heat capacity is not an important parameter.

Reference 5 is considered a standard for defining heat capacity for UO_2. The variation of the UO_2 heat capacity is only a function of temperature. Using the heat capacity consistently in the different codes will yield consistent results. No error estimate or special treatment is used for the UO_2 heat capacity.

4.1.10 Fractional Heat Deposited in Coolant

The fraction of heat deposited in the coolant can affect the relative amount of direct heating of the water and the fuel. The different prompt temperatures of the water and the fuel can result in different feedback between the MTC and DTC during a power pulse. The direct heating of the coolant could have an impact on the results since MTC can vary from small positive to large negative values from BOC to EOC conditions, respectively. This parameter is assumed constant throughout the transient because it has few or no dependencies upon other core parameters. A sensitivity evaluation is used to determine its importance.

4.1.11 Pellet Radial Power Profile

The pellet radial power profile could affect the rate of energy transferred from the fuel pellet to the coolant or it could affect the weighting of the pellet temperature distribution on the DTC. This parameter has very weak dependencies upon other core parameters. A sensitivity evaluation is used to determine its importance.

4.1.12 Rod Peaking Factors

The rod peaking factors are important relative to the weighting of the local powers to the overall core reactivity as well as the local energy deposition during the power pulse. As with the ejected rod worth, the rod peaking is not an input quantity to the 3-D kinetics calculations. If the peaking factors increased, the local fuel temperatures would increase so that the Doppler response would lower the core power. Therefore, the peaking factors that are used in the kinetics calculation are best estimate and the

peaking factors for the fuel rod thermal model are conservatively increased by the expected uncertainties.

4.1.13 Neutron Velocities

Since the dominant fission reactions occur with thermal neutrons, the thermal neutron velocities determine the rate at which the neutrons multiply. The mean generation time in point kinetics is calculated based on the neutron velocities. The impact of neutron velocities on the REA energy deposition is negligible because the energy deposition in the first equation in Section 4.1.9 is not a function of mean generation time. However, the pulse width is roughly inversely proportional to the thermal neutron velocity and narrow pulse widths could become more important when evaluating potential coolability concerns when PCMI failures occur. Since this methodology shows that energy deposition is below the cal/g for PCMI failure criteria for M5™, any reasonable value for thermal neutron velocity is acceptable.

4.1.14 System T-H Conditions

The kinetics solution can be affected by changes in inlet temperature, pressure, and flow. The longer the transient is modeled (greater than 5 seconds) the more the system T-H conditions can influence the neutronic kinetic solution. It is expected that prompt critical excursions will not be affected by the system T-H conditions since the maximum power deposition and maximum fuel temperatures are reached in less than a second. Non-prompt excursions may require modeling for more than a few seconds. Sensitivity studies are performed to assess these impacts.

4.2 Fuel Rod Transient Model for Fuel and Cladding Temperatures and DNBR

The fuel and cladding temperatures are dominated by the initial temperatures and the energy deposition versus time. Similar to the previous section, inlet temperature, core pressure, and flow are relatively constant and the fuel rod transient model can be used independently of a system T-H code. The discussion in this section is a review of the parameters listed in Table 4-2 relative to the fuel rod transient model for fuel and

cladding temperatures. Additional parameters address impacts on DNBR since the scope of Reference 4 was primarily concerned with PCMI type failures and not DNBR.

4.2.1 Pellet and Cladding Dimensions

Pellet and cladding dimensions are considered important and well known. Nominal dimensions are appropriate and application of the uncertainty for manufacturing allowances is acceptable. Approximations of the full core geometry model surrounding the limiting rod can affect the results. These approximations are shown to be appropriate for the REA analysis.

4.2.2 Burnup Distribution

The local rod radial burnup distribution is rated as a relatively low importance parameter and a homogenized pellet is acceptable.

4.2.3 Cladding Oxidation

The cladding oxidation is rated as a relatively low importance parameter and can be modeled on a best estimate basis or ignored.

4.2.4 Power Distribution

The power distribution is assumed to be the radial pellet power distribution and is weighted as an important parameter. The radial pellet power profile is a strong function of pellet burnup and uranium enrichment. A typical or bounding fuel performance power history from an approved fuel performance code can provide this information and is acceptable for the REA. Sensitivity calculations are used to define the impact of this parameter.

4.2.5 Initial Coolant Conditions

Initial coolant conditions for inlet temperature, flow and pressure are defined by the initial power level and operational mode. These parameters are already defined conservatively for other safety analyses. Existing methods are applicable.

4.2.6 Transient Power Specification

The transient core power and peaking factors are defined by the results generated from the plant transient analysis, which also includes the initial power distributions. The uncertainties applied to the REA power distributions are consistent with the current uncertainties applied for $F_{\Delta H}$ and F_Q for other accidents. Initial distributions are representative of the worst conditions allowed by Technical Specifications. The uncertainties of the power peaking factors are addressed.

4.2.7 Heat Resistances in Fuel, Gap, and Cladding

A typical or bounding fuel performance power history from an approved fuel performance code can provide the heat resistances in fuel, gap, and cladding, and is acceptable for the REA. Sensitivity studies are used to define the bounding conditions. Decreased thermal conductivity can increase the maximum fuel temperature but reduce the heat flux (DNBR). Therefore, two calculations modeling the limiting direction of the resistances are needed. One is used for maximum fuel temperature prediction and the other to predict MDNBR.

4.2.8 Transient Cladding-to-Coolant Heat Transfer Coefficient

The importance of the cladding to coolant heat transfer coefficient for prompt critical power excursions is rated of little importance. Since DNBR is a fuel failure criterion, transient cladding-to-coolant heat transfer becomes an important parameter. Transient heat transfer and critical heat flux (CHF) are not as well understood as static CHF. In general, the application of the static heat transfer, CHF, and failure when exceeding MDNBR is considered conservative for rapidly changing conditions. Therefore, the use of existing approved T-H codes, CHF correlations, and MDNBR cladding failure criterion is considered acceptable.

4.2.9 Heat Capacities of Fuel and Cladding

The heat capacity of UO_2 is primarily dependent upon temperature. Therefore, the local rod model requirement for heat capacity is the same as that used in the plant transient

model. Section 4.1.9 addresses the heat capacity as a non-critical parameter for REA when predicting temperatures and no uncertainty is needed.

4.2.10 Coolant Conditions

The transient water temperatures, local flows, and pressure are important to estimate fuel and cladding temperatures and DNBR of the fuel rods. An approved T-H computer code with time dependent capability is used with the approved uncertainties defined for licensing.

4.2.11 System T-H Conditions

The inlet temperature, core flow, and system pressure can affect the fuel rod transient analysis. The longer the transient is modeled (greater than 5 seconds) the more the system T-H conditions can impact the transient fuel rod model. Prompt critical excursions will not be impacted by the system T-H conditions because the maximum power deposition and maximum fuel temperatures are reached in less than a second. Non-prompt excursions may require modeling for more than a few seconds and the impact of plant conditions on the overall results is evaluated.

4.3 Time Dependent Analysis

The sensitivity of the time dependent calculations to time step meshing is addressed.

4.4 Failure Analysis

There are many ways to count the number of rod failures. The failure criteria defined for this methodology in Section 2.1.3 must be used. Rod by rod explicit analysis is acceptable. Rod by rod explicit analysis models the power versus time of every rod and counts each rod that has a DNBR less than the design limit as failed. Also, setting a conservative value for $F_{\Delta H}$ and F_Q and counting any rod above either value as a rod failed is acceptable. Exceeding a 95/95 tolerance/confidence limit on DNBR is conservative as a failure criterion. If the number of rods is statistically counted, only 5 percent or less of the rods having powers equal to the criteria would be failed. This is far less than the 100 percent as defined. Therefore, no additional DNBR propagation

needs to be assumed since the maximum fuel enthalpy is less than 150 cal/g and the maximum cladding temperature is less than **[ ]**.

Table 4-1 PIRT Plant Transient Analysis

Subcategory	Phenomenon	IR*	KR**
Calculation of power history during pulse (includes pulse width)	Ejected control rod worth	100	100
	Rate of reactivity insertion	61	88
	Moderator feedback	38	93
	Fuel temperature feedback	100	96
	Delayed-neutron fraction	95	96
	Reactor trip reactivity	0	96
	Fuel cycle design	92	100
Calculation of rod fuel enthalpy increase during pulse (includes cladding temperature)	Heat resistances in high burnup fuel, gap, and cladding (including oxide layer)	58	67
	Transient cladding-to-coolant heat transfer coefficient	56	64
	Heat capacities of fuel and cladding	94	90
	Fractional energy deposition in pellet	4	93
	Pellet radial power distribution	63	88
	Rod-peaking factors	97	100

Notes:
* Importance Ratio IR>75 Important
**Knowledge Ratio KR<75 Not completely understood

Table 4-2 PIRT Fuel Rod Transient Analysis for Fuel and Cladding Temperatures

Subcategory	Phenomenon	IR*	KR**
Initial conditions	Pellet and cladding dimensions	91	96
	Burnup distribution	55	89
	Cladding oxidation	46	73
	Power distribution	100	89
	Coolant conditions	93	96
	Transient power specification	100	94
Fuel and cladding temperature changes	Heat resistances in fuel, gap, and cladding	75	77
	Transient cladding-to-coolant heat transfer coefficient (oxidized cladding)	50	58
	Heat capacities of fuel and cladding	88	93
	Coolant conditions	85	88

Notes:
* Importance Ratio IR>75 Important
**Knowledge Ratio KR<75 Not completely understood

5.0 U.S. EPR REA METHODOLOGY

The major difference in this methodology compared to past methods is that it replaces the point kinetics model with a 3-D kinetics model. A bounding sample problem analysis is presented in the following sections to define the overall process, computer codes, boundary conditions, uncertainties, and results for the REA event for the U.S. EPR. This methodology also provides the static conditions that a future cycle must meet for this analysis to remain valid. A cycle specific analysis can be repeated for those cycle parameters that do not meet the REA design parameters or a complete re-analysis can be performed to meet more challenging fuel designs. The following sections describe the U.S. EPR REA methodology and describe how the requirements are met.

6.0 COMPUTER CODES

The computer codes used to demonstrate the applicability of this methodology are COPERNIC[2], NEMO-K[6], LYNXT[7], and S-RELAP5[8]. Other approved computer codes which perform the same types of calculations are also acceptable.

6.1 COPERNIC

COPERNIC is used to define the fuel and cladding thermal properties for both NEMO-K and LYNXT. These properties include the fuel and cladding thermal conductivity which includes oxide formation, the heat capacity for the fuel pellet and cladding, the radial power distribution in the fuel pellet, and the gap conductance. Fuel burnup affects the fuel conductivity, the pellet radial power profile, the gap conductance, and cladding oxide. The gap conductance is a complex function of the gap and surface temperatures, gap size (i.e., creep and thermal expansion), contact pressure, and fission gas content. To capture these effects in the downstream codes using a constant fuel geometry model, the gap conductance is interpolated from a table of gap conductances **[**

] Repeating these calculations of gap conductance values at various burnup levels, a complete table is developed that captures the complex effects of burnup on the gap as well as the transient effects due to thermal expansion.

6.2 Plant Transient Model

The approved NEMO-K code is used as the plant transient model. It is a 3-D neutronic kinetics solution with time dependent fuel and coolant models. Benchmarks presented in Reference 6 include three HZP and three HFP ejected rod code benchmarks and confirm that NEMO-K is applicable for calculating core power and peaking response during an ejected rod event. This section provides an overview of the features added to NEMO-K and its applicability to the U.S. EPR.

6.2.1 Trip Function

The U.S. EPR uses an excore power rate lagged trip signal to sense severe RIAs and subsequently shutdown the core. This trip function requires three different models: excore detector signals, a rate lagged processed signal, and a control rod drop model. The excore detectors are located near the minor axis of each quadrant, which causes the excore signal response to differ from the core average value when an asymmetric rod is ejected. These signals are processed with a rate lagged function to compare to the trip values. Once the criteria for trip are reached (2/4 logic when trip signal is exceeded), a time delay is employed before the control rods are moved. The rod position with time in NEMO-K is defined by the safety analysis control rod drop position versus time from an input table. The physical models for the excore signals, the flux lagged signal, and the dropping of the control rods are discussed in the following sub-sections.

6.2.1.1 *Excore Detector Model*

Reactor plant protection systems typically sense and respond to the plant excore power detector signals. These signals measure the fast flux exiting the reactor core and are an indication of the actual incore reactor conditions. The incore assembly powers are multiplied by weighting factors to translate the incore conditions to the excore signals. These weighting factors are typically generated using detailed transport calculations. As demonstrated in Reference 6, a simple weighting of the peripheral location closest to the excore detector provides good simulated results compared to the actual results in an operating reactor when a control rod is dropped.

The excore detector model in NEMO supports a top and bottom detector at four radial locations. Detector response is computed by:

$$E_n^{T/B} = C_n^{T/B} \cdot F\left(T_n^{T/B}\right) \cdot \left[\sum_{j=1}^{J} W_j \cdot \sum_{k=1}^{K} D_k^{T/B} \cdot P_{jk}\right] \cdot P_{th}$$

where:

$E_n^{T/B}$ = top or bottom excore response in terms of percent power for radial detector *n*

$C_n^{T/B}$ = top or bottom excore response calibration factor for radial detector *n*

$F\left(T_n^{T/B}\right)$ = top or bottom excore response correction function for coolant temperature compensation for radial detector *n*

W_j = weighting factor for the assembly *j* contribution to the excore detector response

$D_k^{T/B}$ = weighting factor for the axial level *k* contribution to the top or the bottom detector response

P_{jk} = normalized power density for assembly *j* at axial level *k*

P_{th} = percent thermal power

The calibration factor represents the actual calibration performed at the plant when the excore detectors are periodically normalized to the measured thermal power. The calibration factor is either input or calculated by NEMO-K, if requested. For the requested calibration, the detectors are calibrated to core power using a static case that is run before the transient. The temperature correction factors, the radial and the axial weighting factors are input by the user.

6.2.1.2 *Rate Lagged Processed Signal*

NEMO-K simulates the instrumentation and processing that determines a reactor scram based on excore flux signals. The model combines the top and bottom signals previously described to treat four distinct radial detectors. The user specifies the magnitude of the signal to cause a detector to trip and the number of detectors required to trigger a reactor scram. A maximum (i.e., saturation) signal can be specified, along with a low signal that will reset the state of the detector. The relationship between the rate lagged signal ($F(t)$) that is used for the trip function and the unfiltered excore detector signal ($I(t)$) is defined by the following first order filter equations:

$$F(t) = \tau_d \frac{dP(t)}{dt}$$

$$\frac{dP(t)}{dt} = \frac{1}{\tau}\left(I(t) - P(t)\right)$$

where:

τ_d = the derivative lead time constant

$P(t)$ = the lagged excore signal (power)

τ = the lagged signal time constant

These equations are approximated with a finite difference formulation based on the *dt* as the sampling rate. When the trip criteria are reached, the time to start the rod movement is set based on an input delay time between the trip measured and the start of physical movement.

6.2.1.3 *Control Rod Drop*

Rod movement during a scram is characterized by several distinct conditions:

- An initial acceleration period.
- Free fall above the dashpot.
- Deceleration due to the dashpot.
- Free fall within the dashpot.
- Stop at the bottom position.

The NEMO-K implementation models the movement for each rod or bank regardless of its initial position before scram. This leads to two different starting conditions:

- Rods that begin above dashpot.

- Rods that begin at the top of or within the dashpot.

When rod movement begins from a trip actuation, NEMO-K drops the rods or banks from their current height to the fully inserted position. The position versus time of a rod or bank depends upon the initial position prior to the trip. **[**

] This control rod drop model allows the rods to fall from any initial position in a manner consistent with the safety analysis assumptions without user intervention.

6.2.2 Adiabatic cal/g Edit

An edit is provided that calculates the change in pellet enthalpy during a transient. The method integrates the change in rod segment power produced (relative to the beginning of the transient) over each timestep. The total energy deposited is the change in enthalpy. This method conservatively estimates the cal/g as defined for RIA because it neglects the energy lost from the fuel rod by heat transfer to the coolant. This definition provides a useful means of identifying the relative impact of different conditions in two or more NEMO-K transients.

6.2.3 Adjustment Factors

In NEMO, there are four types of adjustment factors that can be used to account for uncertainty and conservative allowances. These adjustment factors are multipliers on the following parameters:

- Fuel conductivity
- Gap conductance
- Cross section changes due to fuel temperature variation (Doppler adjustment)
- Cross section changes due to control rod insertion (rod worth adjustment)

For the first three parameters the multipliers are applied to every node location. The control rod multiplier can be applied by bank or assembly location. These multipliers are factors that can be applied to examine sensitivities or to formulate a limiting case with uncertainties and/or conservative allowances.

6.2.4 Pellet Weighted Temperature for DTC

The cross sections are generated for NEMO-K using a flat pellet temperature profile. The pellet temperature distribution can vary significantly with time during an REA. For a pellet with a temperature distribution, a simple approach is to use volume averaging to obtain the effective temperature for the cross sections. Another common method uses a weighting of the centerline and surface temperatures as shown below:

$$T_{eff} = T_S \cdot wt_{SC} + T_{CL} \cdot (1 - wt_{SC})$$

where:

T_{eff} = the effective flat temperature

T_S = the fuel surface temperature

T_{CL}= the fuel centerline temperature

wt_{SC} = the weighting factor for the surface/centerline formula

For example, Reference 9 uses this formulation with a weighting factor of 0.7. The disadvantages of this formulation are that it uses only two temperatures of the pellet and that it is based on the typical radius squared variation of the fuel pellet temperature at static conditions. An improved weighting method is employed in NEMO-K [

]

6.2.5 NEMO-K Summary

Some of the results from Reference 6 that are pertinent to the REA are summarized to illustrate the accuracy of NEMO-K to a fine mesh reference solution. Table 6-1 shows the current NEMO-K results for each of the six rod ejection benchmark cases. These results are comparable to Table 4-5 in Reference 6. The six cases include a HZP (x1) and a HFP (x2) rod ejection with three different core geometries (where x is A, B, or C). As stated in Reference 6, the agreement between NEMO-K and the reference solution is excellent. The only item that stands out in the table is case B2, where the time of the peak is predicted to be 0.10 seconds rather than 0.12 seconds as the reference solution. Although this is a large percentage difference, the absolute difference is small considering the relatively flat peak core power in this transient as shown in Figure 6-2.

Additionally, Figure 6-3 through Figure 6-5 show the power distribution comparisons for case A1 at initial, peak core power, and 5 seconds during the transient, respectively. These figures correspond to figures 4-17, 4-18, and 4-19 in Reference 6. As shown in the figures, NEMO-K agrees with the reference PANTHER solutions.

Figure 6-6 and Figure 6-7 show power distribution results that have not been previously published with NEMO-K for cases C1 and C2, respectively. These figures show the assembly planar power at a fixed height along the major axis at maximum transient core

power. This dimensional slice includes the ejected rod location at B08. The power density values are normalized to the maximum value in this slice. The figures show excellent agreement between NEMO-K and the reference solution. The results demonstrate that NEMO-K accurately models REA time dependent phenomena and is applicable for the methodology presented.

6.3 Transient Fuel Rod Model

The fuel rod model in LYNXT[7], an approved code, is used as the transient fuel rod model. Changes to the core thermal-hydraulic code LYNXT are implemented in the fuel rod modeling for the REA analysis. This section contains a brief overview of the approved fuel rod model as well as the changes in the fuel rod model made for the REA and other static and transient fuel rod modeling applications.

6.3.1 General Overview of Existing LYNXT Fuel Rod Models

The approved fuel rod model in LYNXT is based on a two-dimensional conduction equation with a radial and optional axial dependence. The solution is based on the orthogonal collocation method where the solution locations within the fuel and cladding are determined based on the collocation order. Two fuel rod models exist in LYNXT as approved by the U.S. NRC:

- Constant Gap/Constant Properties (CG/CP) – This is the same model in COBRA-IV-I[10], which served as the basis for LYNXT. The fuel-to-cladding gap dimension remains invariant throughout the modeled event as do all the thermal properties, with the exception of the fuel thermal conductivity which can optionally be modeled using a third order temperature dependence.

- Variable Gap/Temperature Dependent Properties (VG/TDP) – This fuel rod model is based on the thermal and mechanical properties of the TAFY[11], TACO[12], and TACO2[13] fuel performance codes. The VG/TDP fuel rod model allows the fuel and cladding dimensions to change during the event due to temperature and pressure difference effects (i.e., pressure difference between

coolant and internal fuel rod pressure), based on the TAFY, TACO, and TACO2 models. The VG/TDP fuel rod model uses the same gap conductance model from TAFY, TACO, and TACO2 with the gas inventory at the start of the event being invariant throughout the event. The LYNXT VG/TDP model allows the radial power profile data from the three fuel performance codes to be used as an optional input, which is held invariant during the modeled event.

6.3.2 Enhancements to the Fuel Rod Models

The enhancements to the approved LYNXT fuel rod models increase the number of solution locations in the fuel pellet and increase the modeling flexibility of the fuel rod model (including the cladding). Increasing the number of solution locations in the fuel allows the fuel rod model to more accurately represent various radial power profiles across the fuel pellet, including those with the peak radial power in the outer portions of the fuel pellet. Expanding the modeling capability allows various fuel performance codes, such as (but not limited to) TACO3[14] or COPERNIC[2], to be used as the basis of a LYNXT time dependent analysis. The enhancements use the same fuel and cladding energy equations and solution process as the CG/CP and VG/TDP models (defined in Equations 2-6 through 2-13 for the energy equations and Equations 2-117 through 2-125 for the solution process in Reference 7), but use input property values for the pellet, gap, and cladding instead of the code specific values relative to TAFY, TACO, and TACO2.

The maximum number of solution locations in the cylindrical fuel is increased from 6^{th} order collocation in Reference 7 to 20^{th} order collocation. The additional solution locations are available for the enhanced fuel rod model and the approved CG/CP and VG/TDP fuel rod models. Table 6-2 contains the collocation locations, both the cylindrical and planar data up to 6^{th} order collocation are from Figure 2-5 of Reference 7, as well as the additional 8^{th}, 10^{th}, 12^{th}, 16^{th}, and 20^{th} order radial locations in the fuel pellet. The planar data is unchanged from COBRA-IV-I[10].

The enhancements to the fuel rod model to expand the modeling capability allow the various temperature dependent properties and radial power profile characteristics used in the fuel/cladding energy equation calculations to be based on a number of potential fuel performance codes. The enhancements provide a fuel rod model that is based on the following parameters being invariant during the modeled event:

- Fuel Dimensions - Thermal and lateral pressure changes to the geometry are not modeled. Gap conductance is allowed to change in a transient [

  ]

- Cladding, gap, and fuel properties dependent on parameters other than temperature, such as pressure difference across the cladding.
- Gas inventory during the event - This is consistent with the VG/TDP model.
- Radial power profile - This is consistent with the VG/TDP model.

The new fuel rod model is called the Constant Gap/Temperature Dependent Property (CG/TDP) model because the fuel-to-cladding gap dimension is invariant and various thermal properties may be temperature dependent.

The CG/TDP model allows the input of the following temperature dependent properties, in tabular form:

- Thermal conductivity for the fuel and/or cladding
- Specific heat for the fuel and/or cladding
- Gap conductance
- Fuel enthalpy

[

] The CG/TDP model also allows the application of a radial power profile across the fuel pellet.

6.3.3 LYNXT Benchmark Review

The LYNXT thermal equations have not changed; only the user inputs to those equations have changed. Therefore, the validation of the code equations remains valid. This subsection reviews the past qualification of the code and provides some example cases with the new input options to illustrate the new coupling of inputs.

6.3.3.1 *Past Qualification*

The benchmarks for the CG/CP and VG/TDP fuel rod models included:

- Analytical solution of the fuel and cladding with the gap conductance assumed as negligible.
- Power ramp comparisons to TACO (Reference 12).
- Non-crossflow transient fuel temperature and DNBR code, RADAR[15], using the four pump coastdown and the four pump locked rotor transients.
- Sensitivity studies using the hot full power ejected rod (HFPER) event.

The Reference 7 CG/CP and VG/TDP benchmark cases indicated the following in terms of the maximum difference:

- Agreement between the CG/CP LYNXT fuel rod model and the analytical solution was within 0.5 percent on the fuel centerline temperature.
- Agreement between the VG/TDP LYNXT fuel rod model (initialized to 102 percent rated power with TACO) and TACO over a power ramp range from 60 to 135 percent rated power was within 2 percent on centerline temperature and 4 percent on fuel surface temperature for BOL conditions.

- Agreement between the VG/TDP LYNXT fuel rod model and the RADAR fuel rod model for the transients was within 3 percent on the fuel centerline temperature, within 4.5 percent on the radial average temperature, and 2.5 percent on the transient minimum DNBR (MDNBR). These comparisons are based on BOL conditions.

The fuel rod model benchmark cases for LYNXT, based on Reference 7, confirm that the VG/TDP LYNXT fuel rod model is capable of predicting consistent results with fuel performance codes (limited to TAFY, TACO, and TACO2). The CG/CP and VG/TDP fuel rod models are capable of predicting the fuel temperatures, cladding temperatures and DNBR from other transient fuel performance and DNBR codes such as RADAR over a wide range of static and transient events typically encountered in plant operations.

These benchmarks are repeated with the new LYNXT version which produced equivalent results (within roundoff). In addition, several cases were repeated with the higher collocation orders and with the CG/TDP fuel option which produced equivalent results. Therefore, the conclusions made for LYNXT in Reference 7 remain valid for the CG/TDP fuel option.

6.3.3.2 *LYNXT-to-COPERNIC Example Cases*

The CG/TDP LYNXT fuel rod model is compared to COPERNIC (Reference 2) using a representative rod ejection transient starting at HZP and HFP conditions. Even though COPERNIC is not approved for fast transients like REA, this comparison highlights any significant differences between LYNXT and a more precise treatment of the fuel rod thermal parameters. These calculations were repeated for both BOL and EOL burnup-based fuel rod conditions. The CG/TDP LYNXT inputs for these rod ejection cases are thermal properties (including gap conductance) and radial/axial power profiles based on static COPERNIC calculations. In addition to any temperature dependence, the COPERNIC-based LYNXT inputs consider the burnup effects, the uranium enrichment, the porosity of the fuel, and the oxide thickness on the cladding. The same transient

boundary conditions for power, $F_{\Delta H}$, axial shape, and cladding outer wall temperature versus time are used in both the COPERNIC and LYNXT transient analyses.

The following four example cases are performed for LYNXT and COPERNIC:

- HZP/EOL – Based on EOL burnup conditions (60 GWD/MTU) for HZP transient boundary conditions.
- HFP/EOL – Based on EOL burnup conditions for HFP transient boundary conditions.
- HZP/BOL – Based on BOL burnup conditions (2.5 GWD/MTU) for HZP transient boundary conditions.
- HFP/BOL – Based on BOL burnup conditions for the HFP transient boundary conditions.

The transient comparisons of the fuel surface, fuel radial average, fuel centerline, fuel maximum, and the cladding maximum temperatures for the four different cases are presented in Figure 6-8 through Figure 6-27 as illustrated in the following table.

Condition	Fuel temperature				Cladding maximum temperature
	Surface	Average	Centerline	Maximum	
HZP/EOL	Figure 6-8	Figure 6-9	Figure 6-10	Figure 6-11	Figure 6-12
HFP/EOL	Figure 6-13	Figure 6-14	Figure 6-15	Figure 6-16	Figure 6-17
HZP/BOL	Figure 6-18	Figure 6-19	Figure 6-20	Figure 6-21	Figure 6-22
HFP/BOL	Figure 6-23	Figure 6-24	Figure 6-25	Figure 6-26	Figure 6-27

Table 6-3 contains a numerical summary for the LYNXT and COPERNIC comparisons for each of the four transient cases when transient time steps are the same in both codes.

With the exception of the HZP/EOL fuel surface temperatures in the 0.15 to 0.20 second time frame, the maximum difference between the transient COPERNIC and LYNXT

CG/TDP fuel temperatures is less than **[ ]** percent. During this 0.05 second interval for HZP/EOL, which represents the time of the neutron power spike due to the rod ejection, the differences between the COPERNIC and the CG/TDP LYNXT fuel surface temperatures are **[**

]. This difference in the gap conductance is for a short duration and has little impact on the maximum fuel temperature comparisons, which are within **[ ]** percent. The maximum difference in the maximum cladding temperatures between COPERNIC and LYNXT is within **[ ]** percent, with LYNXT predicting higher temperatures than COPERNIC. Since this LYNXT model tends to yield higher peak cladding temperatures and accurately predicts peak fuel temperatures, this model with the gap conductance fitting tables is acceptable to predict fuel melt and minimum DNBR conditions for REA.

6.3.4 LYNXT Conclusions

Three different fuel rod models are available in LYNXT (i.e., CG/CP, VG/TDP, and CG/TDP). These models are summarized in Table 6-4. The enhancements used to form the CG/TDP model provide LYNXT the ability to use thermal properties and other conditions from any fuel performance code, such as (but not limited to) TACO3 (Reference 14) or COPERNIC (Reference 2). The CG/TDP fuel rod model allows LYNXT to mimic the behavior of various fuel performance codes without the need to implement each of the various fuel performance code models and properties within LYNXT. The CG/TDP model allows the specification of the following, based on input:

- Temperature dependent thermal properties for the fuel and cladding
- Gap conductance based on the **[ ]**

- Radial power profile across the fuel pellet

The limitations of the CG/TDP LYNXT fuel rod model are as follows:

- Cladding, gap, and fuel dimensions are invariant throughout the event.
- Cladding, gap, and fuel properties are only temperature dependent.
- Cladding, gap, and fuel properties apply throughout the event.
- Radial power profile is invariant throughout the event.
- Gas inventory during the event is invariant.

The last two limitations are also limitations of the VG/TDP fuel rod model.

Three different types of cases to verify that the CG/TDP fuel rod model is accurately predicting the results of various fuel performance codes are as follows:

- Analytical benchmark (same as in Reference 7).
- Original fuel performance code benchmarks using a variable gap conductance fuel rod model (same as in Reference 7).
- Example cases with COPERNIC.

The code comparisons indicate that the CG/TDP fuel rod model predicts the known solution (analytical or from a fuel performance code) to within **[ ]** percent, based on the input gap conductance table accurately predicting the fuel performance code gap conductance behavior. As the burnup increases and the power excursion gets larger it becomes **[**

]. For these higher burnups and large power excursions, the difference between the CG/TDP LYNXT local fuel temperature predictions and COPERNIC is **[** **]**, with LYNXT

producing higher temperatures. Even with these differences for short durations, the maximum difference in the maximum fuel temperature is less than [ ] percent. Therefore, this model with the gap conductance fitting tables is acceptable to predict fuel melt and minimum DNBR conditions for REA analyses.

6.4 System T-H Model

The plant transient model uses a constant pressure, inlet temperature, and flow model. A system T-H model is needed to model the trip functions, primary and secondary systems to address those conditions that may change pressure, inlet temperature and/or flow during an REA. S-RELAP5 (Reference 8) is used for non-LOCA safety analyses and is also used to estimate changing plant conditions during an REA. Its applicability to the U.S. EPR for the maximum pressure boundary consequences of REA is addressed in Reference 16. The only significant change to this model for REA simulations would be to turn off the point kinetics model and substitute the power versus time obtained from NEMO-K.

Table 6-1 NEACRP Kinetic Results

	NEMO-K	Ref	Diff	% Diff
A1				
Maximum Core Power Fraction	1.223	1.179	0.044	3.7
Core Power Fraction @ 5 sec	0.200	0.196	0.004	2.0
Time of Maximum Power	0.550	0.560	-0.010	-1.8
Fuel Temperature at Max Power	294.7	294.5	0.200	0.1
Fuel Temperature @ 5 sec	325.1	324.3	0.800	0.2
A2				
Maximum Core Power Fraction	1.082	1.080	0.002	0.2
Core Power Fraction @ 5 sec	1.036	1.035	0.001	0.1
Time of Maximum Power	0.1	0.1	0.000	0.0
Fuel Temperature at Max Power	544.6	546.5	-1.900	-0.3
Fuel Temperature @ 5 sec	553.0	554.6	-1.600	-0.3
B1				
Maximum Core Power Fraction	2.431	2.441	-0.010	-0.4
Core Power Fraction @ 5 sec	0.324	0.320	0.004	1.3
Time of Maximum Power	0.520	0.517	0.003	0.6
Fuel Temperature at Max Power	301.4	301.4	0.000	0.0
Fuel Temperature @ 5 sec	350.3	349.9	0.400	0.1
B2				
Maximum Core Power Fraction	1.062	1.063	-0.001	-0.1
Core Power Fraction @ 5 sec	1.038	1.038	0.000	0.0
Time of Maximum Power	0.10	0.12	-0.020	-16.7
Fuel Temperature at Max Power	542.1	544.1	-2.000	-0.4
Fuel Temperature @ 5 sec	550.0	552.0	-2.000	-0.4
C1				
Maximum Core Power Fraction	4.735	4.773	-0.038	-0.8
Core Power Fraction @ 5 sec	0.148	0.146	0.002	1.4
Time of Maximum Power	0.268	0.268	0.000	0.0
Fuel Temperature at Max Power	298.2	297.9	0.300	0.1
Fuel Temperature @ 5 sec	316.1	315.9	0.200	0.1
C2				
Maximum Core Power Fraction	1.074	1.071	0.003	0.3
Core Power Fraction @ 5 sec	1.031	1.030	0.001	0.1
Time of Maximum Power	0.1	0.1	0.000	0.0
Fuel Temperature at Max Power	544.5	546.4	-1.900	-0.3
Fuel Temperature @ 5 sec	551.8	553.5	-1.700	-0.3

Table 6-2 Cylindrical and Planar Geometry Collocation Points for LYNXT

Cylindrical geometry

N = 2	N = 3	N = 4	N = 5	N= 6
0.393765	0.297637	0.238965	0.199524	0.171220
0.803087	0.639896	0.526159	0.444987	0.384810
	0.887502	0.763931	0.661797	0.580504
		0.927491	0.833945	0.747443
			0.949455	0.877060
				0.962780

[ ]

Planar Geometry

N = 2	N = 3
0.285232	0.209299
0.765055	0.591700
	0.871740

Notes:

1. All collocation points are normalized, based on fuel pellet/plate outer surface.
2. The point, based on a normalized location, of 1.0 is a collocation point for all orders. This represents the fuel surface.
3. N denotes the collocation order.

Table 6-3 LYNXT and COPERNIC Transient Temperature Ratio Comparisons

Comparison parameter	Fuel temperature				Cladding maximum temperature
	Surface	Average	Centerline	Maximum	
HZP EOL					
Average	[				]
Std. dev.					
Maximum					
Minimum					
Sample size	[				]
HFP EOL					
Average	[				]
Std. dev.					
Maximum					
Minimum					
Sample size	[				]
HZP BOL					
Average	[				]
Std. dev.					
Maximum					
Minimum					
Sample size	[				]
HFP BOL					
Average	[				]
Std. dev.					
Maximum					
Minimum					
Sample size	[				]

Notes:

1. The data is based on (COPERNIC result) / (LYNXT CG/TDP result).
2. “Std. dev.” is the standard deviation of the data about the average. Sample size is the number of transient time steps.

Table 6-4 LYNXT Fuel Rod Model Options

Fuel/cladding parameter	CG/CP	VG/TDP	CG/TDP
Collocation orders	See Note 1	See Note 1	All values in Table 6-2
Fuel thermal conductivity	Constant or user-supplied third order polynomial	TAFY, TACO, TACO2 property	User-supplied function of fuel temperature
Fuel specific heat	Constant	Temperature-dependent function	
Cladding thermal conductivity		TAFY, TACO, TACO2 property	User-supplied function of cladding temperature
Cladding specific heat		Temperature-dependent function	
Fuel-to-cladding gap dimension		Variable	Constant
Gap conductance		TAFY, TACO, TACO2 model	User-supplied function of [ ]
Radial power profile	Uniform	User-supplied as a function of fuel pellet radial location	User-supplied as a function of fuel pellet radial location
Fuel enthalpy	Not available	Not available	User-supplied function of fuel temperature

Notes:

1. The collocation orders in Reference 7 are 2, 3, 4, 5, and 6 (cylindrical). The potential collocation orders were expanded to include all the locations in Table 6-2.
2. In the CG/TDP fuel rod model the input of each of the user-supplied functions is optional and if used is supplied in tabular form.

Figure 6-1 Scram Position Versus Drop Time

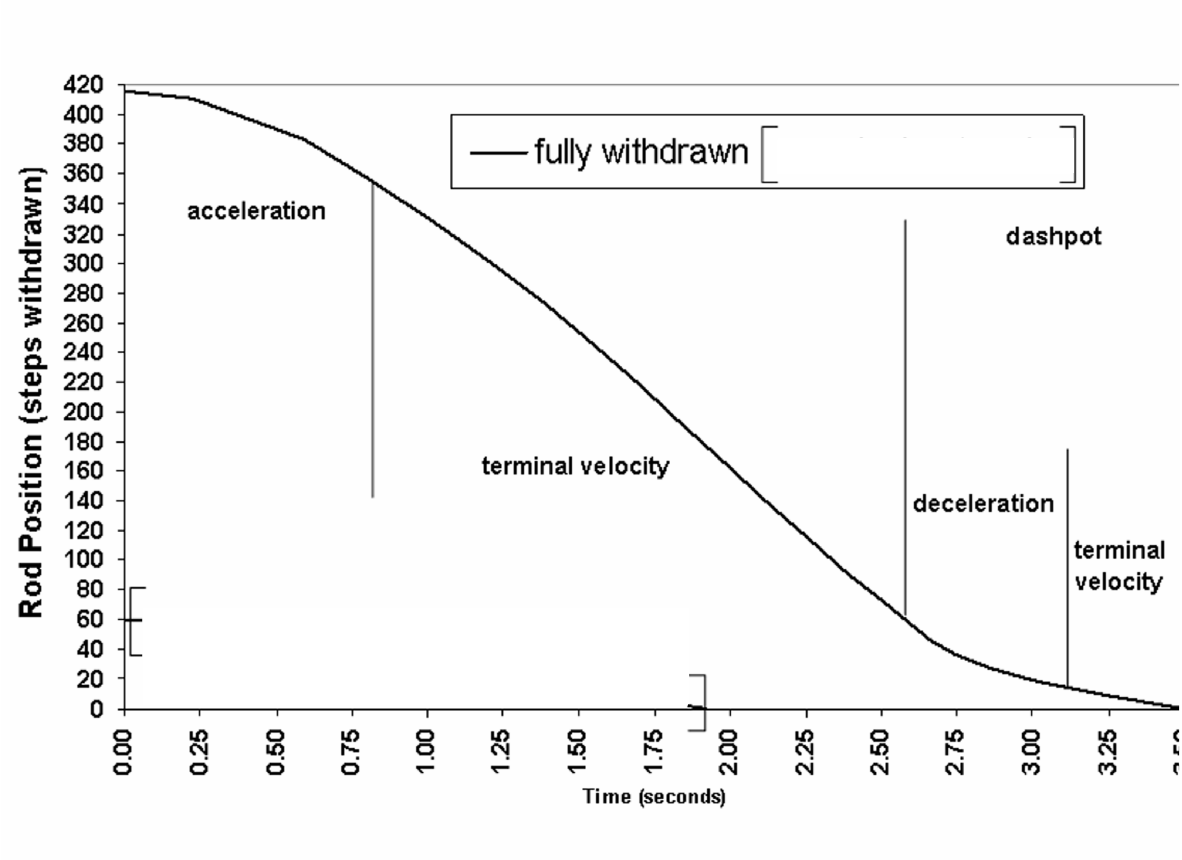

Figure 6-2 Core Power Fraction – Case B2

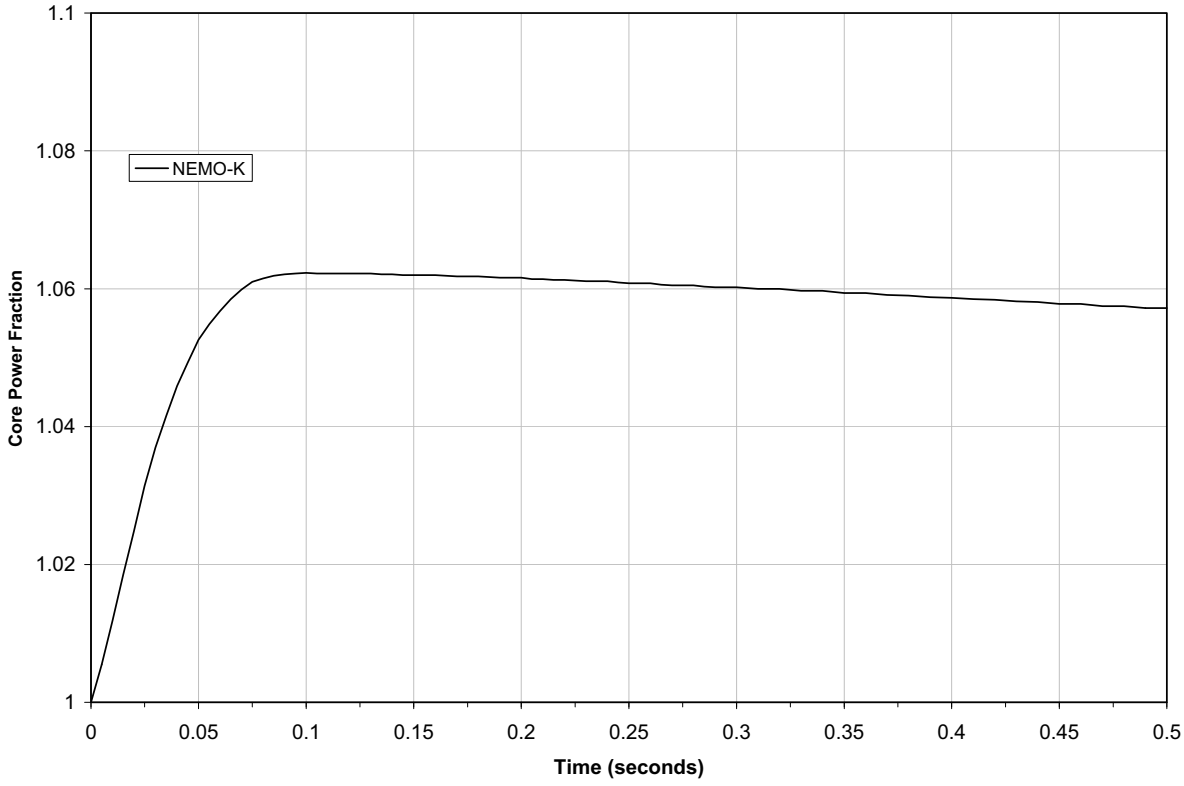

Figure 6-3 Power Distribution at Initial Conditions – Case A1

1/8th Core Assembly Power Map at Plane 6

PANTHER

				0.293	0.354		
			0.752	0.533	0.497	0.285	
		0.545	0.757	0.393	0.380	0.206	
	0.964	0.867	1.000	0.745	0.301	0.294	0.226
0.533	0.793	0.575	0.945	0.951	0.527	0.214	0.285

NEMO-K

Nodal Layer Peak		2.372		0.284	0.353		
			0.752	0.532	0.496	0.284	
		0.530	0.757	0.382	0.380	0.200	
	0.965	0.868	1.000	0.745	0.292	0.293	0.225
0.518	0.794	0.559	0.945	0.950	0.527	0.207	0.284

DIFFERENCE (N-P)

STD	0.006			-0.009	-0.001		
			0.000	-0.001	-0.001	-0.001	
		-0.015	0.000	-0.011	0.000	-0.006	
	0.001	0.001	0.000	0.000	-0.009	-0.001	-0.001
-0.015	0.001	-0.016	0.000	-0.001	0.000	-0.007	-0.001

Figure 6-4 Power Distribution at Maximum Core Power – Case A1

1/8th Core Assembly Power Map at Plane 6

PANTHER

				0.128	0.150		
			0.362	0.242	0.214	0.120	
		0.316	0.390	0.188	0.169	0.088	
	0.790	0.562	0.540	0.371	0.140	0.126	0.093
1.000	0.778	0.390	0.513	0.474	0.248	0.093	0.117

NEMO-K

Nodal Layer Peak		4.357		0.124	0.149		
			0.362	0.242	0.213	0.119	
		0.307	0.391	0.183	0.169	0.085	
	0.790	0.562	0.540	0.371	0.136	0.126	0.093
1.000	0.778	0.379	0.513	0.474	0.248	0.090	0.117

DIFFERENCE (N-P)

STD	0.003			-0.004	-0.001		
			0.000	0.000	-0.001	-0.001	
		-0.009	0.001	-0.005	0.000	-0.003	
	0.000	0.000	0.000	0.000	-0.004	0.000	0.000
0.000	0.000	-0.011	0.000	0.000	0.000	-0.003	0.000

Figure 6-5 Power Distribution at 5 Seconds – Case A1

1/8th Core Assembly Power Map at Plane 6

PANTHER

				0.143	0.168		
			0.392	0.266	0.239	0.135	
		0.333	0.417	0.205	0.188	0.099	
	0.802	0.581	0.569	0.397	0.153	0.142	0.106
1.000	0.785	0.403	0.540	0.505	0.269	0.104	0.134

NEMO-K

Nodal Layer Peak		4.554		0.139	0.169		
			0.392	0.266	0.239	0.135	
		0.323	0.417	0.199	0.188	0.096	
	0.802	0.582	0.570	0.397	0.149	0.142	0.106
1.000	0.785	0.392	0.541	0.505	0.270	0.101	0.134

DIFFERENCE (N-P)

STD	0.003			-0.004	0.001		
			0.000	0.000	0.000	0.000	
		-0.010	0.000	-0.006	0.000	-0.003	
	0.000	0.001	0.001	0.000	-0.004	0.000	0.000
0.000	0.000	-0.011	0.001	0.000	0.001	-0.003	0.000

Figure 6-6 Comparison of Radial Power at Max Power – C1

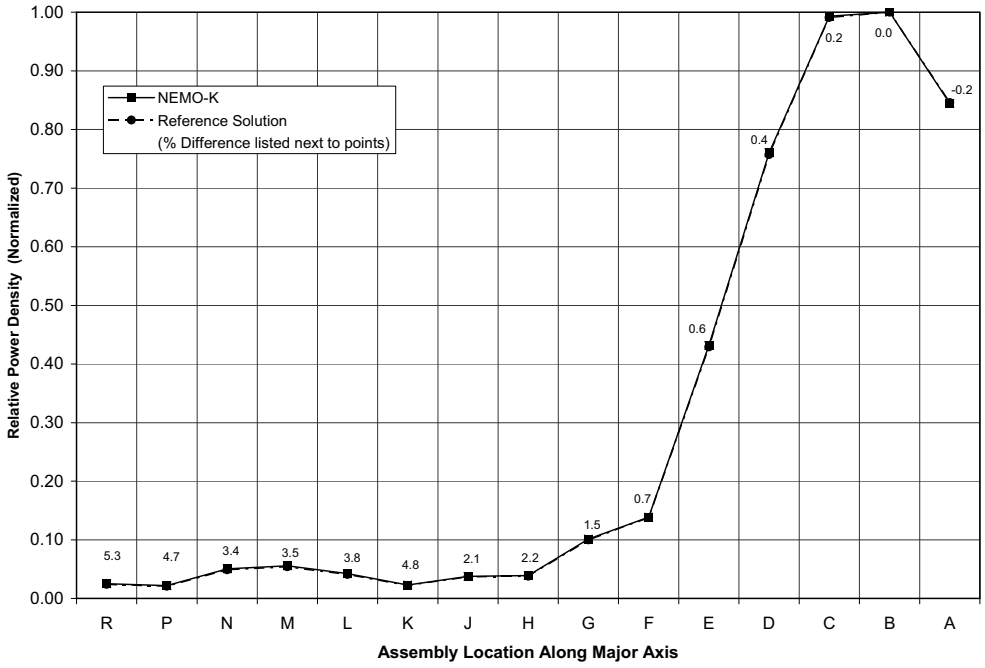

Figure 6-7 Comparison of Radial Power at Max Power – C2

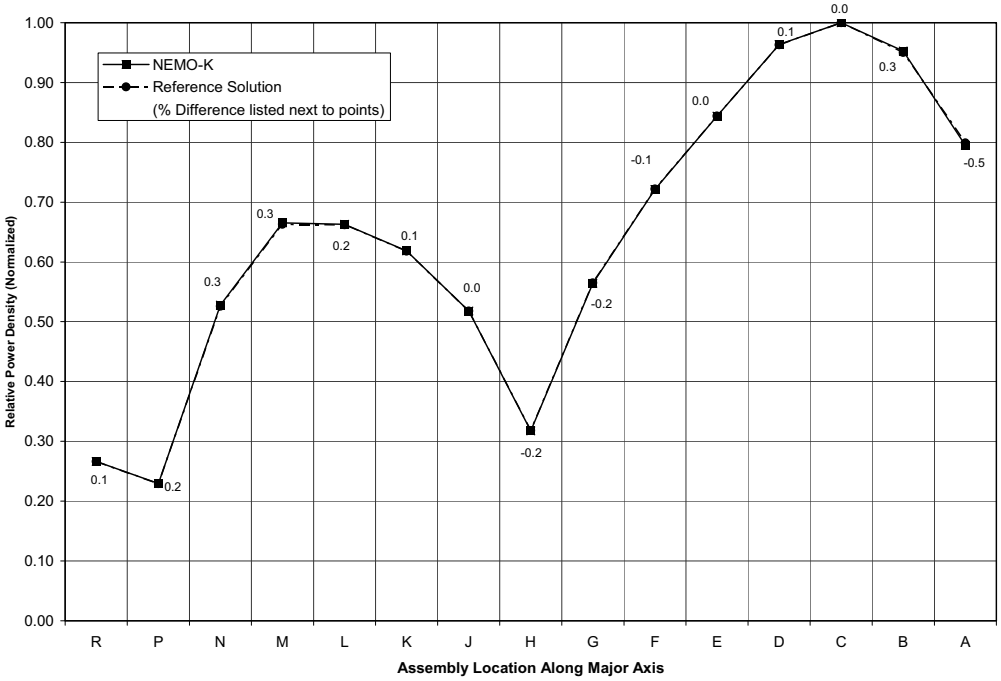

Figure 6-8 HZP/EOL Transient Fuel Surface Temperature

Figure 6-9 HZP/EOL Transient Fuel Average Temperature

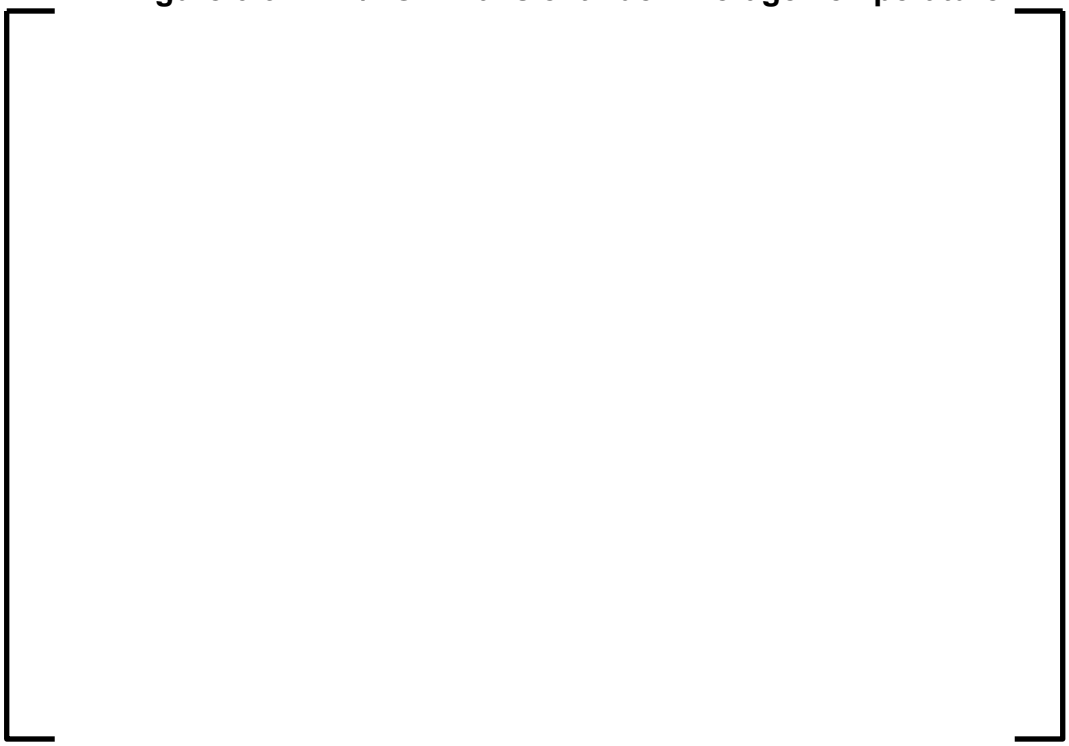

Figure 6-10 HZP/EOL Transient Fuel Centerline Temperature

Figure 6-11 HZP/EOL Transient Fuel Maximum Temperature

Figure 6-12 HZP/EOL Transient Cladding Maximum Temperature

Figure 6-13 HFP/EOL Transient Fuel Surface Temperature

Figure 6-14 HFP/EOL Transient Fuel Average Temperature

Figure 6-15 HFP/EOL Transient Fuel Centerline Temperature

Figure 6-16 HFP/EOL Transient Fuel Maximum Temperature

Figure 6-17 HFP/EOL Transient Cladding Maximum Temperature

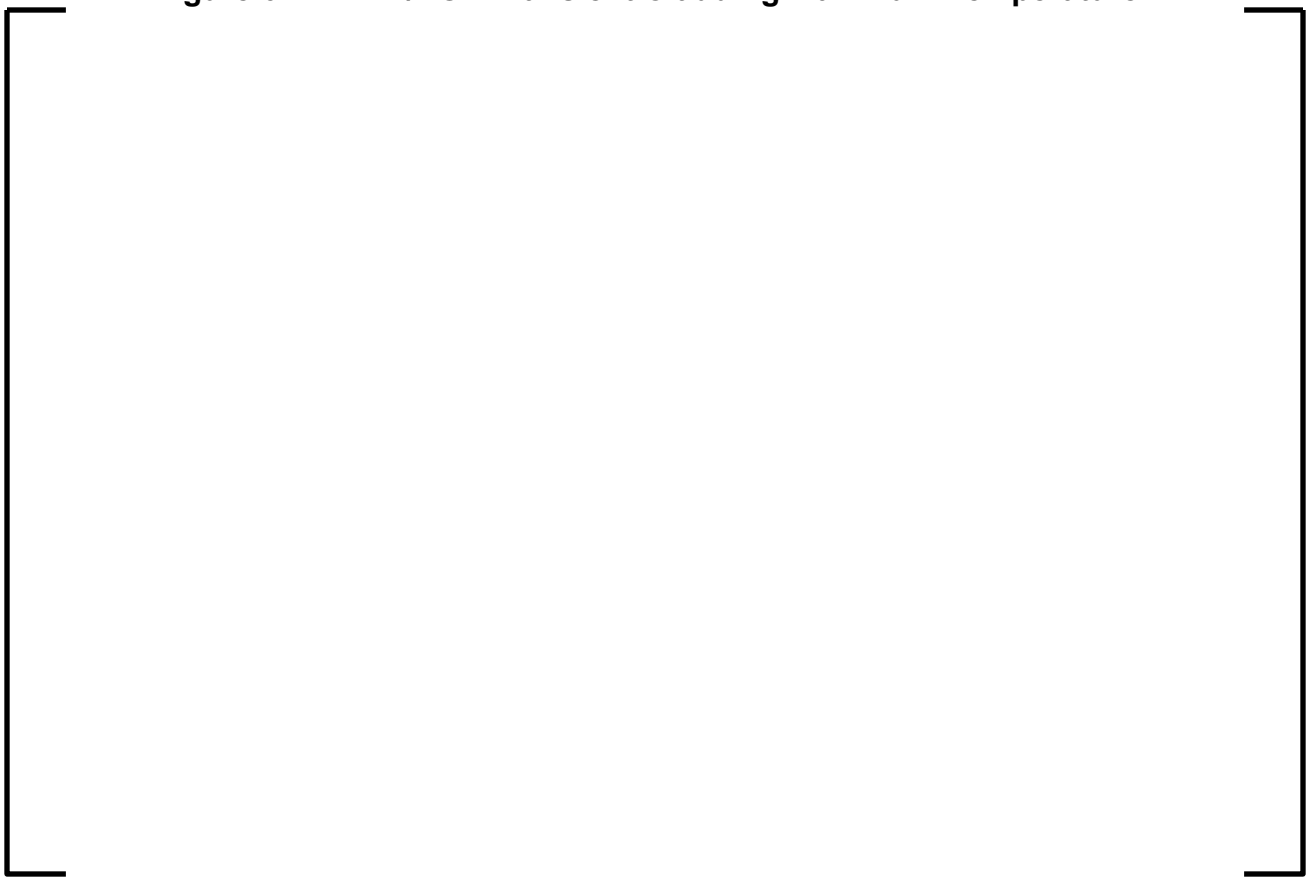

Figure 6-18 HZP/BOL Transient Fuel Surface Temperature

Figure 6-19 HZP/BOL Transient Fuel Average Temperature

Figure 6-20 HZP/BOL Transient Fuel Centerline Temperature

Figure 6-21 HZP/BOL Transient Fuel Maximum Temperature

Figure 6-22 HZP/BOL Transient Cladding Maximum Temperature

Figure 6-23 HFP/BOL Transient Fuel Surface Temperature

Figure 6-24 HFP/BOL Transient Fuel Average Temperature

Figure 6-25 HFP/BOL Transient Fuel Centerline Temperature

Figure 6-26 HFP/BOL Transient Fuel Maximum Temperature

Figure 6-27 HFP/BOL Transient Cladding Maximum Temperature

7.0 APPLICATION OF BOUNDARY CONDITIONS AND UNCERTAINTIES

This section discusses the REA analysis boundary conditions and uncertainties for the plant transient model, the fuel rod model, and the failure analysis. The minimum requirement is to analyze/bound the limits of operation from BOC to EOC and from HZP to HFP. The U.S. EPR average temperature versus power level is shown in Figure 7-1. Since DNBR is one of the main failure criteria and it can be sensitive to the coolant temperature, the core powers of 0, 25, 35, 60, and 100 percent (i.e., at the transition temperatures) are analyzed to demonstrate where the limiting conditions occur relative to initial power level.

7.1 NEMO-K Boundary Conditions and Uncertainties

The treatment of the NEMO-K boundary conditions and uncertainties is addressed in this section. The parameters which have conservatisms and/or uncertainties and sensitivity results are presented to illustrate the conservatisms in the calculations. The application of conservatisms and uncertainties of the ejected rod worth, MTC, DTC, β_{eff}, fuel cycle design, and rod power peaking is addressed in the following sections.

7.1.1 Ejected Rod Worth

The uncertainty for the ejected rod worth is 15 percent for NEMO-K. This uncertainty is consistent with the currently employed methods that use NEMO[17]. The initial rod position prior to rod ejection and the change in fuel assembly cross sections due to the presence of control rods can be conservatively changed to bound the cycle-to-cycle variation of the observed ejected control rod worths and the uncertainty of 15%. The rod position insertion limit for the U.S. EPR is shown in Figure 7-2 and is compared to the assumed position in the REA analysis. The maximum calculated ejected rod worths for BOC and EOC at HFP and HZP are shown in Table 7-1 for the proposed cycles 1, 2, 3, and equilibrium cycle with PRISM and the bounding analysis values in NEMO-K for the REA example analysis.

7.1.2 MTC

A 2 pcm/^{o}F uncertainty is used. The MTC uncertainty of 2 pcm/^{o}F has been used as the acceptance criterion for current licensed cores. Both PRISM and NEMO comparisons to measurement results support a value lower than 2 pcm/^{o}F.

7.1.3 DTC

A DTC uncertainty of 10 percent is used.

7.1.4 β_{eff}

A β_{eff} uncertainty of 5 percent is used. **[**

] and

therefore a 5 percent β_{eff} uncertainty is a reasonable upper bound.

7.1.5 Fuel Cycle Design

Eighteen month core designs for cycle 1, cycle 2, cycle 3 and an equilibrium cycle are used to define the bounding initial conditions. The base REA analysis model uses the equilibrium cycle. The proximity of the fuel to the ejected rod location will affect the local cal/g. Since there are no burnup dependencies of the limits (see Section 2.1.1) and the MDNBR is evaluated for the full range of burnups (see Section 7.2.5), only the maximum ejected rod worth is investigated to determine the maximum power response of the peak assembly. Table 7-1 lists the nominal range of the key parameter values and the REA analysis values at BOC and EOC for both HZP and HFP for the available core designs.

A point kinetics model has very few inputs and the applicability to core designs has been demonstrated by using conservative reactivity core coefficients. To demonstrate that 3-D kinetics can be used similarly, sensitivity studies are performed with the [ ] and compared to the equilibrium core design. [

]

Figure 7-3 through Figure 7-6 show the power versus time for both cores at BOC 25 percent power, BOC HFP, EOC HZP, and EOC HFP conditions, respectively. Very similar power excursions for the initial pulse are shown for these cases. Figure 7-5 shows that the [ ]. Figure 7-7 shows the EOC HZP core power [ ]. The equilibrium cycle is now more limiting than [

] The results show that the selected base case is bounding and representative of the REA conditions for the U.S. EPR.

In Figure 7-3 and Figure 7-4, the ejected rod location at BOC is in assembly J03 for [ ] and in assembly N05 for the equilibrium cycle. A different location of the ejected rod does not significantly change the results and indicates a low sensitivity to ejected rod location. Therefore, future cycle results can be compared to the equilibrium cycle results to verify the applicability of this analysis for the U.S. EPR.

7.1.6 Transient Power and Rod Power Peaking

The example uncertainties and peaking allowances that are used for the REA analyses are shown in Table 7-2. These values are consistent with values employed for other chapter 15 events. The $F_{\Delta H}$ and F_Q uncertainty components are statistically combined (square root sum of the squares) and determined to be **[ ]** percent on $F_{\Delta H}$ and **[ ]** percent on F_Q. An overall allowance of **[ ]** percent is also applied to the calculated local $F_{\Delta H}$ and F_Q values. This allowance is defined as the maximum expected difference between measured to predicted values of $F_{\Delta H}$ and F_Q. These uncertainties will only be applied to the fuel rod model.

7.1.7 Sensitivity Calculations for Plant Transient Calculations

Table 7-3 provides a list of parameters, the range of transients sampled, and the estimated range of sensitivity in terms of estimated power differences. The difference in core power, core power times peaking factor ($F_{\Delta H}$ and F_Q), and/or maximum adiabatic cal/g (see section 6.2.2) are compared at the time of peak power and after the pulse has flattened out. The largest of the range of results are tabulated. The first sensitivity case is the base model with the uncertainties removed on ejected rod worth, β_{eff}, DTC, and MTC. The results can be significantly different for a prompt critical rod ejection calculation versus a non prompt critical rod ejection. The prompt critical excursion at EOC HZP has approximately **[ ]** percent conservatism or a delta of **[ ]** cal/g over the first second. The BOC HZP ejected rod worth is not prompt critical and is not as limiting as a higher initial power. Therefore, the BOC 25 percent power transient is used to replace the sensitivities of the analysis for BOC HZP. The BOC 25 percent power case has between **[ ]** percent conservatism. The HFP cases have the least conservatism **[ ]** depending on the time of the comparison. The minimum conservatism at peak power is **[ ]** percent. The smaller value corresponds to the near static condition at greater than 5 seconds. The trend of decreasing conservatism as power increases is expected. The uncertainties are applied to

maximize the resultant power change for a given reactivity insertion and the full power cases have the smallest change for the ejected rod worth.

For the remaining studies it is shown that [

] These conclusions are applicable to the results presented in this report. If in future analyses, the cal/g of the analysis exceeds the cal/g presented herein, the HZP sensitivity cases would need to be repeated for those conditions.

7.2 LYNXT Boundary Conditions and Uncertainties

The treatment for the LYNXT boundary conditions and uncertainties demonstrates which parameters need to be modeled and what conservatisms and uncertainties are applied. The application of boundary conditions and uncertainties for the pellet and cladding dimensions (geometry), cladding oxidation, coolant conditions, transient power, heat resistances, transient coolant heat transfer coefficient, and transient coolant conditions is addressed in the following sections.

7.2.1 Pellet and Cladding Dimensions (Geometry)

The LYXNT geometry model used for the rod ejection accident analysis is based upon a base 17-channel model used for the majority of the thermal-hydraulic and MDNBR evaluations. The model is developed to be consistent with the methods and geometries described in References 7 and 16. The fuel assembly is a 17x17 array of lattice locations with 265 fuel rods and 24 guide tubes. The U.S. EPR fuel assembly has 165.4 inches of active fuel height and a fuel rod in the center location. The LYNXT core model uses a $1/8^{th}$ symmetric model with [

] Figure 7-8 shows the baseline geometry for the radial layout of LYNXT model, which is constant for each axial node.

The geometry model for the temperature and enthalpy calculations within the fuel rod is based on the nominal cold dimensions for all cases. Engineering hot channel factors on the local heat flux and enthalpy rise are used to account for the off nominal dimensions and other manufacturing tolerances not covered by the power factors applied to NEMO-K peak rod powers.

The fuel rod selected to be modeled is the U.S. EPR reference fuel rod described in Reference 16. Axially, the overall cladding length for the coolant heat transfer model is extended beyond the active fuel length to 179.1 inches to account for the lower and upper gas plenums.

7.2.2 Cladding Oxidation

The thermal conductivity of a zirconia corrosion layer on the cladding is lower than the M5™ cladding. The LYNXT code does not currently allow two regions of cladding properties to be used, but the decrease in the effective cladding thermal conductivity can be modeled with the CG/TDP property sets. To determine the impact of the maximum anticipated oxide layer thickness on DNBR and temperatures, a sensitivity study was performed using a cladding conductivity reduced to 60 percent of the nominal temperature dependent values. The study was run on the BOC HFP and EOC HZP rod ejection cases. The results showed that the peak cladding temperatures increased by less than [ ] and the peak fuel temperatures increased by less than [ ]. The timing of the DNBR response was minimally impacted and results indicated higher DNBR values. For the evaluation of the spectrum of rod ejections, the cladding

conductivity properties with no oxide thickness are used in order to provide lower predictions of the MNDBR.

7.2.3 Coolant Conditions

The coolant boundary conditions used in the LYNXT models are the system pressure, inlet coolant temperature, and inlet mass flux. For the system pressure, the pressurizer pressure is used instead of the core exit pressure. This is conservative because the pressurizer pressure is typically 40 psi lower than the core exit pressure. The minimum thermal design volumetric flow rate, which is 4 percent below the nominal, is reduced by 5.5 percent for the core bypass to obtain the inlet mass flux boundary condition for the core. An additional local reduction in the inlet mass flux is applied to the bundle of interest. This provides a low value estimate of the inlet mass flux. The inlet temperature and mass flux are determined by a heat balance performed in conjunction with the coolant average temperature as a function of power level. The average coolant temperature as a function of the core power is given in Figure 7-1. In the LYNXT calculations no further temperature or pressure errors are applied to the determined values. For transients less than 5-10 seconds, these thermal boundary conditions are held constant. For longer duration transients, time varying inputs may be used. Boundary conditions generated with S-RELAP5 are evaluated to estimate the thermal performance for the 25 percent power case at BOC and the HFP cases for both BOC and EOC.

7.2.4 Transient Power

Each fuel rod node is assigned time dependent normalized axial power shapes and radial peaking factors. The fraction of core power is also assigned a time dependent array of values. These are used to approximate the relative global and local heating rates as determined by the NEMO-K neutronics calculations within the number of time-step limitations of the LYNXT code. For DNBR performance, one assembly of the core is considered as the “assembly of interest.” A detailed channel analysis is performed for the peak rod from this assembly. The transient axial shape factors are taken to be that of the fuel assembly of interest and are used for the entire core.

The rod powers for the 17 fuel rod nodes in the assembly of interest are conservatively assumed for this analysis to have [

]

No sensitivities are performed because this is a conservative model.

7.2.5 Heat Resistances in Fuel, Gap and Cladding

A representative approach is used to treat the heat resistances of the fuel and gap. The effect of the cladding resistance is addressed in section 7.2.2. A single uranium enrichment at the extreme burnups is evaluated. Sensitivity studies are run for burnup, uranium enrichment, and gadolinia content to illustrate the analysis conditions.

The EOC HZP power excursion is run with 2.0 and 5.0 w/o U_{235} at two different burnup conditions to determine the uranium enrichment and burnup dependence. The two different burnup conditions are maximum gap (near BOL) and end of life. [

] The practical maximum burnup for a 2.0 and 5.0 w/o U_{235} pellet is estimated to be 50 and 70 GWD/MTU, respectively. The MDNBR performance is shown in Figure 7-9 for these cases. [

] This is due to higher gap conductance values and higher pellet rim power peaking. Calculations are performed with 5.0 w/o U_{235} fuel at 2.5 and 50 GWD/MTU burnup levels for the BOC cases and 20 and 70 GWD/MTU burnup levels for the EOC cases in order to bound the potential burnup thermal property states of the fuel rods.

Fuel loaded with gadolinia has a lower thermal conductivity than pure UO_2. The higher the gadolinia content, the lower the thermal conductivity of the fuel pellet. This increases the fuel temperatures of the gadolinia fuel if operated at the same LHGR as a UO_2 fuel rod. However the gadolinia rods typically have low maximum powers because of lower fuel uranium enrichments and parasitic neutron absorption by the residual gadolinium isotopes. To determine if the analysis can be performed using only UO_2 properties, a sensitivity study was run on the BOC HFP power excursion with gadolinia loadings of 4 w/o and 8 w/o gadolinia. The gadolinia rods were run with the same power history as the pure UO_2 rod and with the maximum power level anticipated for a gadolinia loaded rod. [

] Figure 7-10 shows the peak fuel temperatures for 0, 4, and 8 w/o gadolinia loadings. Note that the fuel temperatures with gadolinia are higher when operating at the same linear heat rate as UO_2 and the transient temperatures for gadolinia fuel adjusted by the power reduction factor are bounded by the UO_2 temperatures. For the thermally limiting transient for HFP at BOC, the temperatures never exceed the lowest fuel melt limit for a rim burnup, even when the peak power is not decreased by the maximum expected value for a gadolinia rod. Because the UO_2 rod bounds the temperatures, the LYNXT calculations use the [

]

7.2.6 Coolant Heat Transfer Coefficient and Transient Coolant Conditions

Minimum flow is used and if the local DNBR is less than a LYNXT code input safety design limit, the heat transfer correlation conservatively switches from Dittus-Boelter to include consideration of the inception of film boiling and post-CHF conditions. The DNBR safety design limit used for this sample problem is **[ ]** (Reference 21).

For the short duration scenarios (i.e., 0-5 seconds), the coolant boundary conditions are assumed constant and only the power distribution history is modeled. For the events that do not have an excore neutron flux rate trip (usually occurs within the first 2 seconds), coolant boundary conditions from S-RELAP5 calculations using the NEMO-K core power history instead of the point kinetics were used to further degrade the LYNXT transient boundary conditions for the calculation of the thermal performance of the fuel rods.

7.3 Failure Boundary Conditions

For a core that has a peak rod exceeding the DNBR criterion or has melted the fuel, a fuel census will be performed. The minimum DNBR Safety Design Limit criterion is **[ ]** from Reference 21.

The UO_2 melting temperature is a function of burnup. The best estimate melt temperature is adjusted downward by a **[ ]** The limiting centerline fuel melt (CFM) temperature is represented by the following equations from Reference 2 (Equation 12-3, pg 12-7):

[

]

where:

T_{LC} = *reduced melt temperature*, *C*

T_{LF} = *reduced melt temperature*, *F*

Bu = *pellet burnup*, GWD/tU

For very fast transients, when the maximum pellet temperature may be close to the rim, the melting temperature limit must also account for local burnup levels being higher than the pellet average. During pellet irradiation, the radial pellet power distribution shifts from **[ ]** the pellet average power on the rim. So at the point of maximum pellet average burnup, the ratio of the rim burnup to the average burnup will be no higher than **[ ]**. This factor is used conservatively to lower the fuel melt limit for these regions. Using 70 GWD/MTU as the maximum average pellet burnup, the maximum rim burnup is no larger than **[ ]**. The peak fuel temperature can not exceed this temperature.

The magnitude of assembly power distribution change due to the ejected rod varies relative to its proximity to the ejected rod location. Several different power shapes versus time are run in LYNXT with different changes in the peaking. The $F_{\Delta H}$ of the assembly is either scaled up or down until the rod DNBR reaches **[ ]** or higher. Peaking conditions between the rods analyzed are linearly interpolated for the failure value. Rods with powers higher than this value in terms of $F_{\Delta H}$ and F_Q are considered failed.

Table 7-1 Design and REA Analysis Conditions

Parameter		Unc[1]	BOC, HZP	BOC, HFP	EOC, HZP	EOC, HFP
Ejected Rod Worth (pcm)	PRISM[2]	+15%	180 to 242	17 to 22	264 to 402	22 to 25
	REA Analysis	-	433	64	634	97
MTC (pcm/ºF)	PRISM[2]	+2	-5.57 to -2.36	-11.89 to -7.68	-26.94 to -22.29	-38.81 to -31.73
	REA Analysis	-	2.16	0.01	-19.40	-28.47
DTC (pcm/ºF)	PRISM[2]	-10%	-1.59 to -1.53	-1.40 to -1.34	-1.82 to -1.81	-1.63 to -1.61
	REA Analysis	-	-1.22	-0.96	-1.52	-1.28
Beta Effective (10^{-5})	PRISM[2]	-5%	640 to 740	640 to 740	510 to 530	510 to 530
	REA Analysis	-	550	550	470	470

Notes:

1. Unc = Uncertainty to be applied to nominal conditions.
2. PRISM conditions are without uncertainties, rod position at rod insertion limits, and nominal Xenon.

Table 7-2 Peaking Uncertainties

3-D Uncertainty	**%**
Measurement	[ ]
HCF	[ ]
Rod Bow	[ ]
Assembly Bow	[ ]
Core Power	[ ]
Total SRSS	[ ]
2-D Uncertainty	**%**
Measurement	[ ]
Assembly Bow	[ ]
Core Power	[ ]
Total SRSS	[ ]

Table 7-3 Plant Transient Sensitivity Study Summary

Parameter	Δ Case Conditions	Range of Evaluation	% difference (Δ /base-1) *100% [a]	Comments
Ejected rod worth, DTC, β_{eff}, and MTC	-15% ejected rod worth 10% increase in Doppler magnitude 5% increase in β_{eff} -2 pcm/°F MTC	BOC 25 BOC HFP EOC HZP EOC HFP	[ ]	
Rate of Reactivity Insertion	0.1 to 0.2 sec for full length ejection	BOC 25 BOC HFP EOC HZP EOC HFP		
Reactor Trip Reactivity	9% increase in trip worth Base analysis is 9% less than nominal	BOC 60 EOC HZP		
Power Peaking	13%	Not tested in plant model		
Heat Resistances and Transient cladding to Coolant Heat Transfer				
Fuel conductivity,	-20% change in Fuel conductivity	EOC HZP		
Gap Conductance	Gap conductance increased by 100%	BOC 25 BOC HFP EOC HZP EOC HFP		
Coolant Heat Transfer	-4% flow assumed by fuel rod model	BOC 25 EOC HZP EOC HFP		

Parameter	Δ Case Conditions	Range of Evaluation	% difference (Δ /base-1) *100% [a]	Comments
Others				
Fractional Heat Deposited in Fuel	0.974 to 0.966	BOC 25 BOC HFP EOC HZP EOC HFP	[	]
Pellet Radial Power Profile	5 w/o fuel to 2 w/o fuel	BOC 25 BOC HFP EOC HZP EOC HFP		
Neutron Velocities	+10%	BOC HFP EOC HZP EOC HFP		
Time step	Flux Δt 2x Fuel Δt =4x Moderator Δt =4x	BOC 25 BOC HFP EOC HZP EOC HFP		
Number of Fuel Rod Nodes	15 to 20 fuel nodes 3 to 5 cladding nodes	BOC HFP EOC HZP EOC HFP		
Effective Temperature	Weighting by the pellet average temperature	BOC 25 BOC HFP EOC HZP EOC HFP		

Notes:

[a] Negative values indicate that the base case yields more conservative results.

Figure 7-1 Average Coolant Temperature with Power

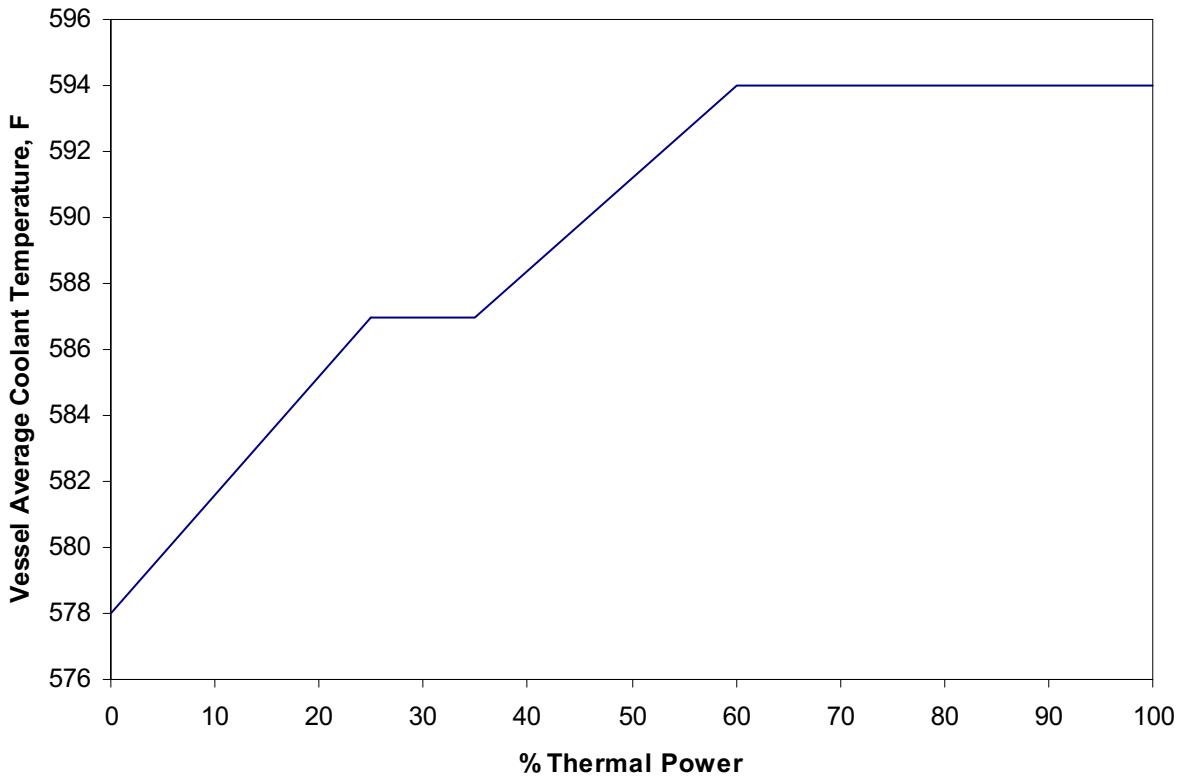

Figure 7-2 Rod Position Technical Specification Limits/Analysis

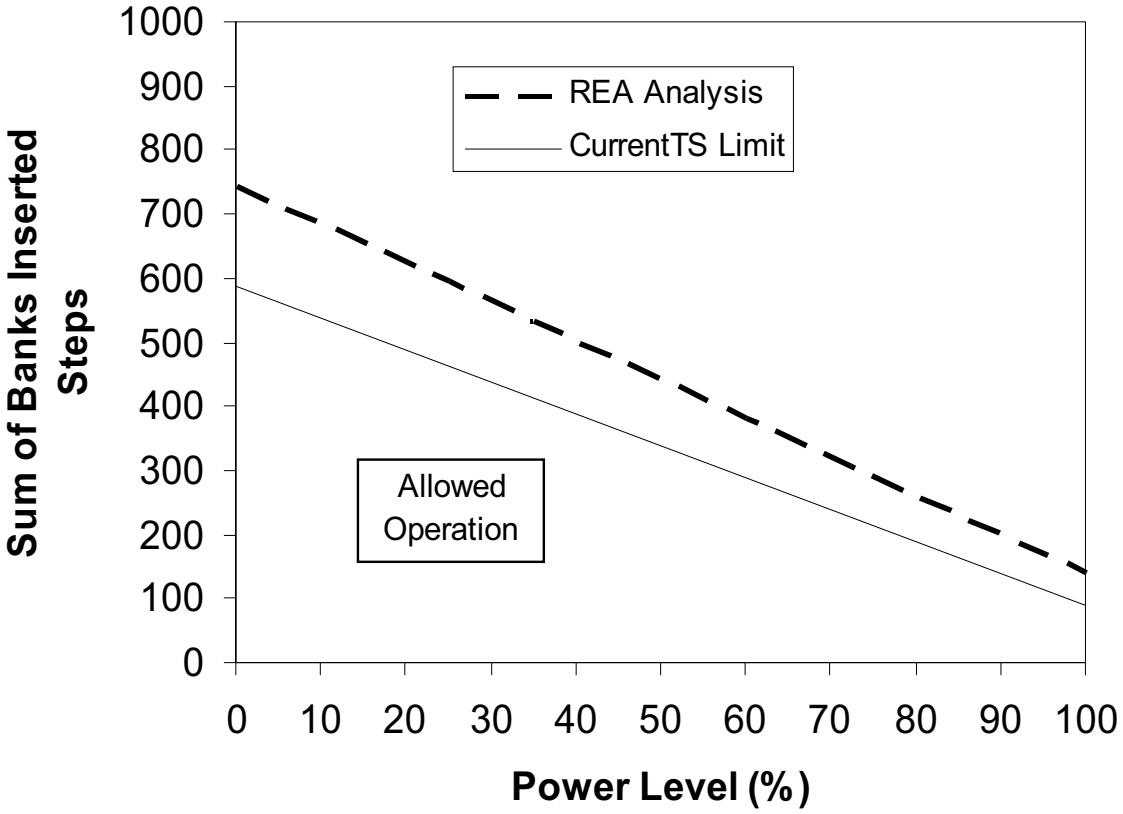

Figure 7-3 BOC 25%, FOP Comparison between Equilibrium Cycle and [ ]

Figure 7-4 BOC HFP, FOP Comparison between Equilibrium Cycle and [ ]

Figure 7-5 EOC HZP Equilibrium Cycle and [ ] Comparison

Figure 7-6 EOC HFP Equilibrium Cycle and [ ] Comparison

Figure 7-7 EOC HZP Equilibrium Cycle and [ ]

Figure 7-8 17-Channel LYNXT Model Diagram

NOTE: channel numbers are shown in normal font and rod numbers are shown in **bold**

Figure 7-9 MDNBR Uranium Enrichment Response for EOC HZP

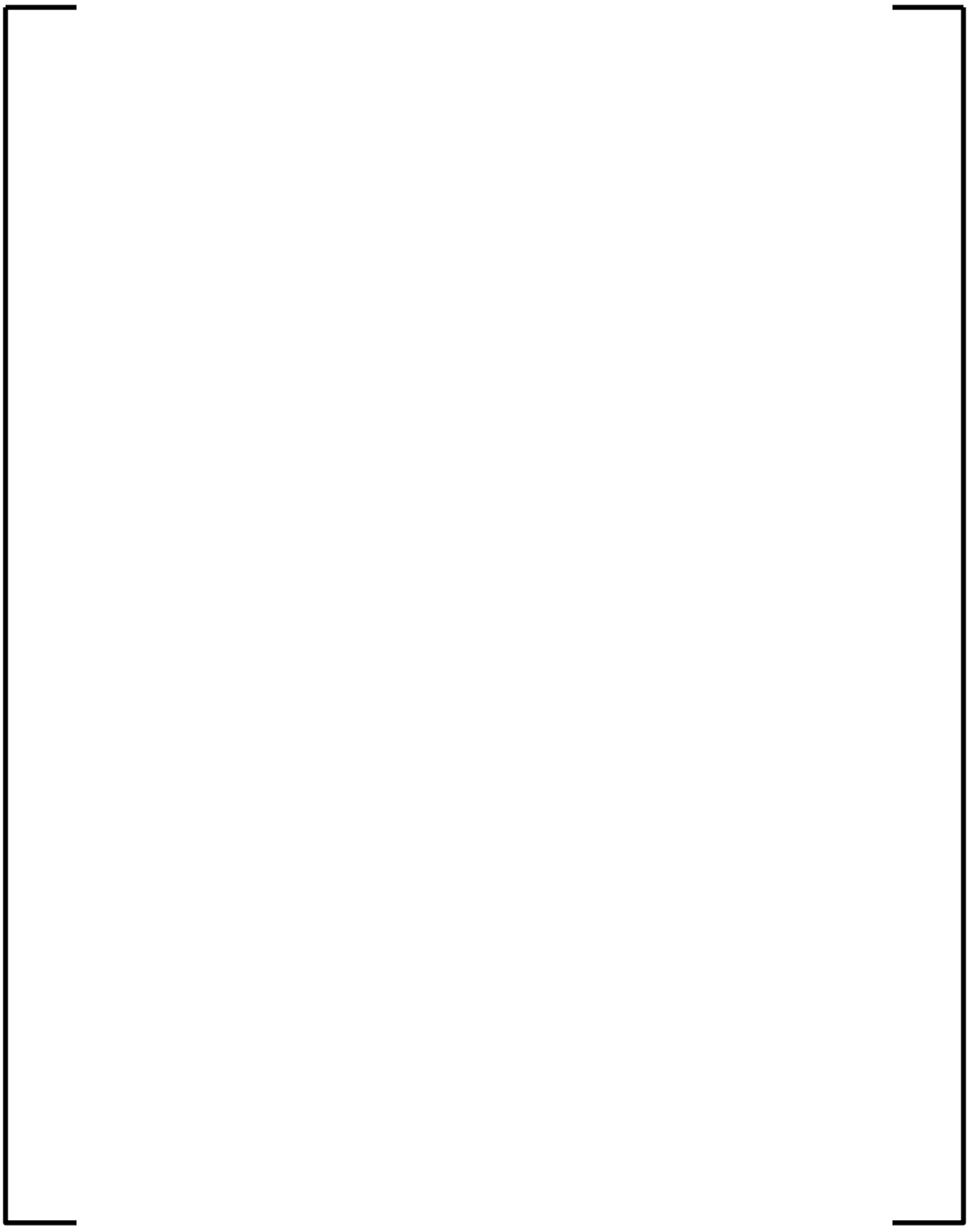

Figure 7-10 UO_2 and Gadolinia Fuel Temperatures for BOC HFP

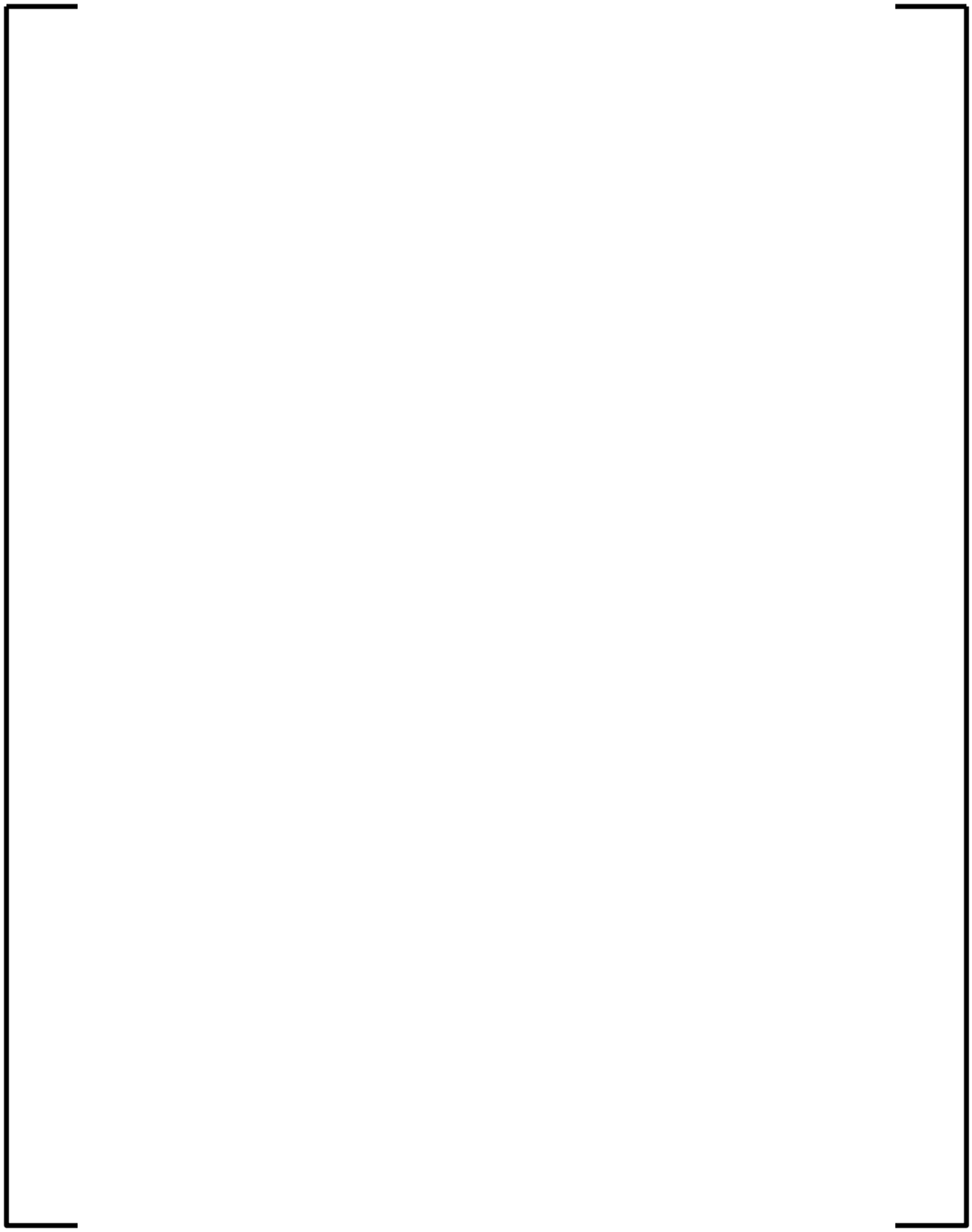

8.0 U.S. EPR SAMPLE PROBLEM RESULTS

The U.S. EPR sample problem results section contains the detailed results of this REA methodology. The trip functions that are used by this sample problem are shown in Table 8-1.

8.1 NEMO-K Results

The transient simulations for 0, 25, 35, 60, and 100 percent full power are performed at BOC and EOC. The results for core power, $F_{\Delta H}$ and F_Q are shown in Figure 8-1 through Figure 8-10. Because the ejected rod starts out at a lower power than the surrounding assemblies a separate analysis can be performed for the ejected rod location. As an example, Figure 8-11 shows the nominal peaking from NEMO-K for the ejected rod and peak locations for the BOC HFP condition. The HZP BOC ejected rod worth is not prompt critical and does not trip on the high flux rate trip. To bound the results below 25 percent power at BOC where the reactor may not trip on the flux rate trip, the transient model is run with and without the trip function. Core pressure, flow, and inlet temperature are held constant during these simulations. BOC and EOC HFP transients do not reach a trip signal. Those conditions without trip require a S-RELAP5 analysis, which is described in the following section.

8.2 S-RELAP5 Evaluation

The S-RELAP5 evaluation section reviews the consequences of using a constant pressure, inlet temperature and flow in the NEMO-K and estimates its impact on the fuel rod model. For the plant model in NEMO-K, two conditions are reviewed:

- an increase in pressure due to the power insertion.
- operation without trip.

A calculation is performed to determine how an increase in pressure affects the core reactivity. The power pulse after the ejection could cause an increase in the pressure if

there is no hole in the primary system from the ejected rod. A pressure increase of 40 psia is estimated for the EOC HFP REA. A power search is performed at EOC HFP at +40 psia. The temperature increase occurred after the peak power and would only affect the static power thereafter. The power difference is **[**

].

For the condition of no trip with a leak in the primary, two S-RELAP5 calculations, a full power and 25 percent power transient, are performed to estimate the range of thermal conditions that could be reached. The break area is calculated using the 75 mm (0.246 ft) inside diameter of the control rod flange as the break diameter and applied to the top of the upper head volume. The simulations continue until a trip in the S-RELAP5 model is reached. This simulation did not include any actions for the non-safety control systems that would tend to improve the situation. The S-RELAP5 results for 25 percent power and HFP are shown in Figure 8-12 and Figure 8-13, respectively. The REA simulations for the 25 percent and HFP initial conditions without a high flux rate trip eventually tripped on high secondary steam pressure and low primary pressure, respectively. For these cases, the duration is slow enough that the core is in near equilibrium with the thermal conditions. Rather than running this specific transient in NEMO-K, several static power searches are performed with the rod ejected at various thermal conditions from S-RELAP5 to determine the limiting power that may be reached after the initial ejection. These results are shown in Table 8-2. The maximum power and the time dependent range of thermal conditions from these cases are evaluated using the fuel rod model with LYNXT.

8.3 LYNXT Results

The transient simulations are performed for 0, 25, 35, 60, and 100 percent full power at BOC and EOC. The BOC HZP ejected rod worth is not simulated in LYNXT because the results are bounded by the 25 percent power response and are not presented. The results for the MDNBR, peak fuel temperature, peak cladding temperature, and peak radially averaged enthalpy rise are shown in Figure 8-14 through Figure 8-40.

The BOC 25 percent power, BOC HFP, and the EOC HFP transient simulations did not trip. The LYNXT models the S-RELAP5 thermal boundary conditions with time. The NEMO-K power results for the first 5 to 8 seconds are followed by a linear progression to the highest power predicted by the static NEMO-K cases. For the 25% power BOC case with no trip, the minimum DNBR for the peak power assembly does not exceed the design limit until after 16 seconds into the transient. After this point the post-CHF heat transfer mode is simulated causing the rapid rise in the peak cladding temperature.

For the BOC and EOC 100 percent power cases, the power level stabilizes at a power level to balance the reactivity. A conservative estimate of 108 percent for BOC and 104 percent for EOC with no void reactivity feedback in NEMO-K is used. The minimum DNBR for the peak power assembly rapidly drops below the DNBR design limit and continues to degrade as the plant heats up and system pressure drops. The thermal boundary conditions continue to degrade and increase the peak fuel and cladding temperatures. The rate of increase reduces as the system approaches thermal equilibrium. The S-RELAP5 simulation did not include the low DNBR reactor trip function, which would terminate the transient before the plant system trip on low pressure. There is a design requirement for the low DNBR reactor trip function to trip at any static power, temperature, and pressure combination of conditions that would compromise the minimum DNBR design criteria for a non skewed design peak type condition. This requirement provides added protection in the event that the core achieves different powers, temperatures, and pressures than analyzed by the S-RELAP5 by enabling the same relative DNBR protection. Based on this requirement applied to the S-RELAP5 core conditions, a trip is estimated to occur before 30 seconds for the HFP REA transients.

Even though the DNBR design limit is exceeded for five of the evaluated cases, in no case did the peak fuel temperatures exceed the fuel melt limit for the expected higher burnup fuel **[**

]. The maximum temperatures calculated were 4014°F for the fuel and 1461°F for the cladding with the limiting temperature case of BOC HFP at 30 seconds into the

transient (time of estimated RCSL trip). The maximum prompt radially averaged fuel enthalpy rise determined for the entire spectrum of cases was less than 20 cal/g (EOC HZP) and a maximum integrated total enthalpy was less than 110 cal/g (BOC HFP).

8.4 Rod Census

The number of rods failed was estimated for BOC 25 percent, BOC 60 percent, BOC HFP, EOC 60 percent and EOC HFP. For each transient, the rods may need to be counted for two different thermal conditions, the prompt response (i.e., 0-5 seconds) and the delayed response (i.e., greater than 5 seconds) when trip does not occur from the power pulse. The latter case reduces to a static case where the neutron power is in equilibrium with the thermal output of the core. None of the assemblies experienced an enthalpy rise of more than 20 cal/g so that the fuel failure analysis does not need to consider the elevated dose requirements outlined in Section 2.3.

LYNXT cases are run for each condition to determine the power at which the limiting fuel rod has a MDNBR of **[ ]**. The $F_{\Delta H}$ and F_Q for this condition are used as the failure criteria. Any rod with an $F_{\Delta H}$ or F_Q exceeding this value is assumed failed. For the prompt response at power, each location has a different amount of thermal margin to the limit based on its initial power. This dependence is captured **[**

] in LYNXT to determine when a rod may fail.

A correlation is then made between the **[**

]. In Figure 8-41 **[**

].

The failed rod counting can be based on the static peaking rather than detailed time dependent evaluations. For each transient condition the limiting transient $F_{\Delta H}$ and F_Q values are correlated to **[** **]**. All rods

exceeding the static $F_{\Delta H}$ or F_Q for these cases are counted as failed for the prompt response.

The cases with no trip (delayed response) can be treated simply as a static case and therefore, only one assembly of interest distribution is needed to define the limiting $F_{\Delta H}$ and F_Q prior to reaching the MDNBR. Table 8-3 contains the estimated rod failures for each of the transients.

8.5 Summary Results

The overall REA results for the plant transient analysis and fuel rod model are shown in Table 8-4 and Table 8-5 for BOC and EOC, respectively. The maximum prompt ∆cal/g is calculated at one pulse width after the peak. For those cases that have no discernable pulse, the value at 1.0 second is used. For all the transients modeled, the maximum ∆cal/g is less than the threshold value (31.2 ∆cal/g) to consider increased fission gas release and there is no fuel melt. Therefore, no equivalent pin failure adjustments are needed to the DNBR failures calculated. The results are within the criteria listed in Table 2-1. Also, the limiting conditions for all the criteria are at either HZP or HFP.

Table 8-1 Trip Signal Parameters in Analysis

Parameter	Value
Type of Trip Signal	Flux Rate
Trip Signal, %	13(1)
Sampling Rate, seconds	0.025
Scram Lag, seconds	$\leq$ 0.7(2)
Number of Detectors Required to Trip	3(3)
Lag Rate Constant, seconds	30
Gain Constant, seconds	30
High Steam Generator Pressure (Setpoint/Analysis), psia	1384.7/1414.7
Low Saturation Margin (Setpoint/Analysis), BTU/lbm	430/0
Low Pressurizer Pressure (Setpoint/Analysis), psia	2005/1980
High Pressurizer Level (Setpoint/Analysis), % range	75.0/80.5
High Pressurizer Pressure (Setpoint/Analysis), psia	2414.9/2439.9

Notes:

(1) 11% plus 2% uncertainty.

(2) Conservatively used 0.725 in analysis.

(3) Need 3 to account for 2 out of 4 logic with 1 detector assumed failed.

Table 8-2 Static Power Search

Core Condition	ΔPressure (psi)	ΔTinlet (°F)	Flow, (%)	Resultant FOP
BOC HFP	0 to -250	0 to +10	0 to -2.5%	1.0034 to1.0817
EOC HFP	0 to -250	0 to +10	0 to -2.5%	0.8405 to 1.0399
BOC 25%	0 to -100	0 to +10	0 to -2.0%	0.5246 to 0.5507

Table 8-3 Estimated Rod Failures

Core Condition	% Failed Rods in Census	
	Prompt	Static
BOC 25% (no trip)	-	1.8
BOC 60%	none*	-
BOC HFP	0.3	7.2
EOC 60%	none*	-
EOC HFP	none*	1.9

Note:

* Although MDNBR [ ] for the conservative peak analysis to bound future cycles, the actual distribution did not result in any failures.

Table 8-4 Ejected Rod Analysis Results for BOC

Parameter	Criterion	0	25	35	60	100
Maximum Ejected Rod Worth, pcm	-	433	362	346	286	64
β_{eff}	-	0.0055	0.0055	0.0055	0.0055	0.0055
MTC, pcm/°F	-	2.16	1.32	1.35	0.34	0.01
DTC, pcm/°F	-	-1.22	-1.14	-1.11	-1.05	-0.96
Initial F_Q	-	NA[a]	3.01	2.88	2.63	2.36
Maximum Transient F_Q	-	9.46	5.75	5.23	5.06	2.70
Initial $F_{\Delta H}$	-	NA[a]	2.15	2.09	1.94	1.70
Maximum Transient $F_{\Delta H}$	-	5.21	3.75	3.58	3.01	2.11
Maximum Neutron Power, FOP	-	0.32	0.55	0.69	0.98	1.10
Maximum cal/g	$\leq$ 150	-	70.4	50.4	63.9	109.4
Maximum Δcal/g, prompt	$\leq$ 110	-	10.0	10.9	11.8	7.2
Maximum Fuel Temperature, °F	[ ]	-	2655	1901	2529	4014
Maximum Cladding Temperature, °F	[ ]	-	1098	727	951	1461
MDNBR/SAFDL Ratio For Failure	$\leq$ 1.0	-	0.71	1.86	0.96	0.33
Time of Trip (initiation of safety bank insertion), seconds	-	No Trip	No Trip[b]	0.850	0.825	No Trip
Equivalent nominal rods failed, %	$\leq$ 30	0	1.8	0	0	7.2

Notes:

[a] Not applicable since initial stored energy above the coolant temperature is zero.

[b] Trip is disabled to bound consequences of powers lower than 25%.

Table 8-5 Ejected Rod Analysis Results for EOC

Parameter	Criterion	0	25	35	60	100
Maximum Ejected Rod Worth, pcm	-	634	516	484	389	97
β_{eff}	-	0.0047	0.0047	0.0047	0.0047	0.0047
MTC, pcm/°F	-	-19.40	-23.44	-23.31	-26.68	-28.47
DTC, pcm/°F	-	-1.52	-1.41	-1.40	-1.35	-1.28
Initial F_Q	-	NA[a]	5.28	4.24	3.28	2.10
Maximum Transient F_Q	-	20.10	13.32	10.91	7.38	3.30
Initial $F_{\Delta H}$	-	NA[a]	2.15	2.09	1.94	1.70
Maximum Transient $F_{\Delta H}$	-	6.51	4.87	4.53	3.61	2.22
Maximum Neutron Power, FOP	-	2.04	1.75	1.75	1.58	1.17
Maximum cal/g	≤ 150	33.9	62.2	64.6	73.1	103.4
Maximum Δcal/g, prompt	≤ 110	13.8	10.2	9.0	6.0	7.9
Maximum Fuel Temperature, °F	[ ]	1140	2402	2534	2987	3856
Maximum Cladding Temperature, °F	[ ]	741	777	774	1062	1337
MDNBR/SAFDL Ratio For Failure	≤ 1.0	1.82	1.36	1.33	0.97	0.46
Time of Trip (initiation of safety bank insertion)	-	1.000	0.850	0.850	0.825	No Trip
Equivalent nominal rods failed, %	≤ 30	0	0	0	0	1.9

Notes:

[a] Not applicable since initial stored energy above the coolant temperature is zero.

Figure 8-1 BOC 0% Power Transient

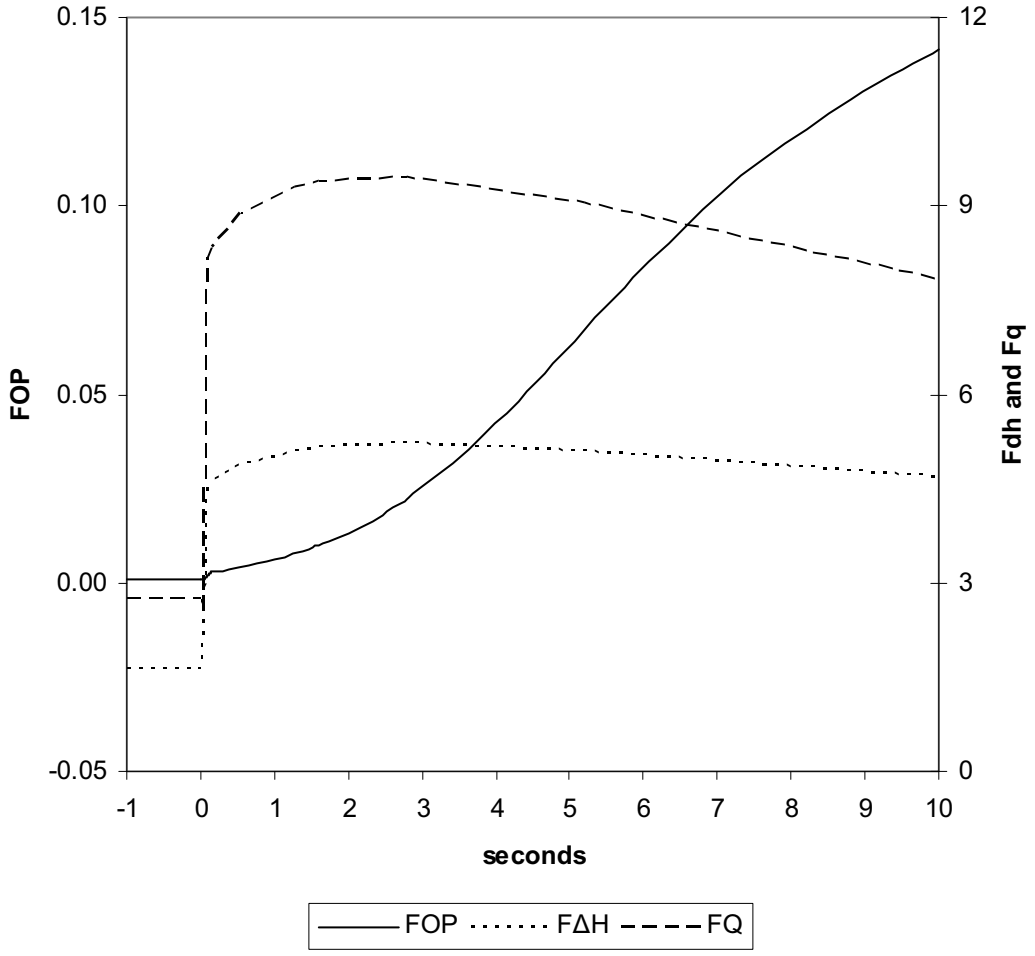

Figure 8-2 BOC 25% Power Transient

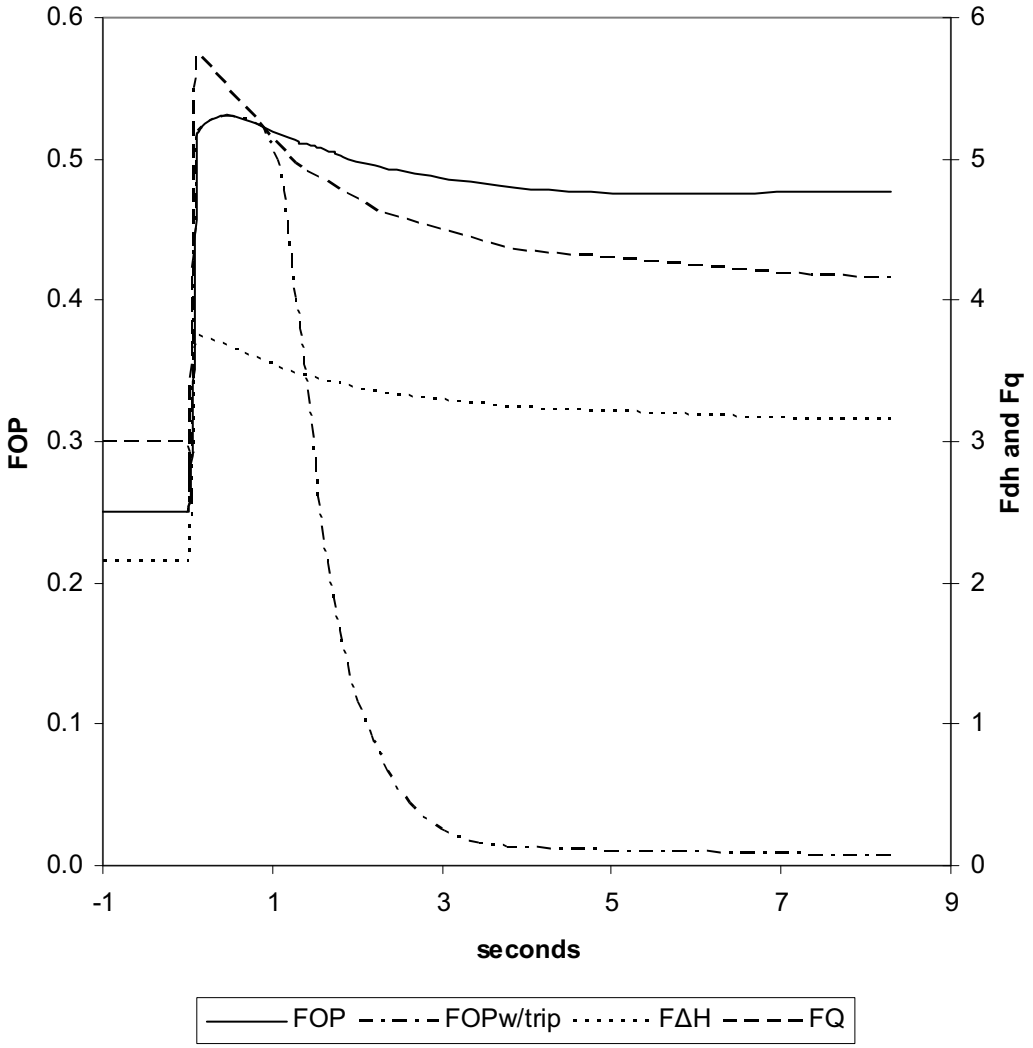

Figure 8-3 BOC 35% Power Transient

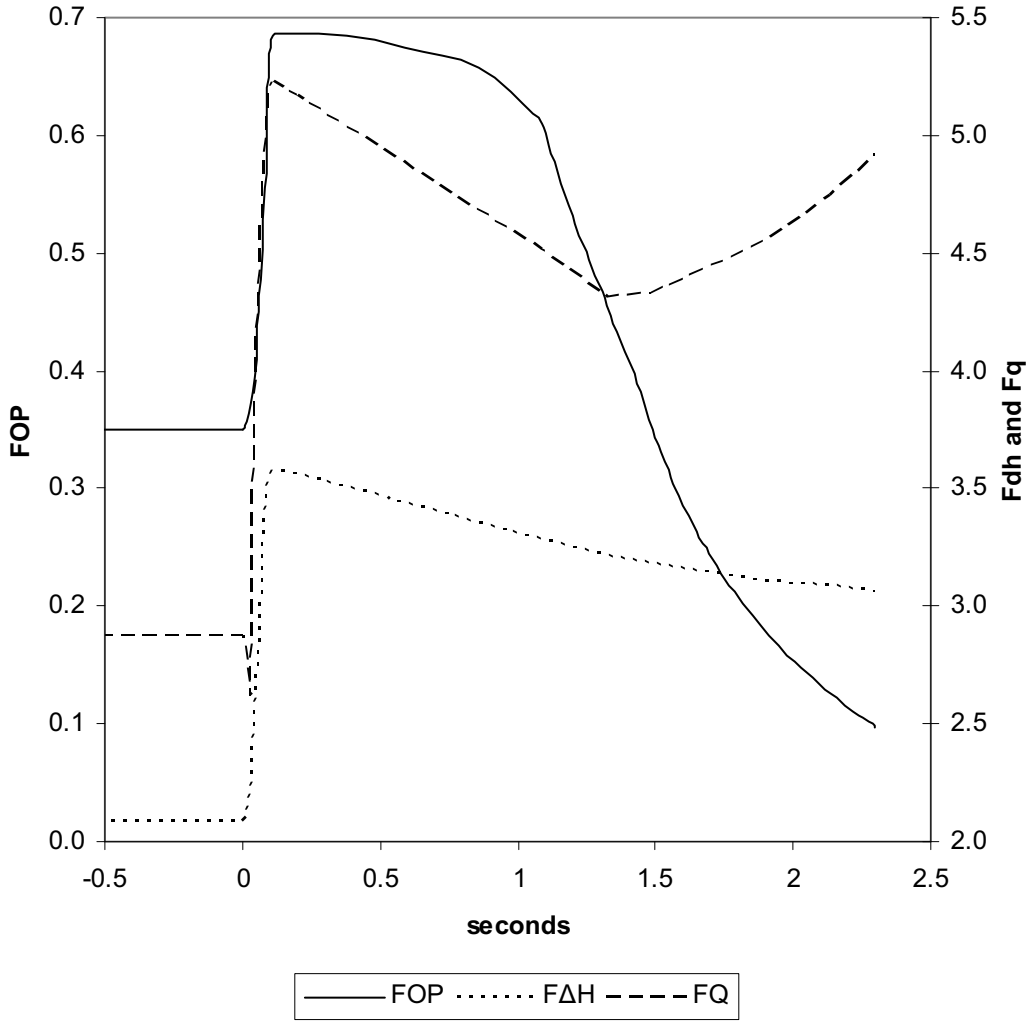

Figure 8-4 BOC 60% Power Transient

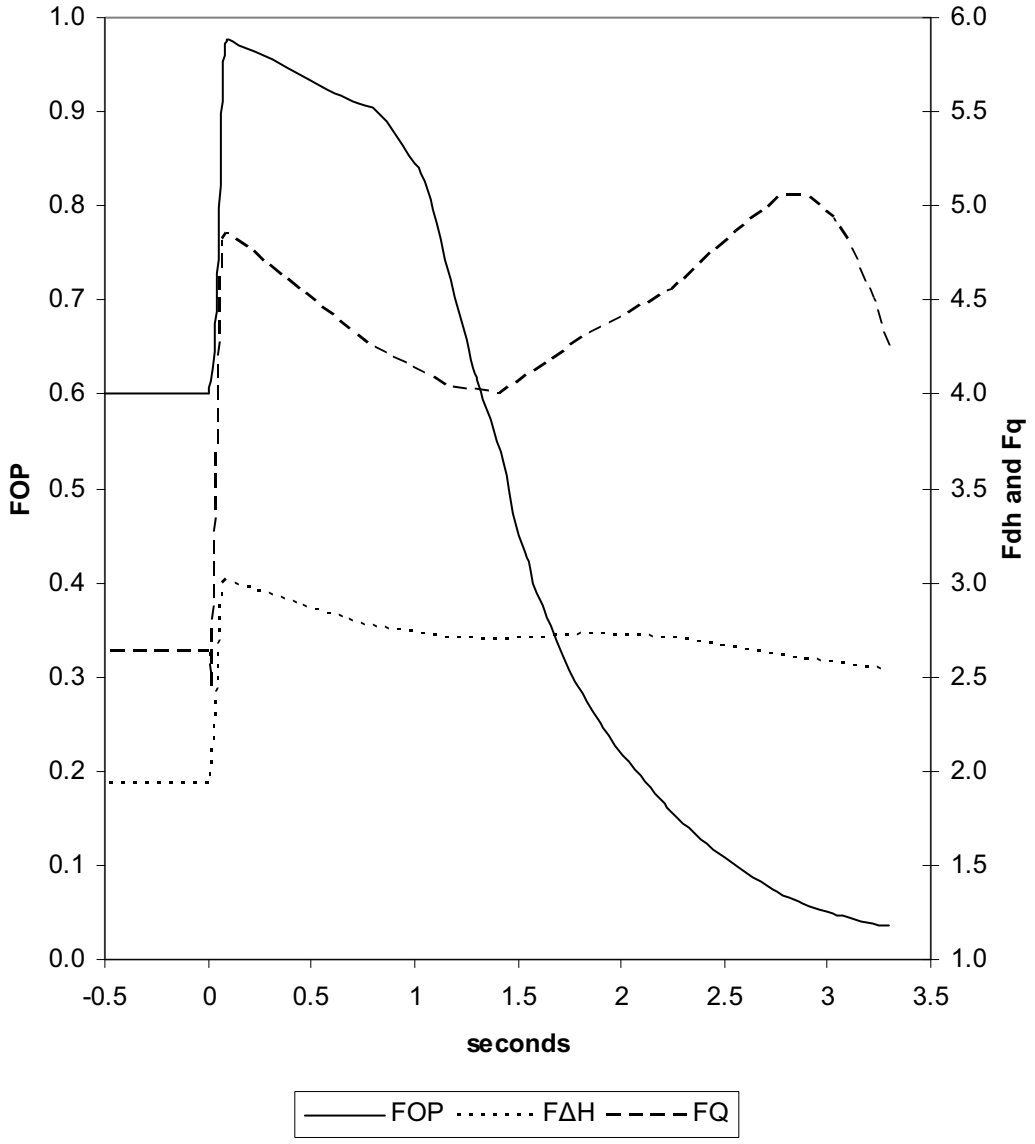

Figure 8-5 BOC 100% Power Transient

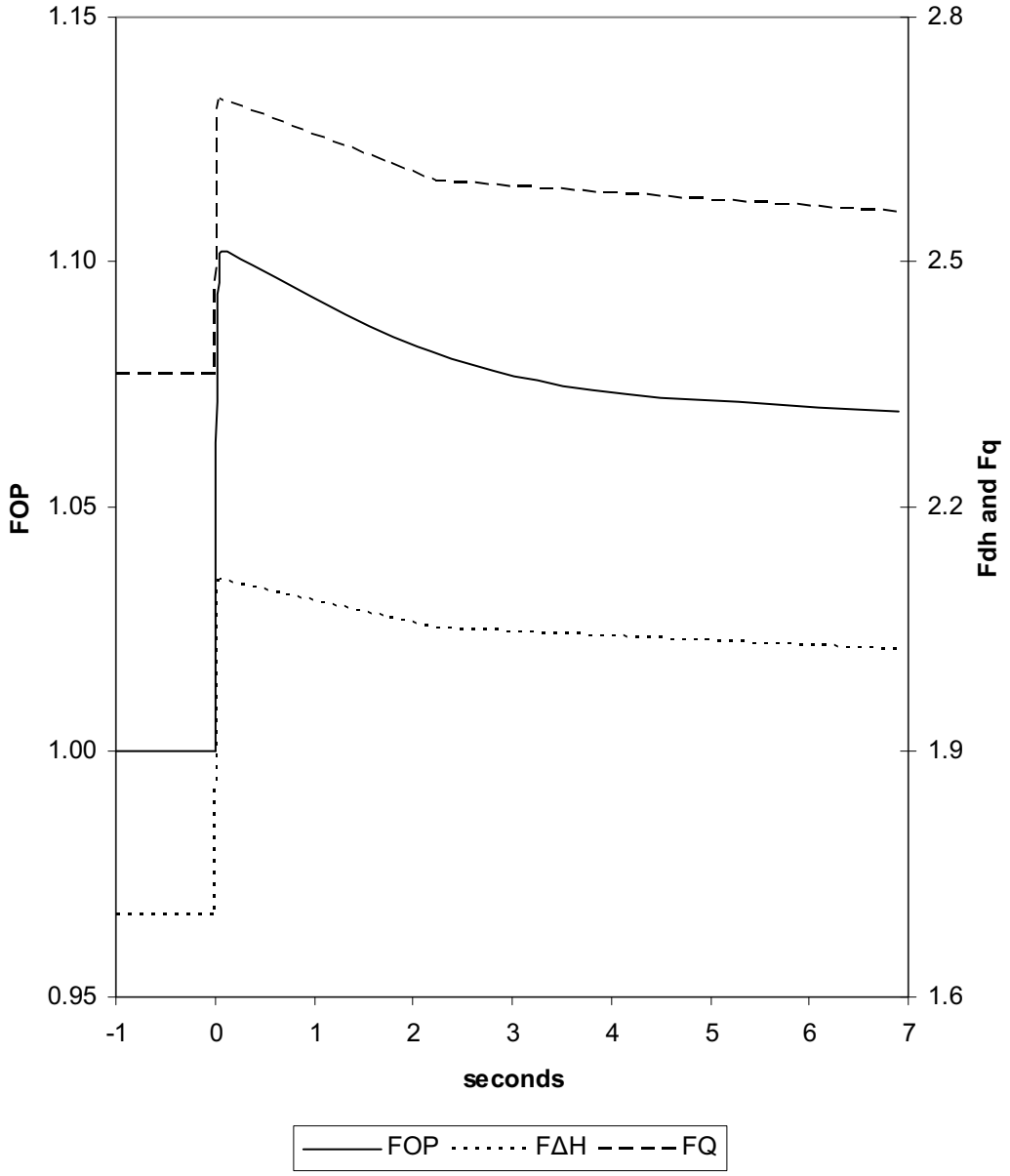

Figure 8-6 EOC 0% Power Transient

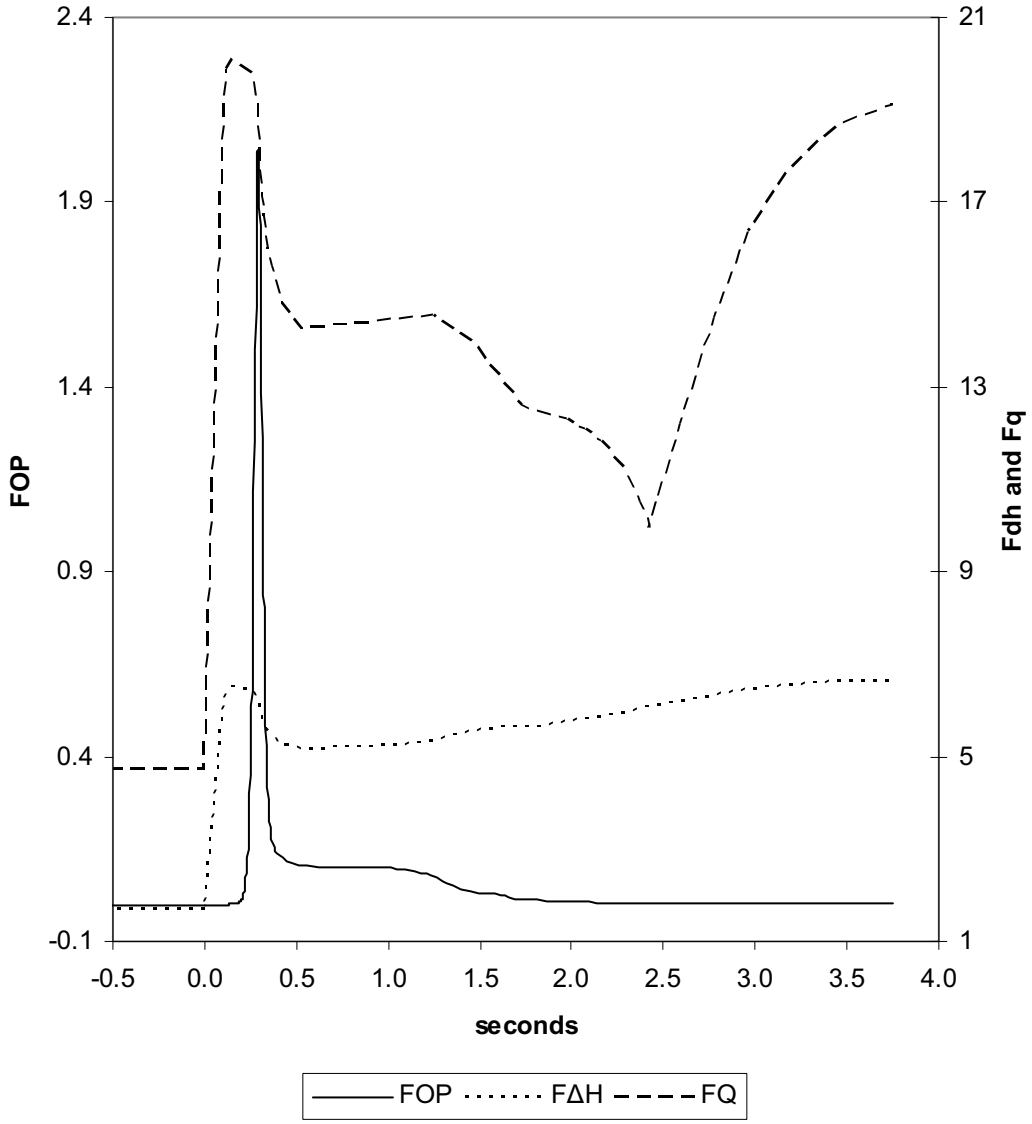

Figure 8-7 EOC 25% Power Transient

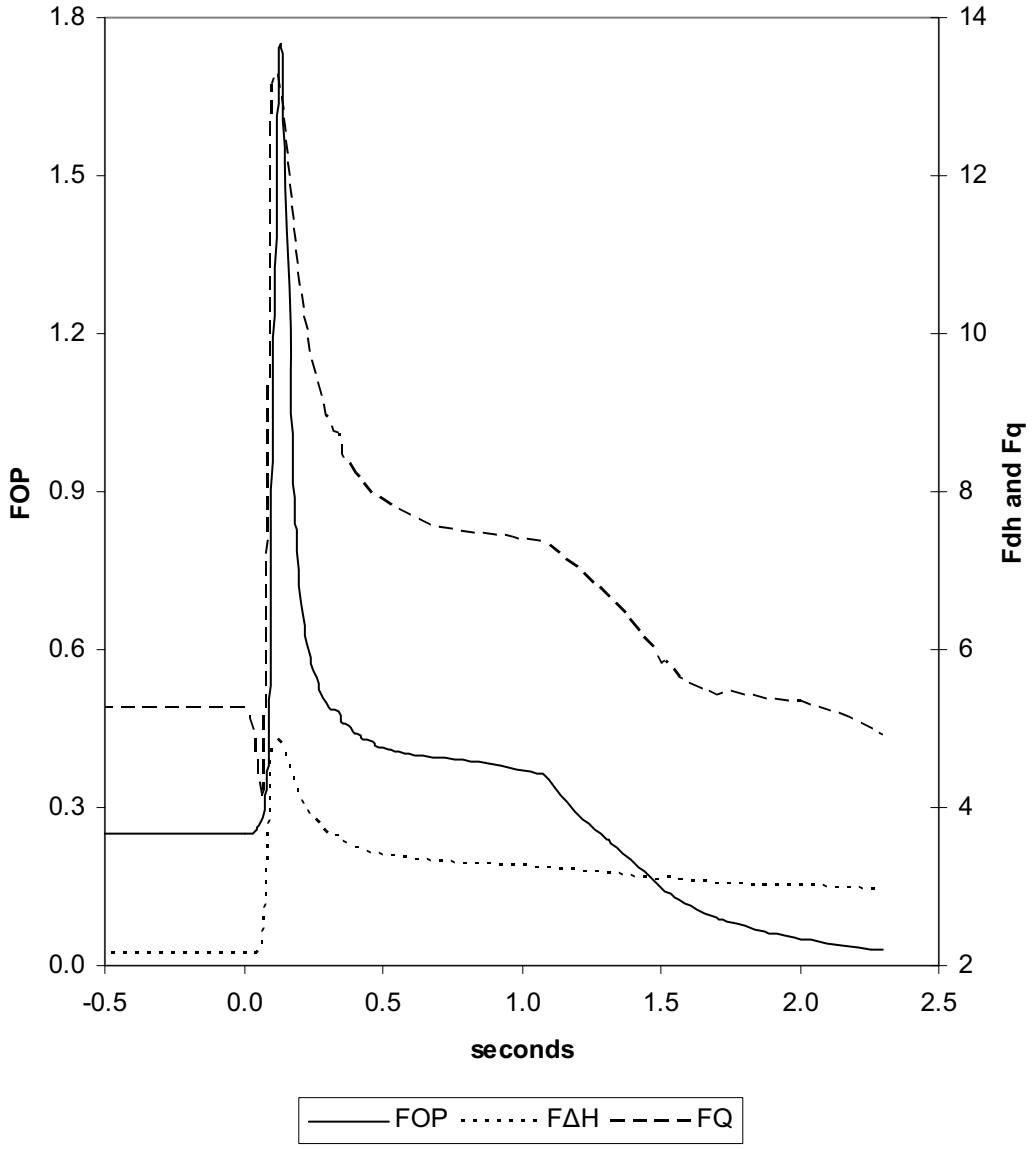

Figure 8-8 EOC 35% Power Transient

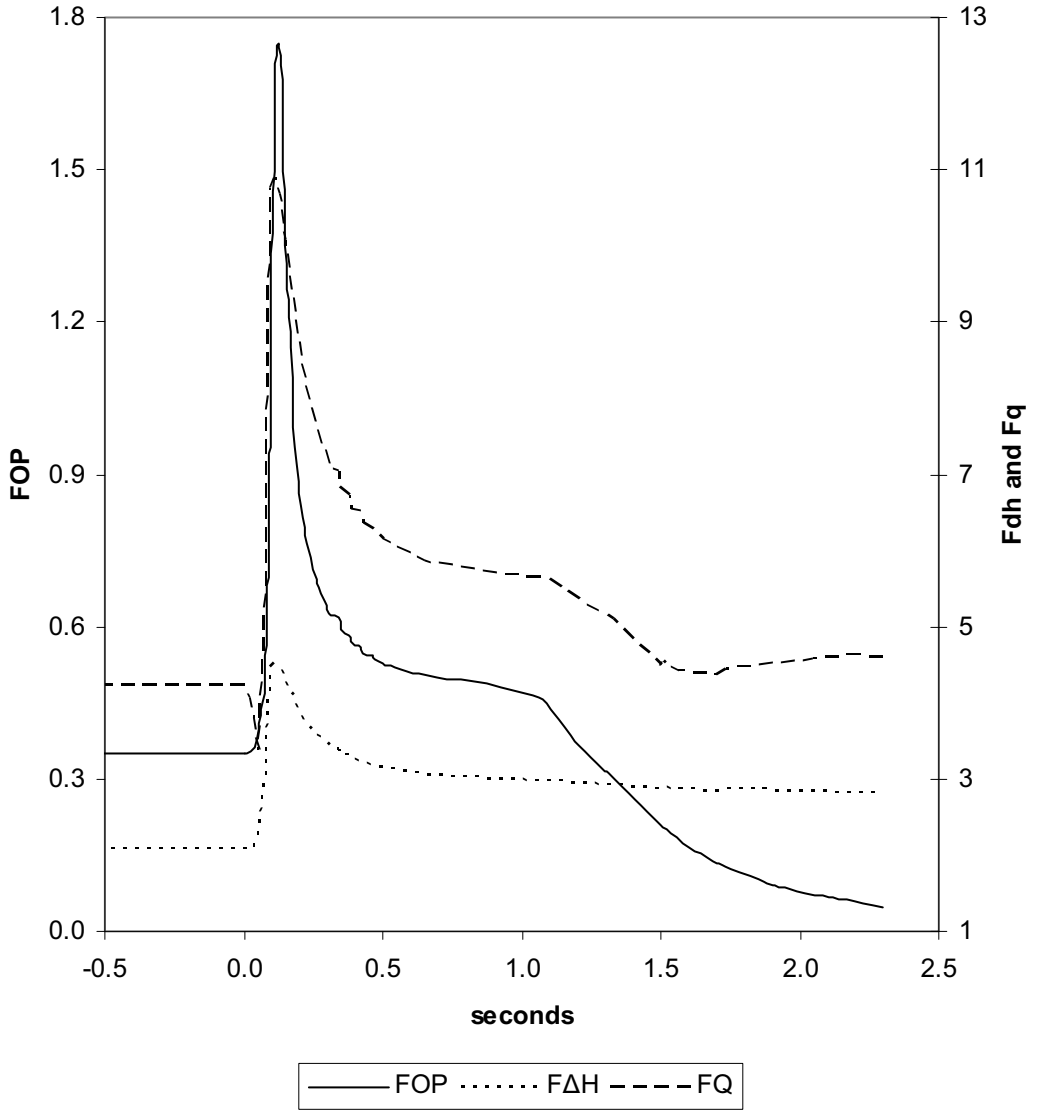

Figure 8-9 EOC 60% Power Transient

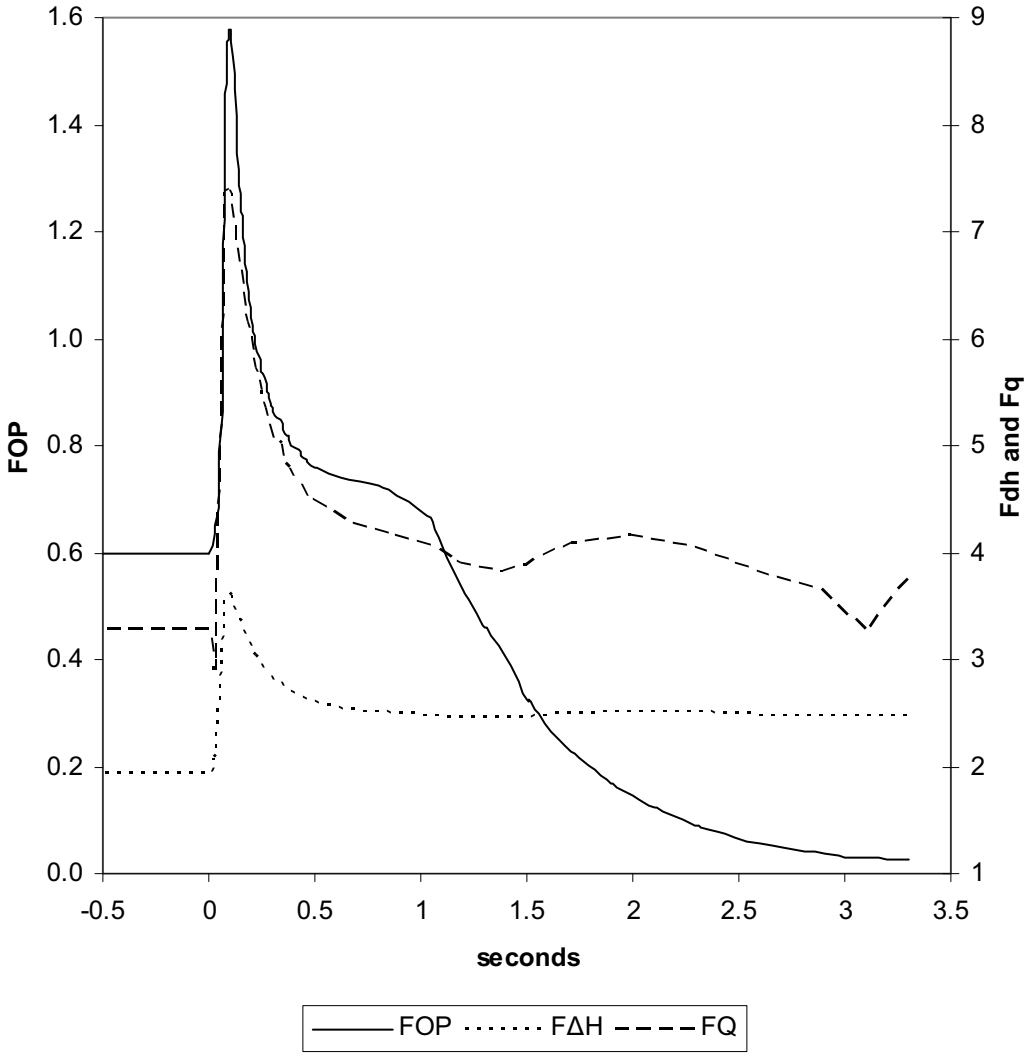

Figure 8-10 EOC 100% Power Transient

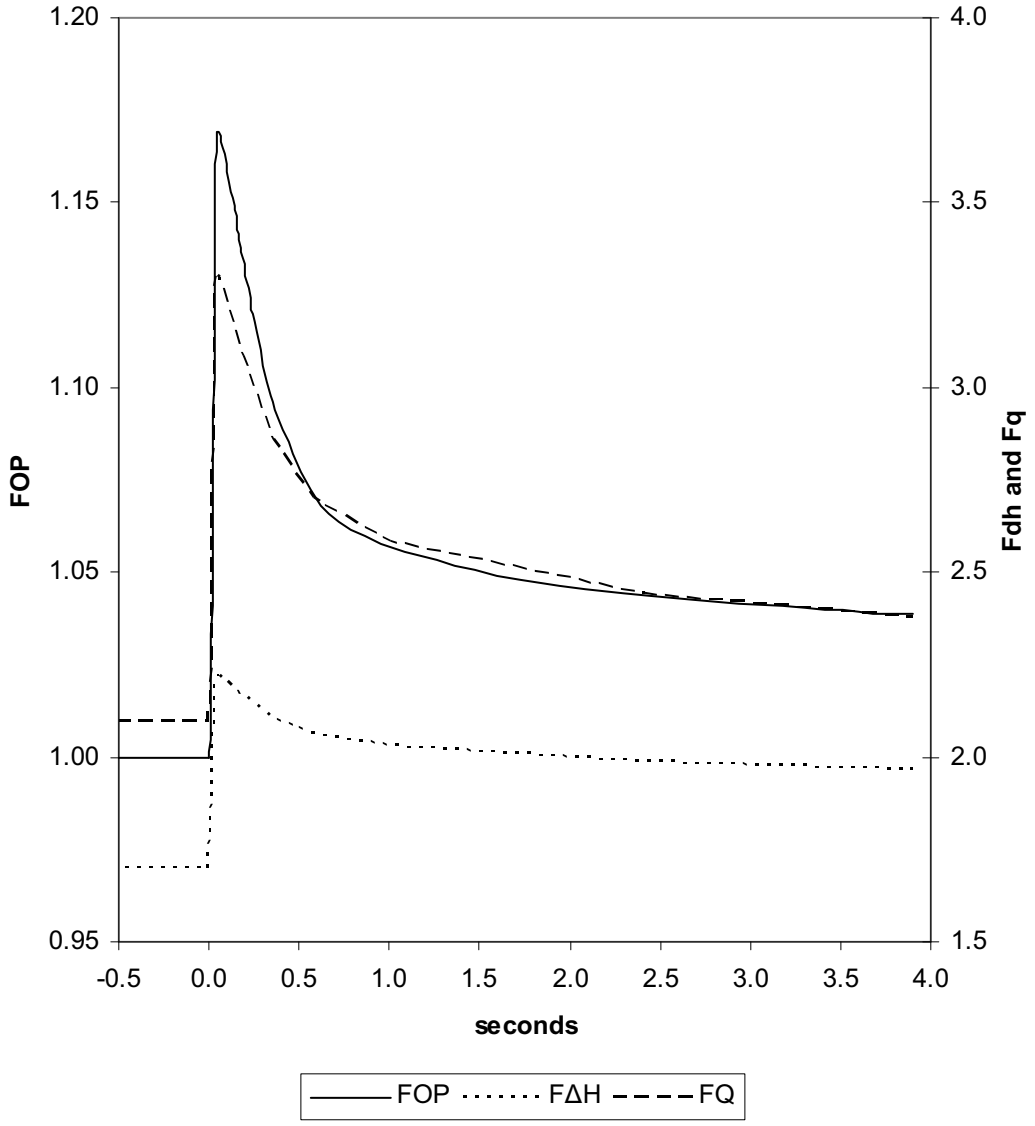

Figure 8-11 BOC 100% Power Transient for N05 Ejected

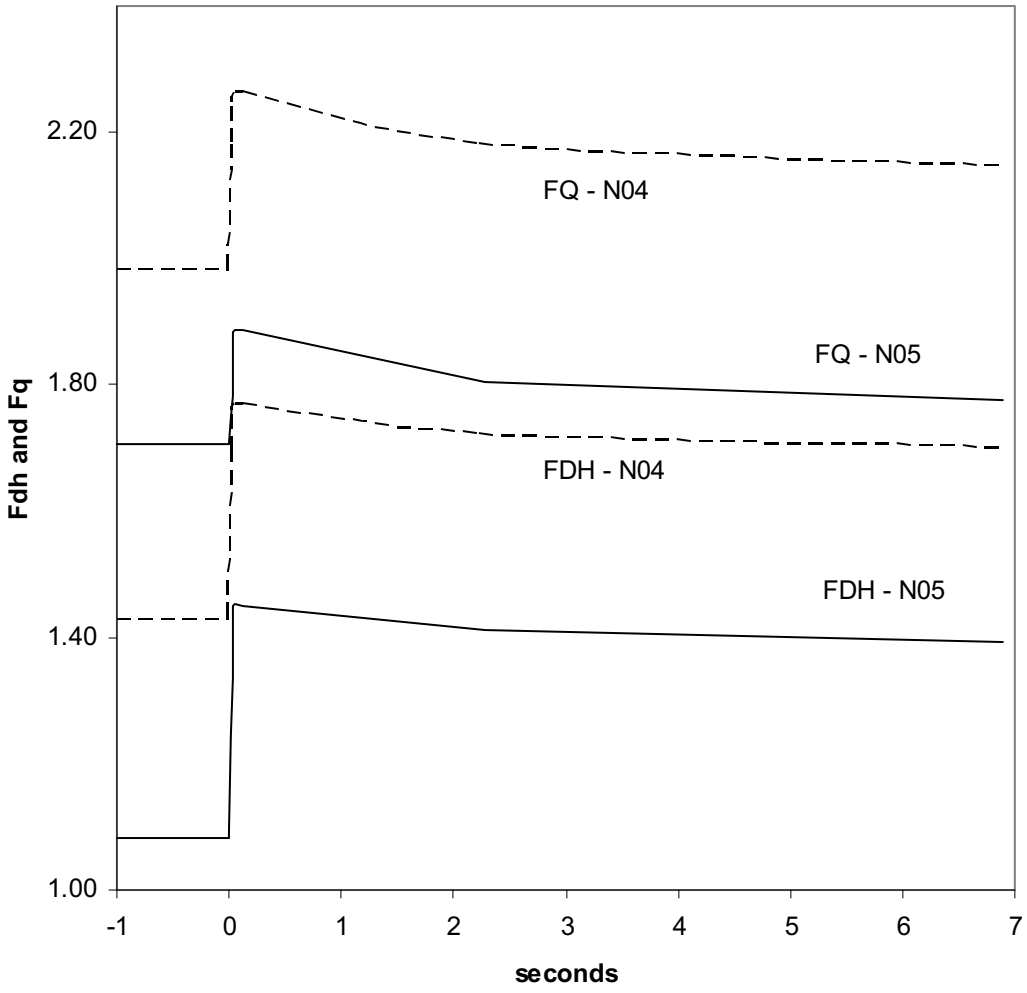

Figure 8-12 S-RELAP5 Results for BOC 25%

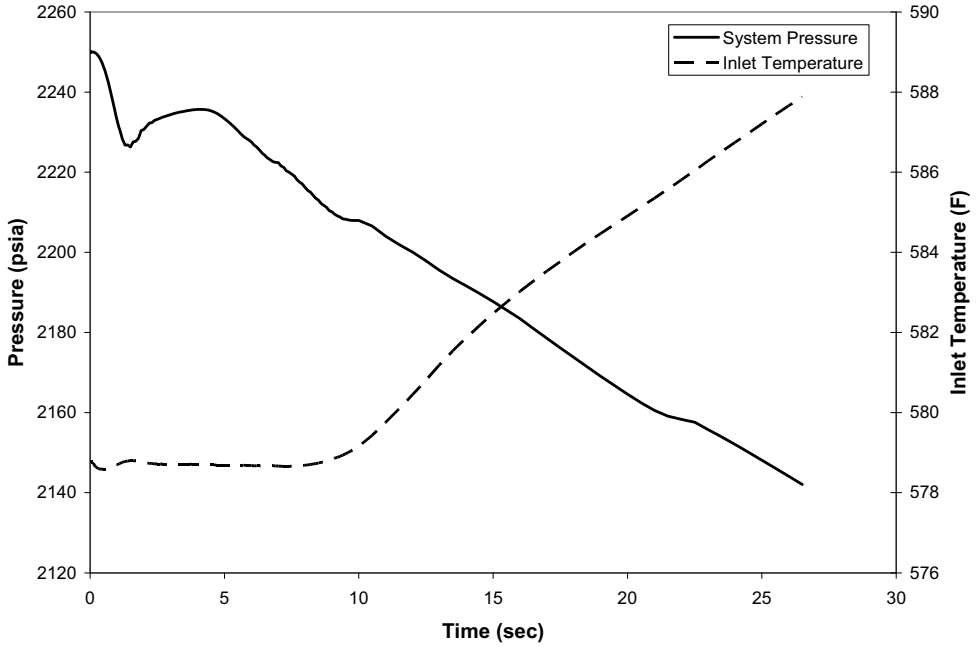

Figure 8-13 S-RELAP5 Results for HFP

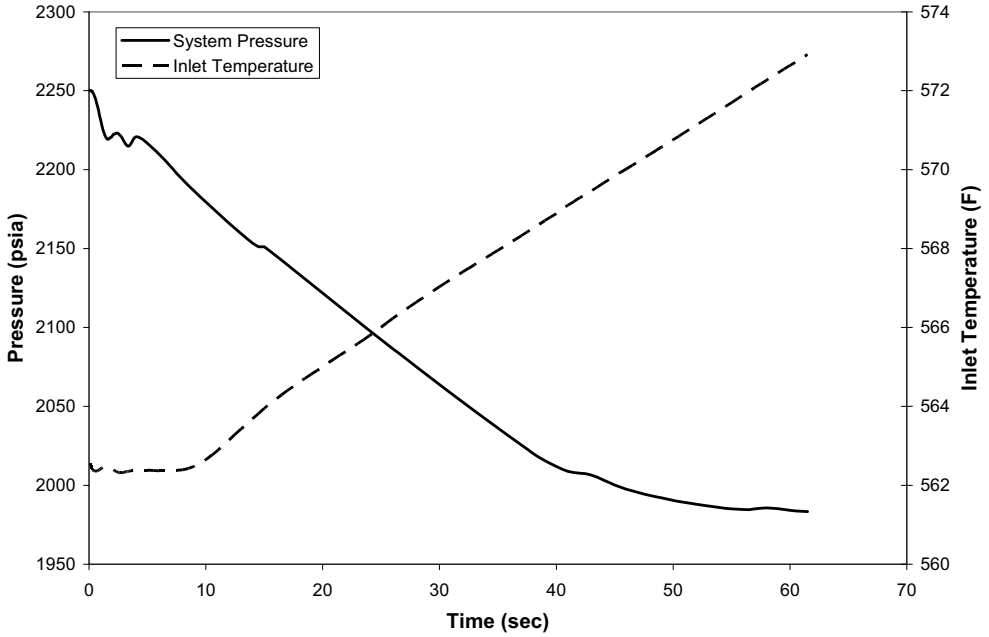

Figure 8-14 MDNBR for BOC 25%

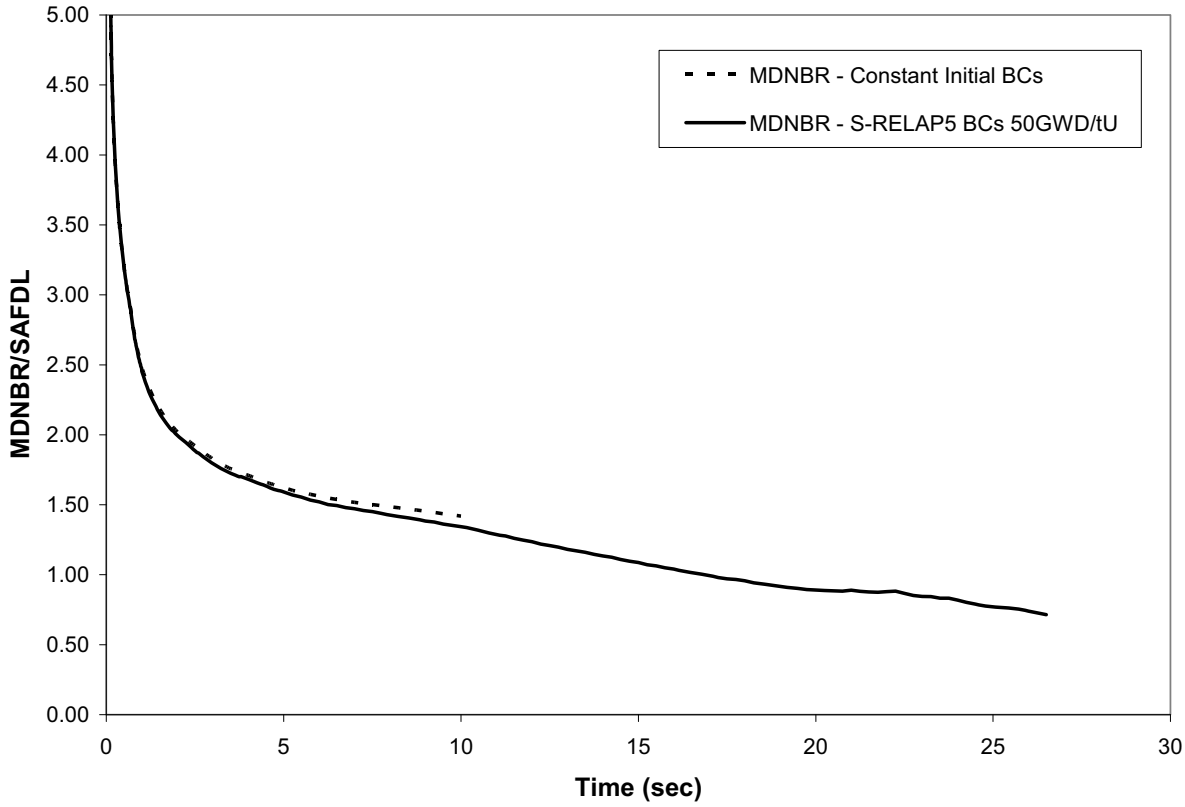

Figure 8-15 Fuel and Cladding Temperatures for BOC 25%

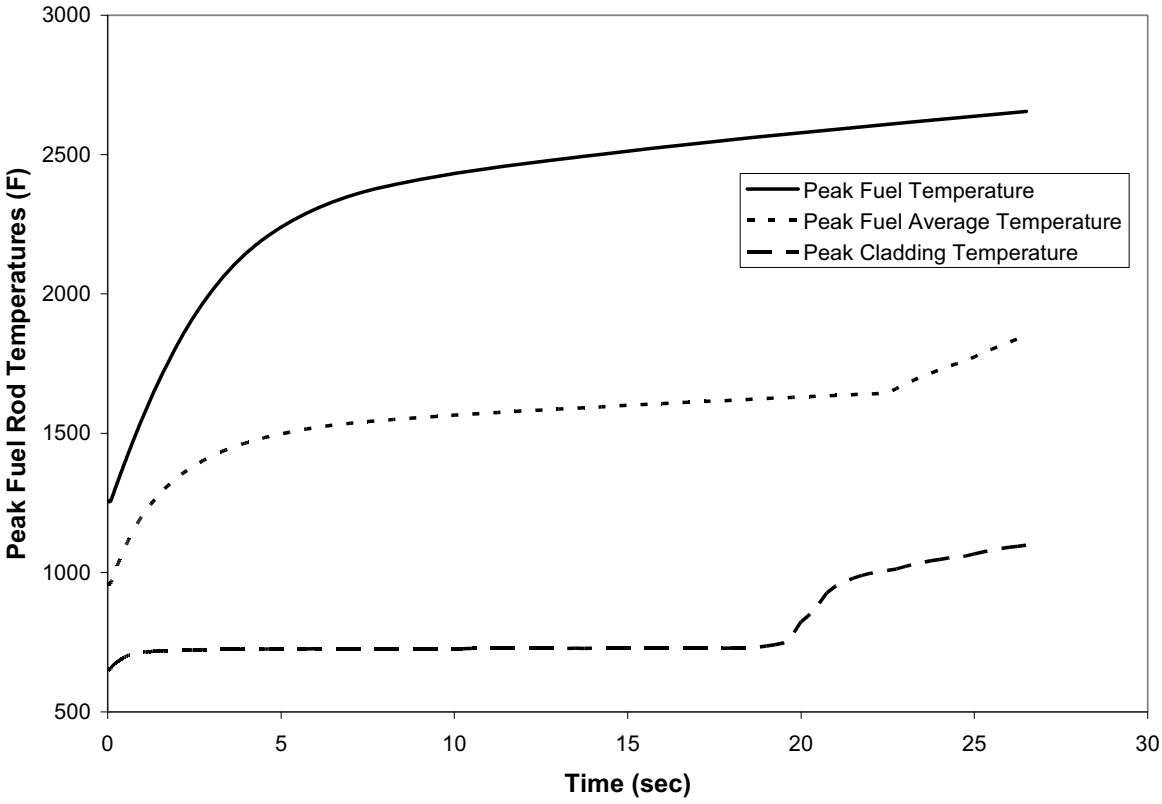

Figure 8-16 Peak Enthalpy Rise for BOC 25%

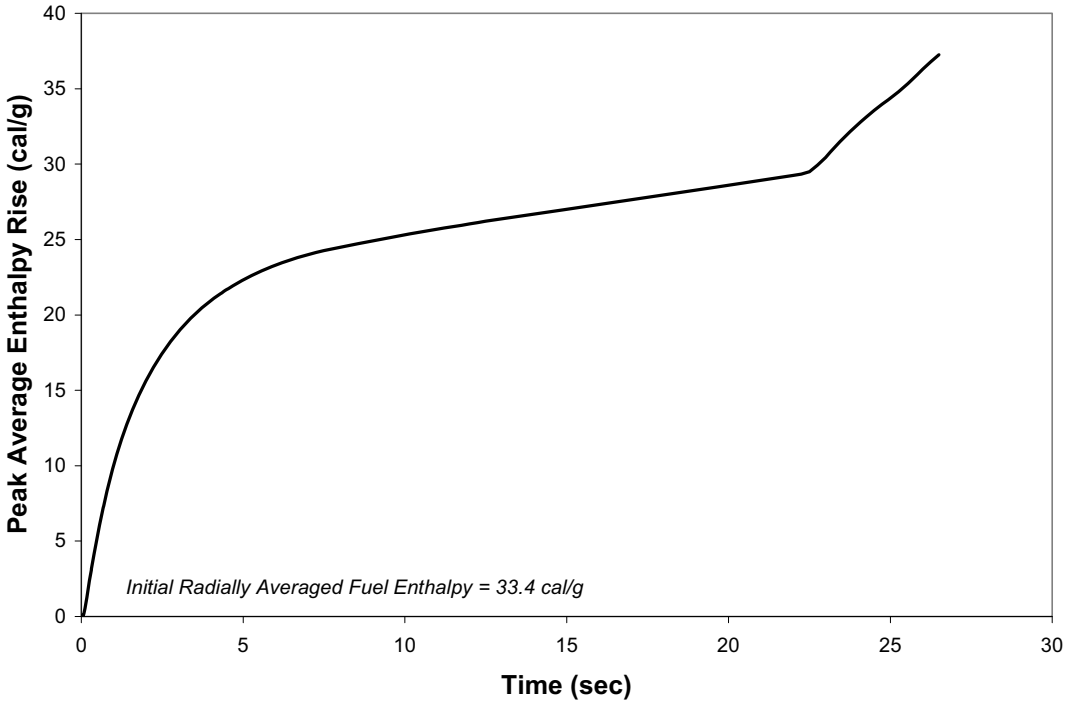

Figure 8-17 MDNBR for BOC 35%

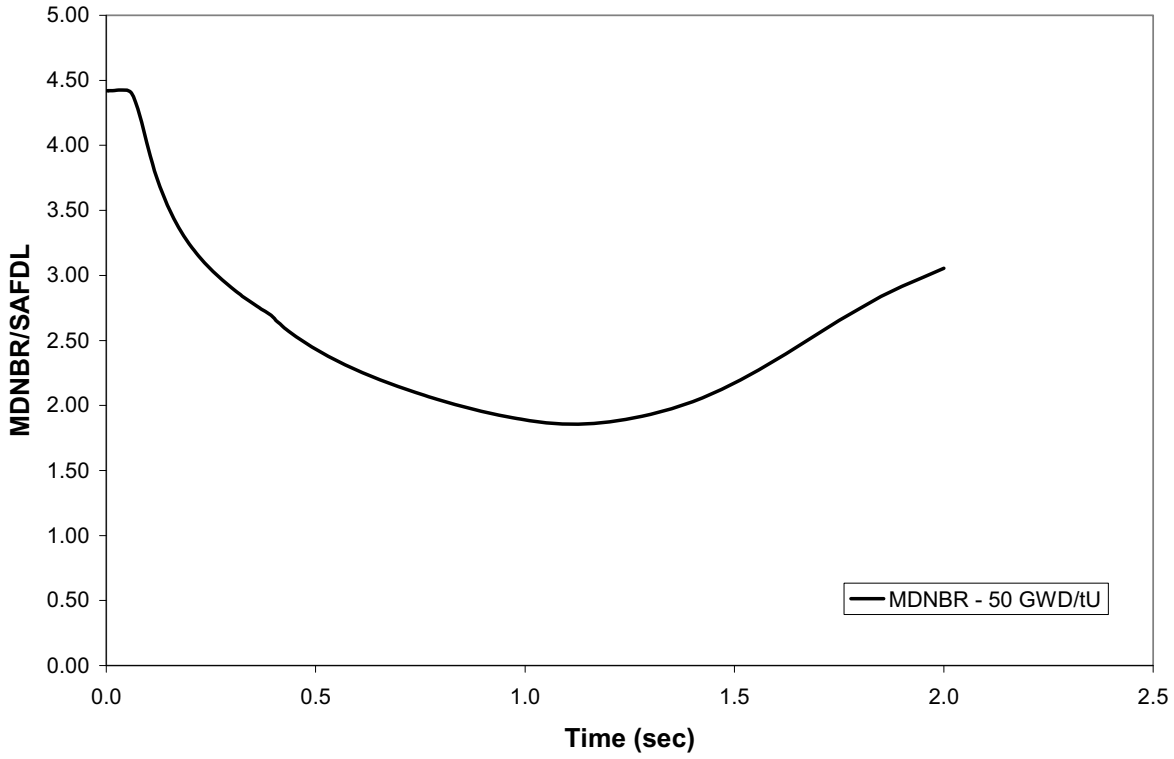

Figure 8-18 Fuel and Cladding Temperatures for BOC 35%

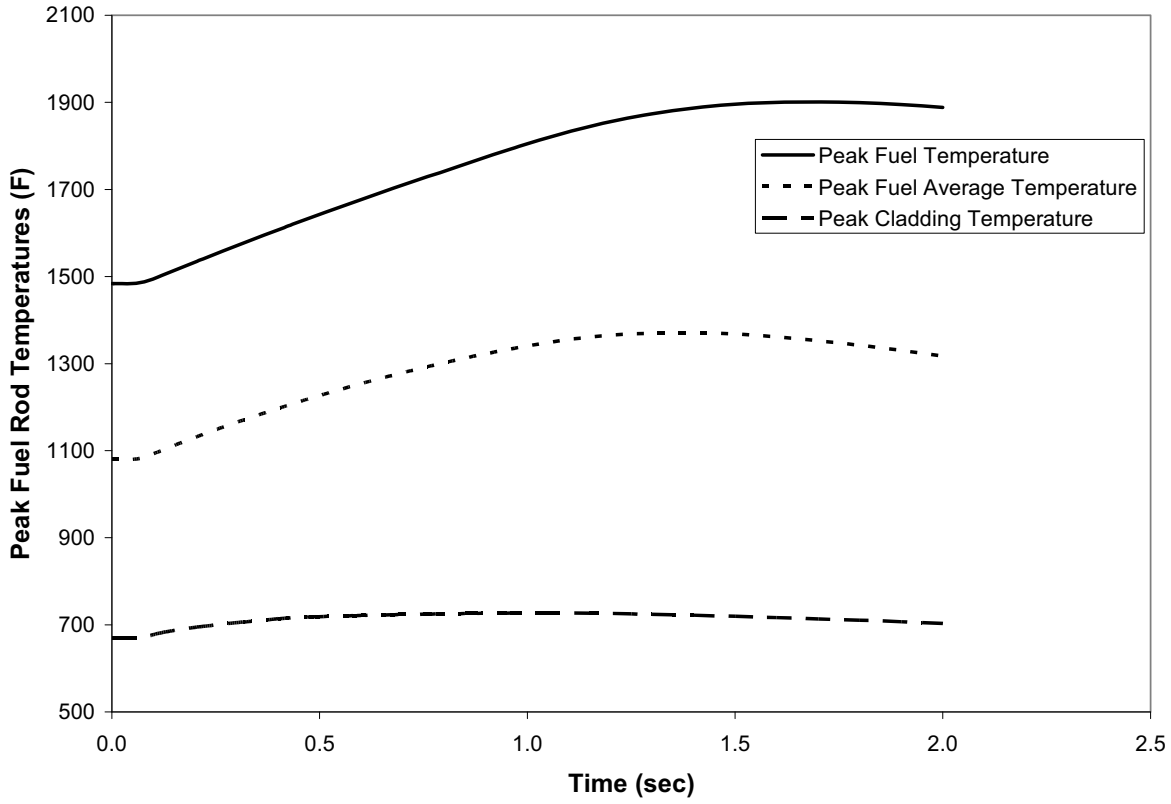

Figure 8-19 Peak Enthalpy Rise for BOC 35%

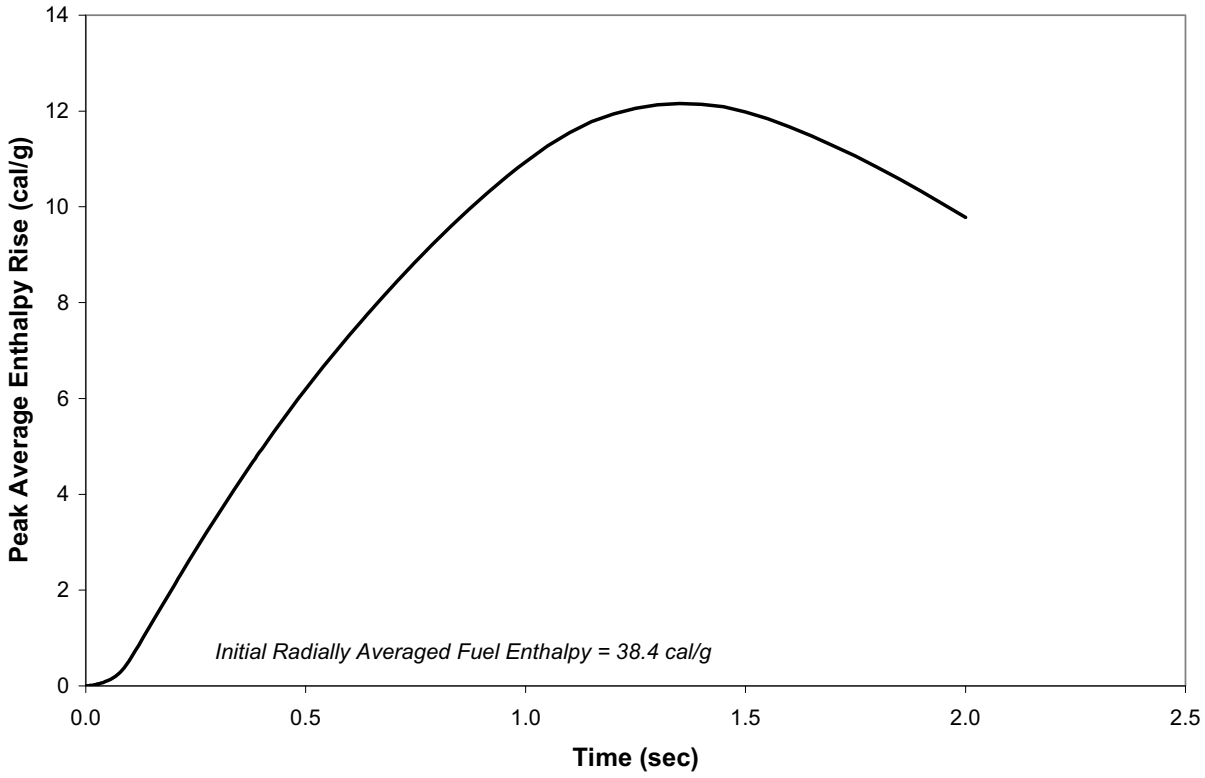

Figure 8-20 MDNBR Excursion for BOC 60%

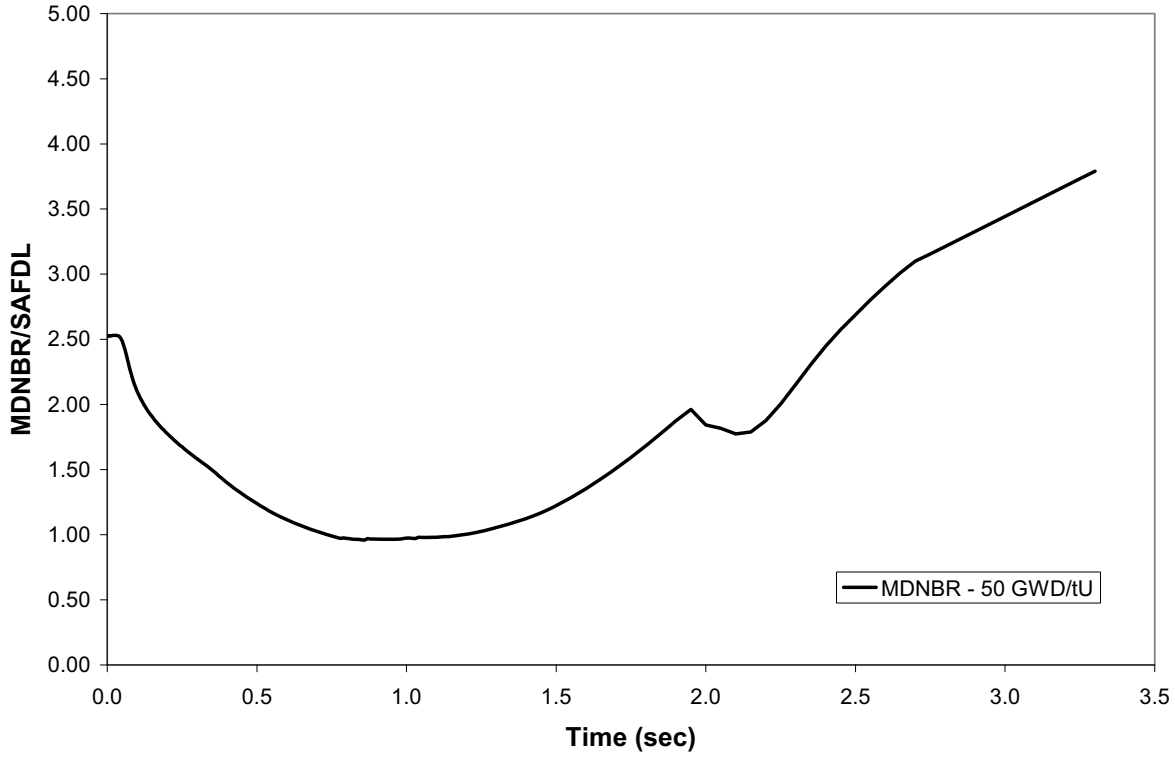

Figure 8-21 Fuel and Cladding Temperatures for BOC 60%

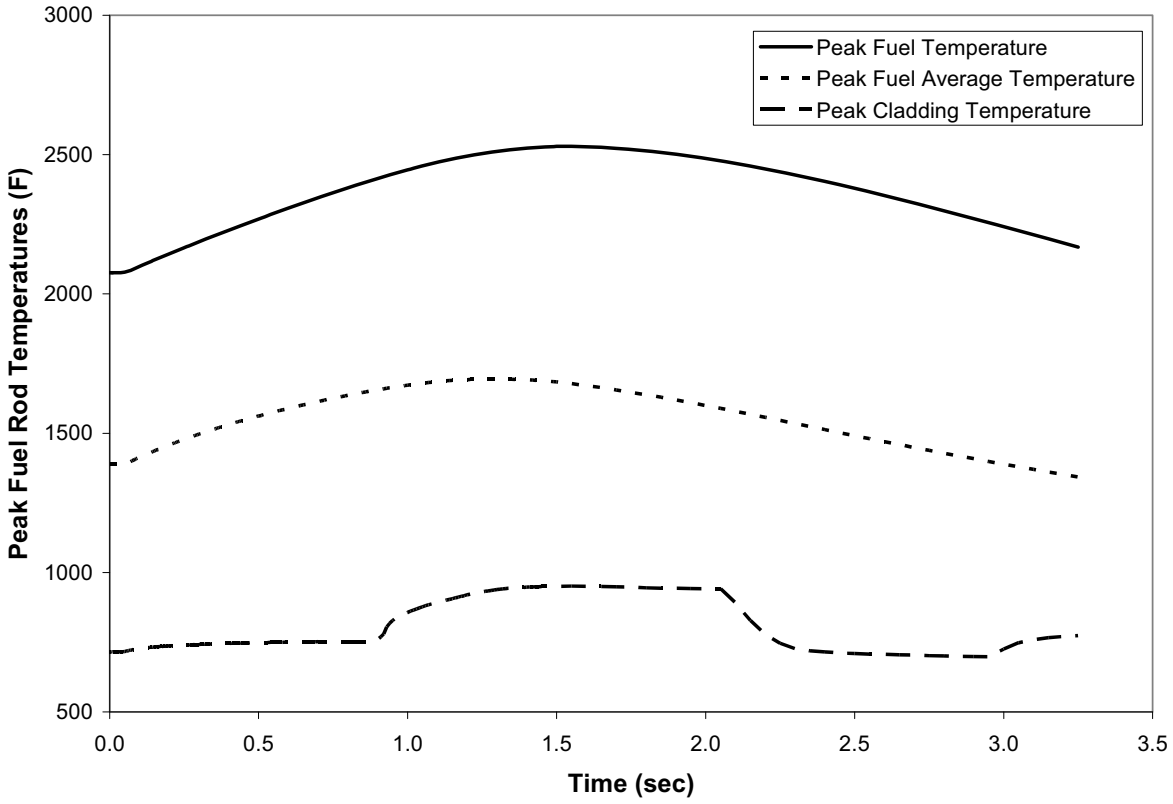

Figure 8-22 Peak Enthalpy Rise Excursion for BOC 60%

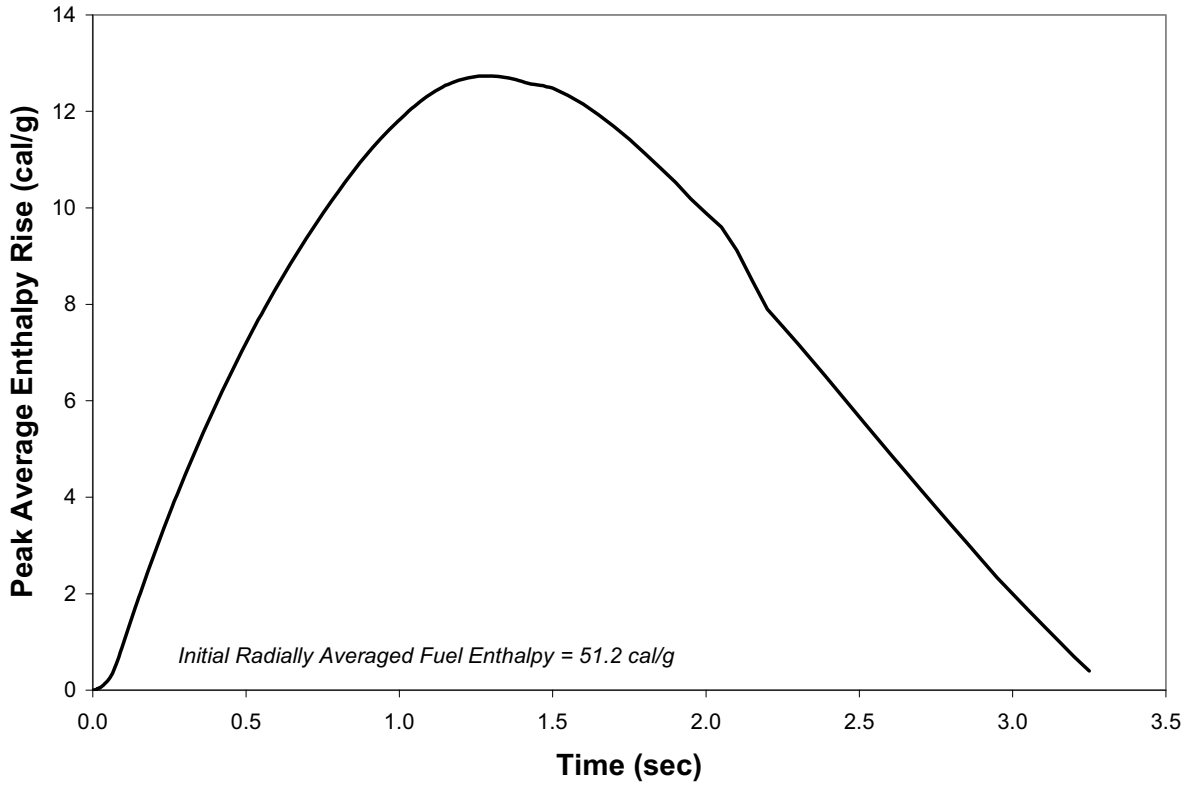

Figure 8-23 MDNBR for BOC HFP

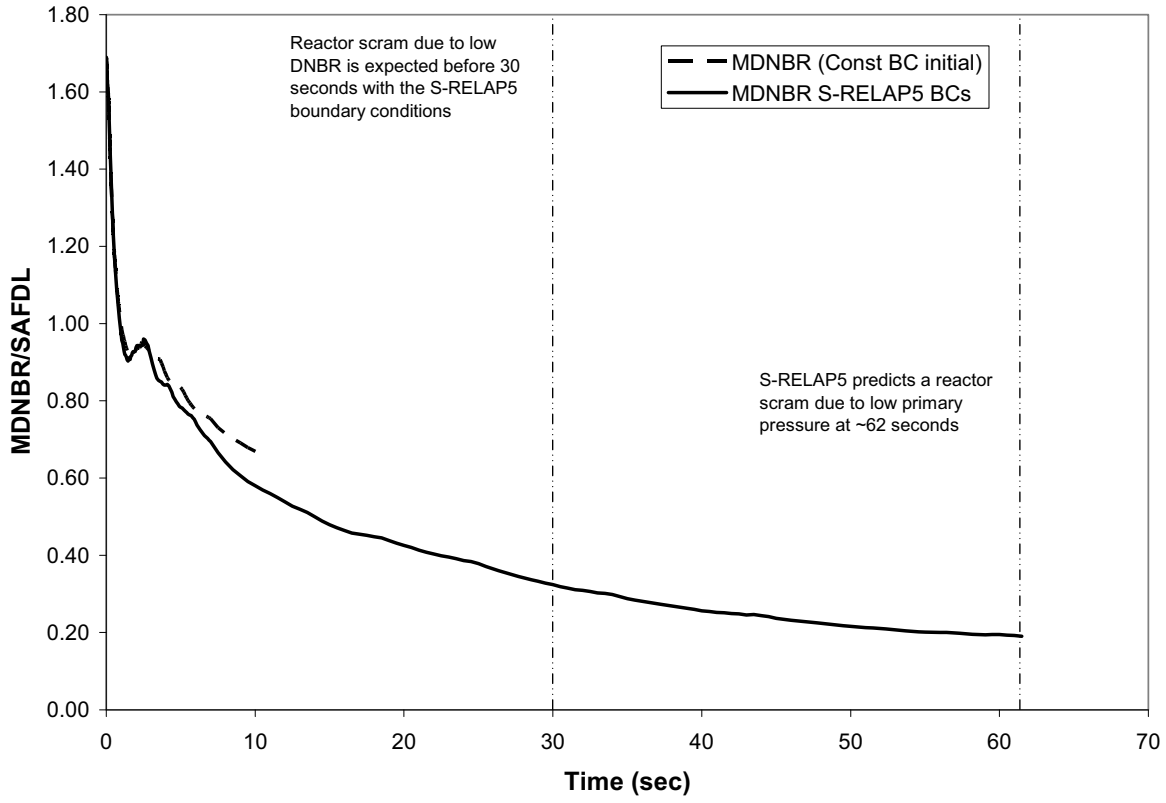

Figure 8-24 Fuel and Cladding Temperatures for BOC HFP

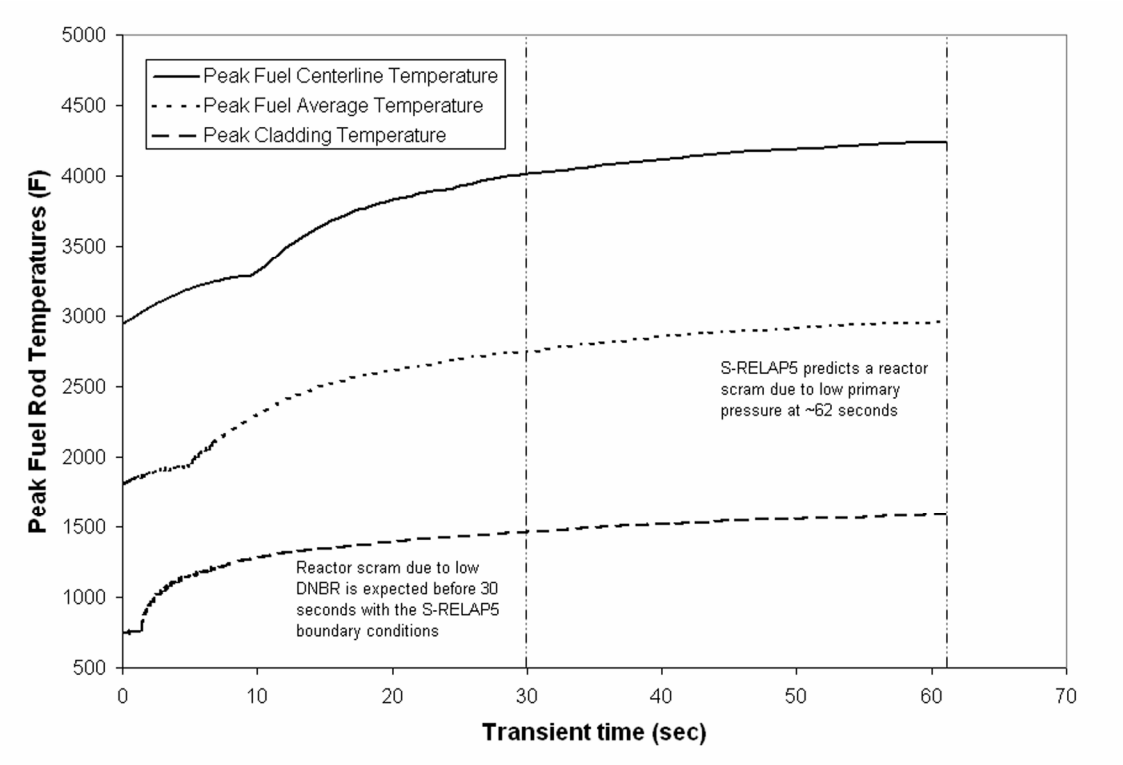

Figure 8-25 Peak Enthalpy Rise for BOC HFP

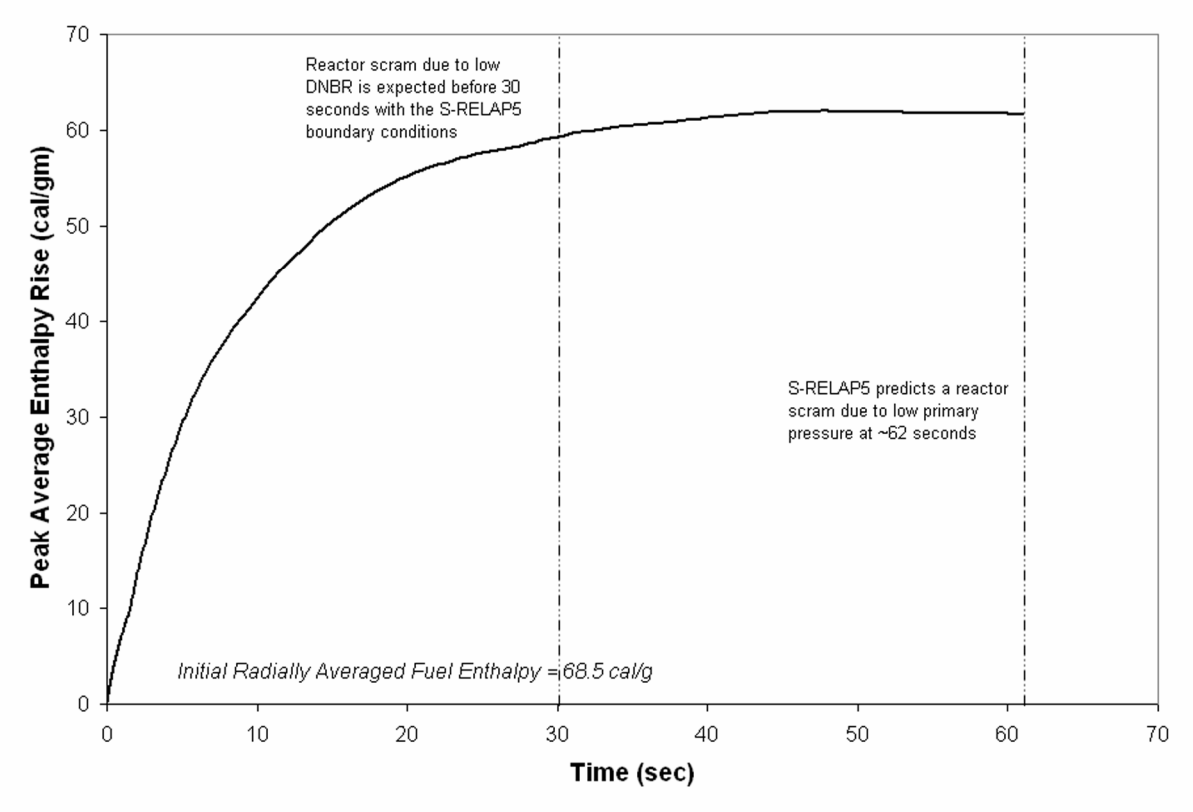

Figure 8-26 MDNBR for EOC HZP

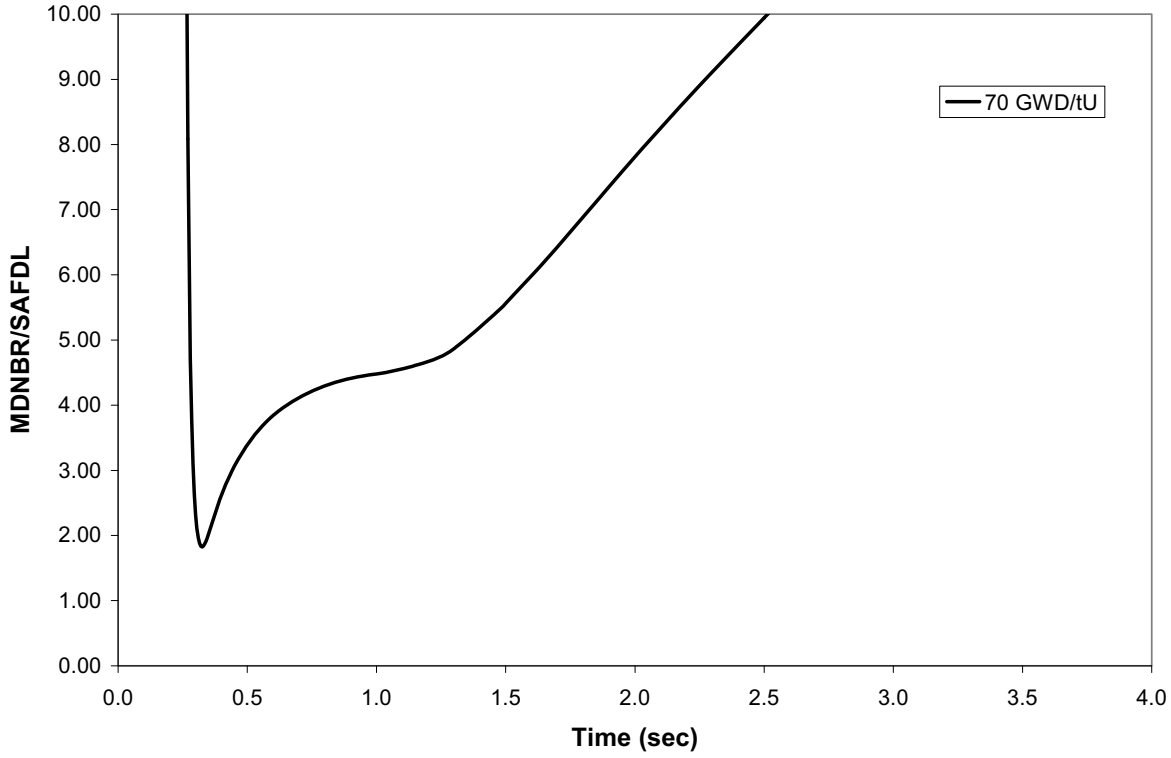

Figure 8-27 Fuel and Cladding Temperatures for EOC HZP

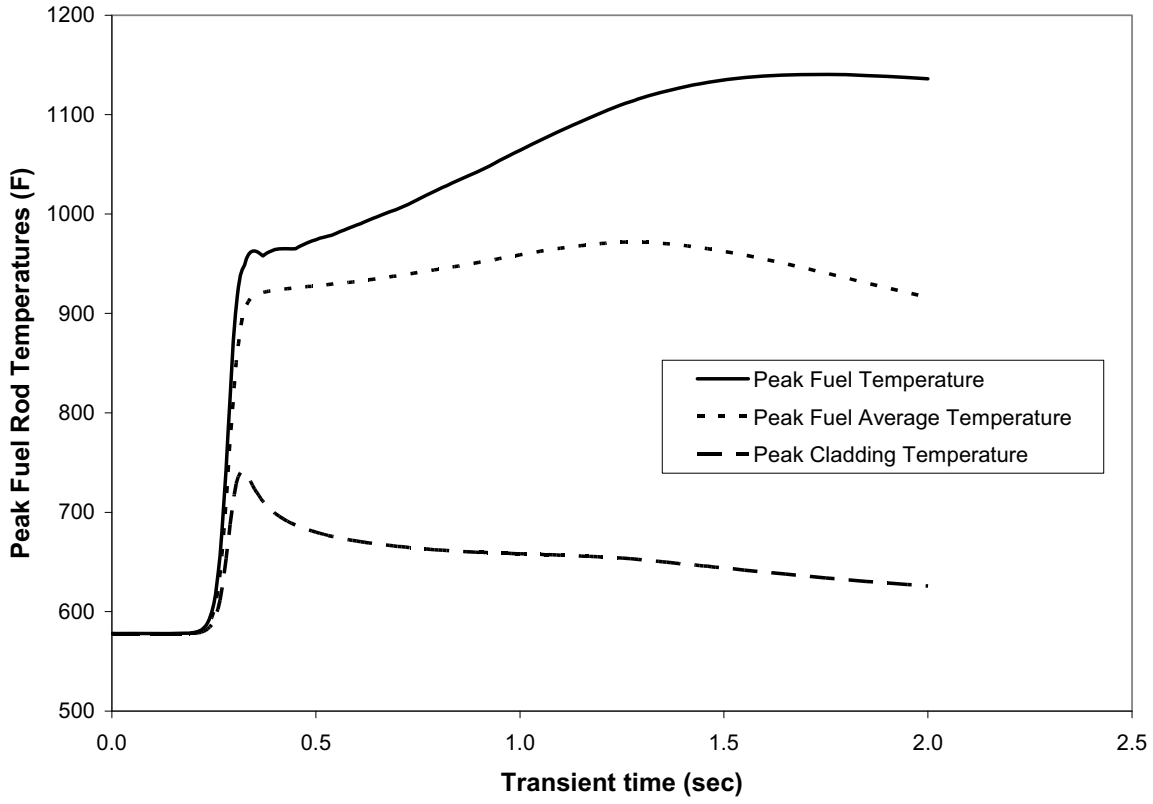

Figure 8-28 Peak Enthalpy Rise for EOC HZP

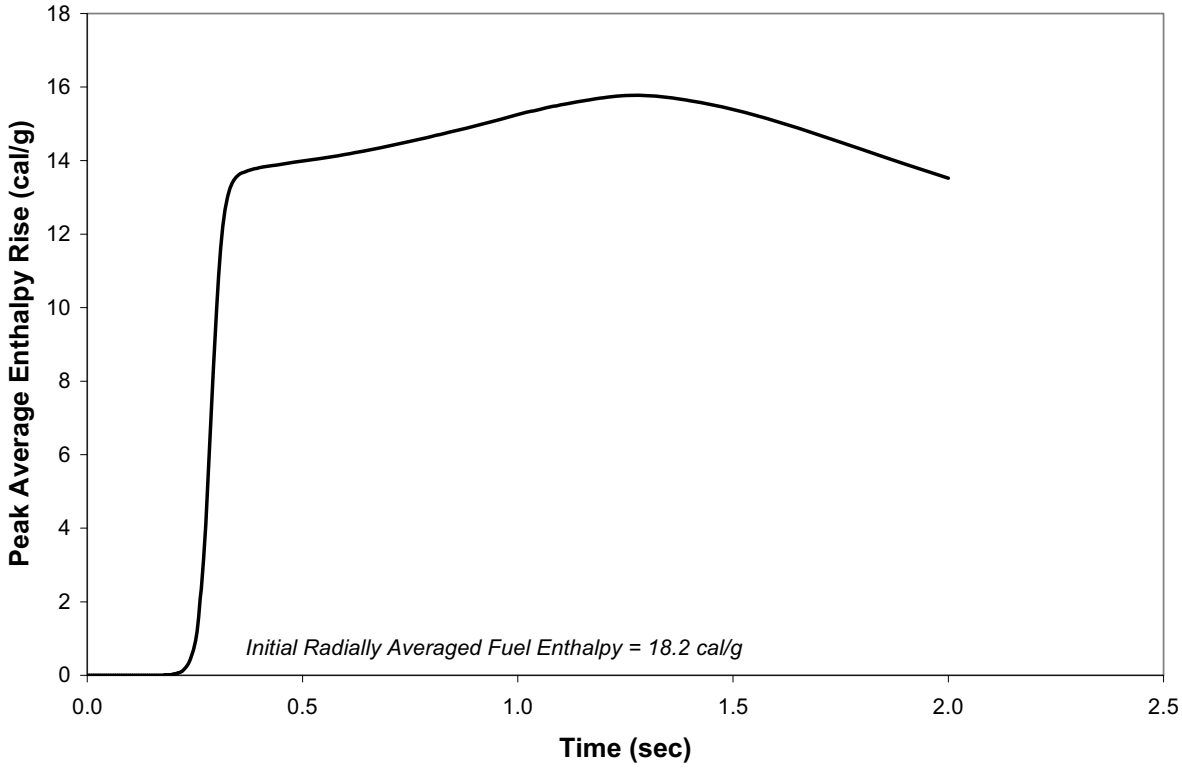

Figure 8-29 MDNBR for EOC 25%

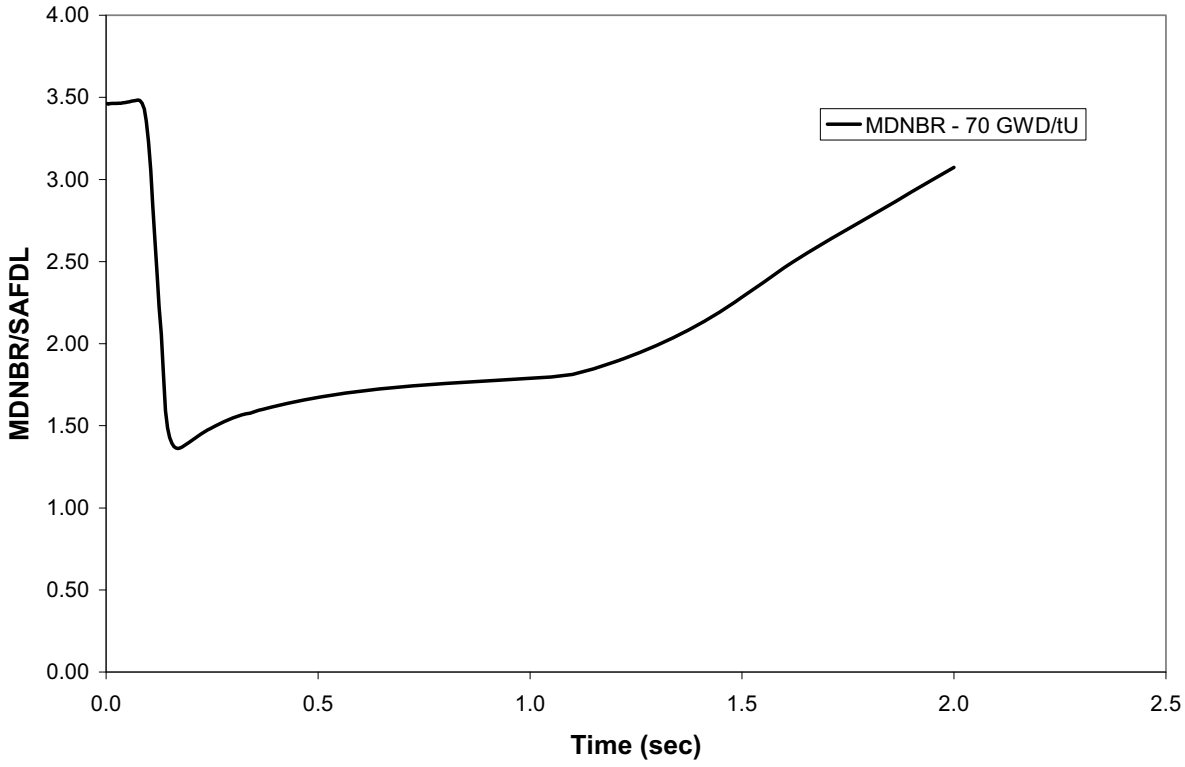

Figure 8-30 Fuel and Cladding Temperatures for EOC 25%

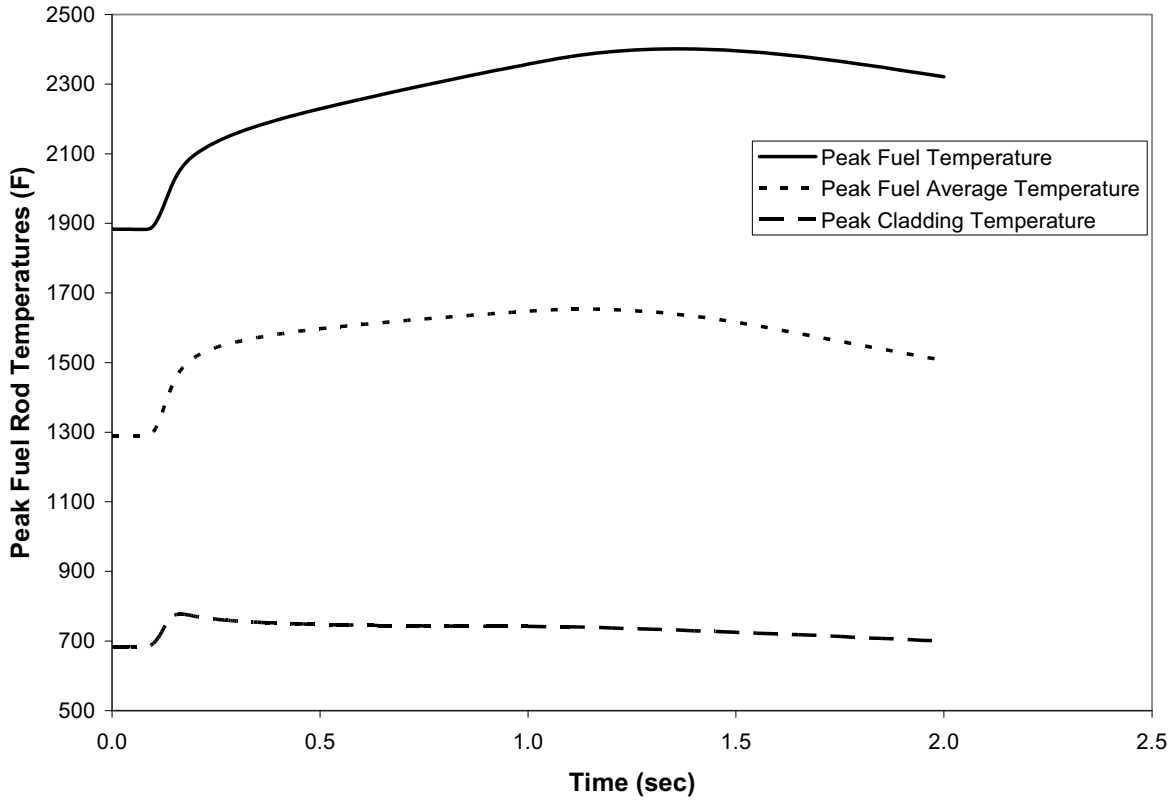

Figure 8-31 Peak Enthalpy Rise for EOC 25%

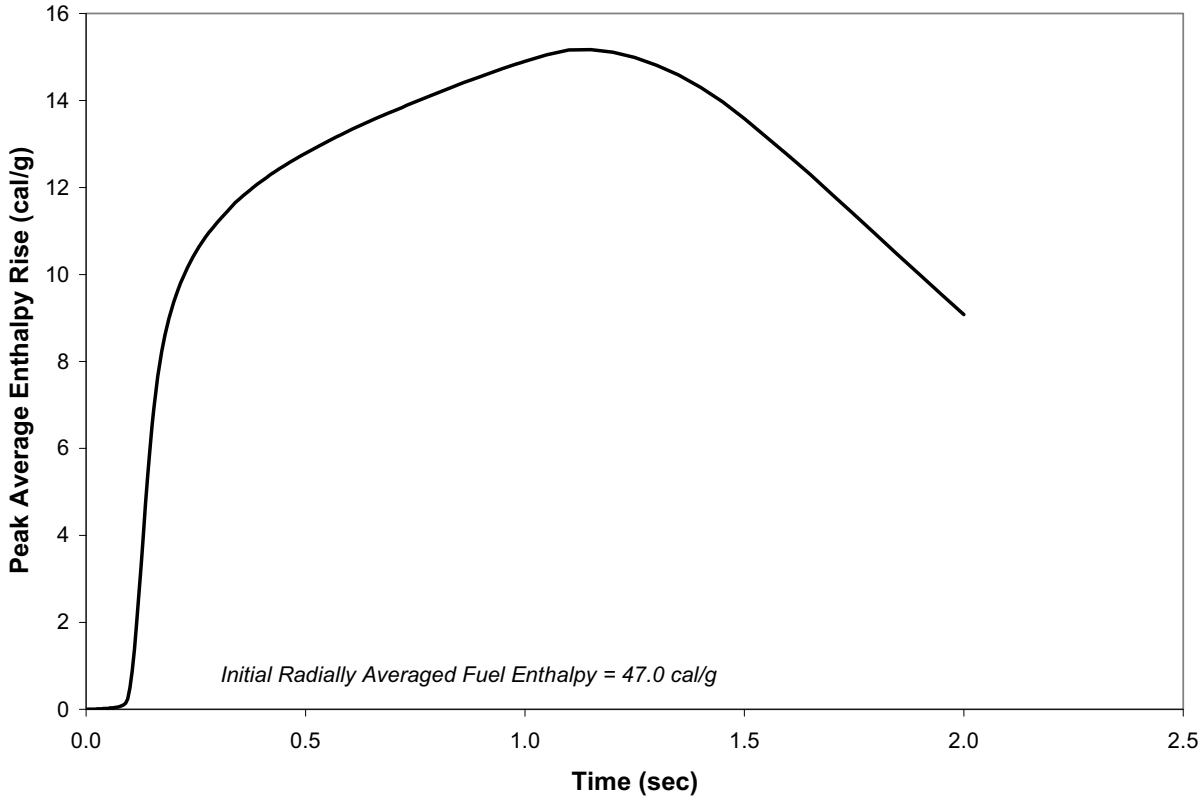

Figure 8-32 MDNBR for EOC 35%

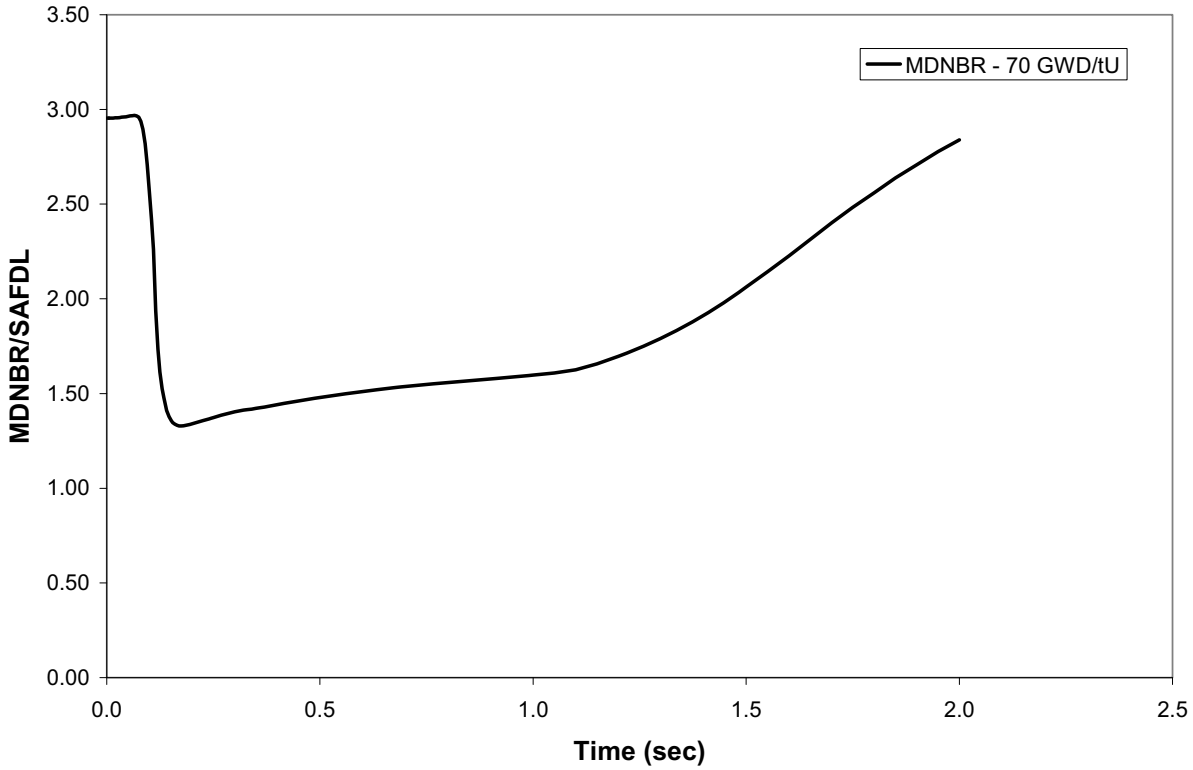

Figure 8-33 Fuel and Cladding Temperatures for EOC 35%

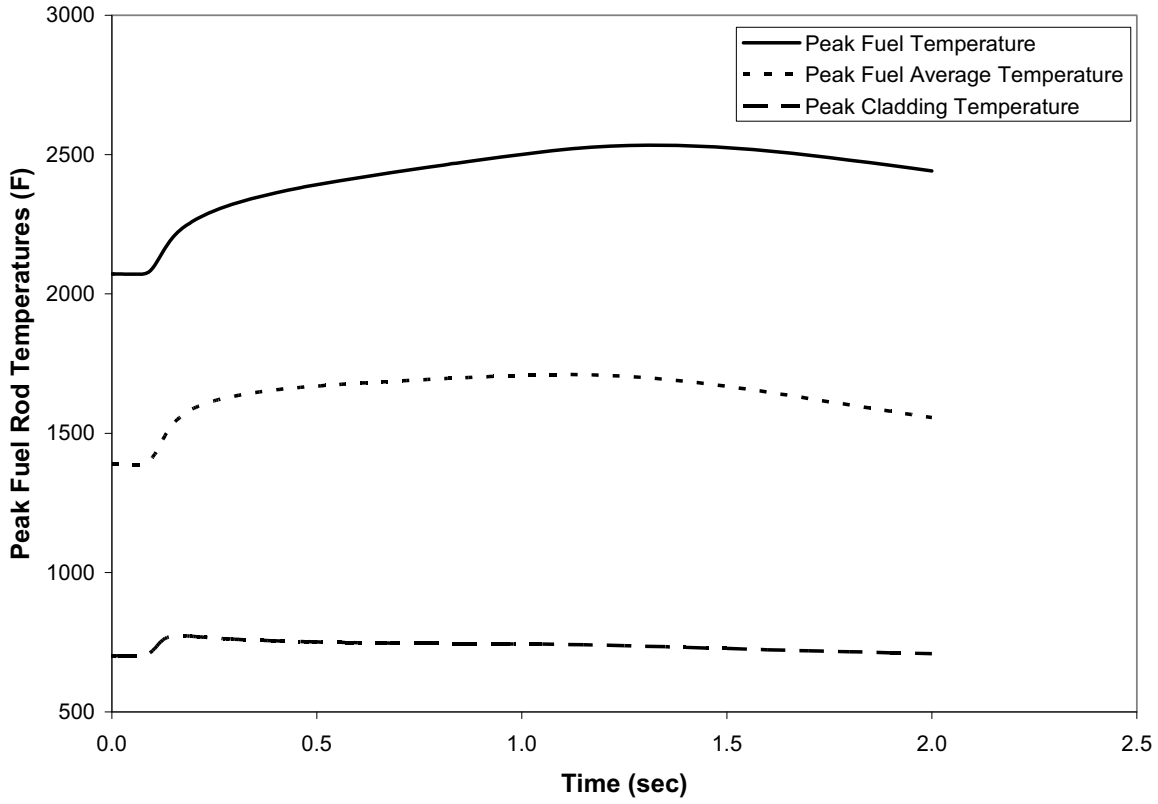

Figure 8-34 Peak Enthalpy Rise for EOC 35%

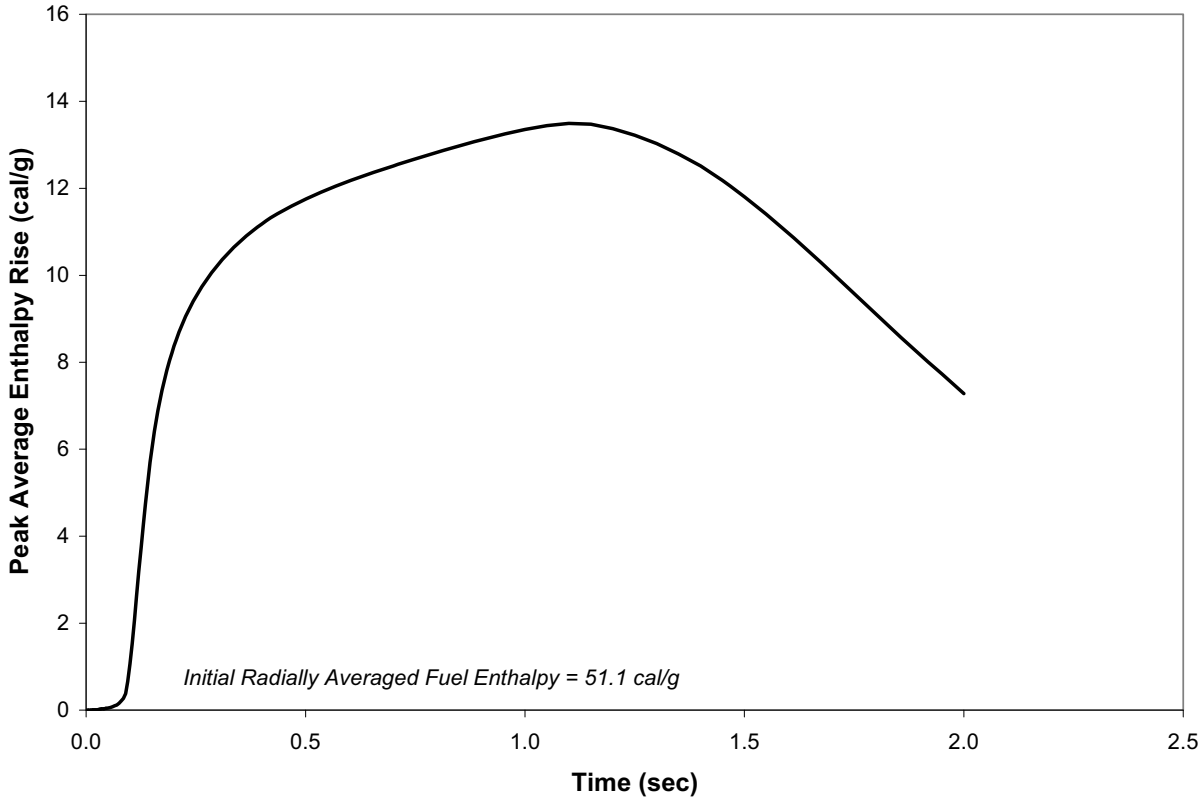

Figure 8-35 MDNBR for EOC 60%

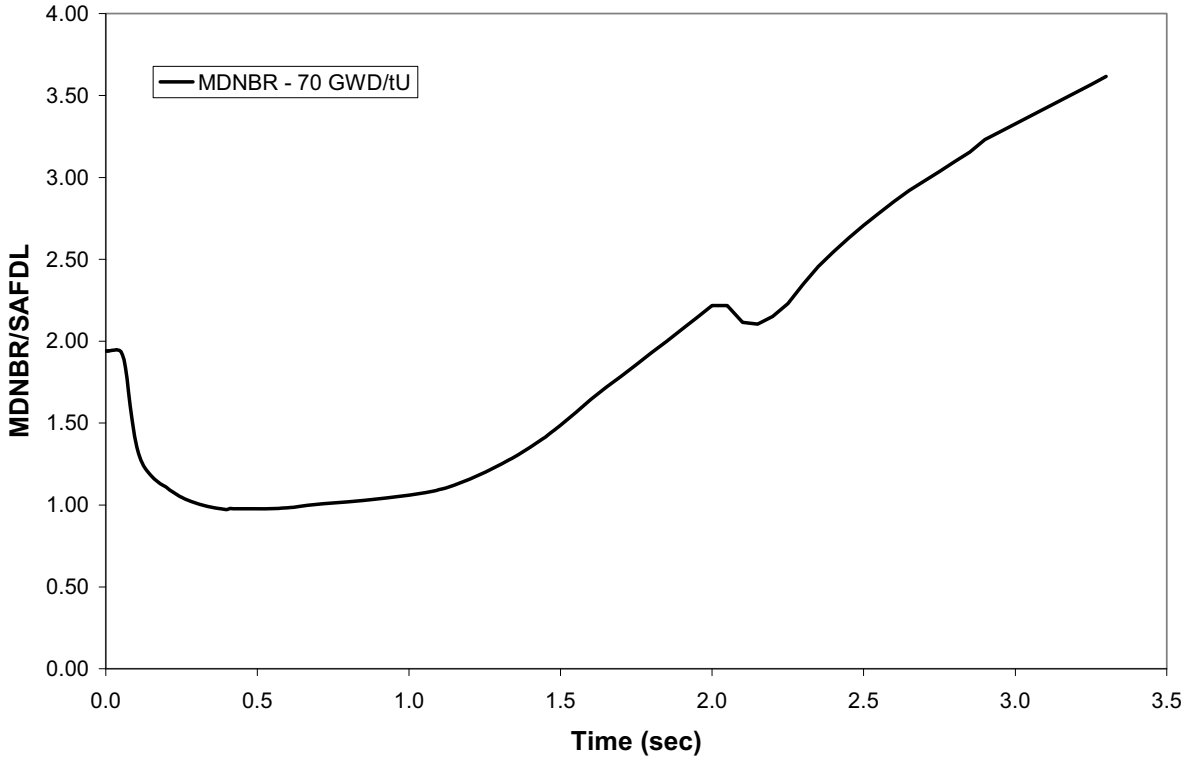

Figure 8-36 Fuel and Cladding Temperatures for EOC 60%

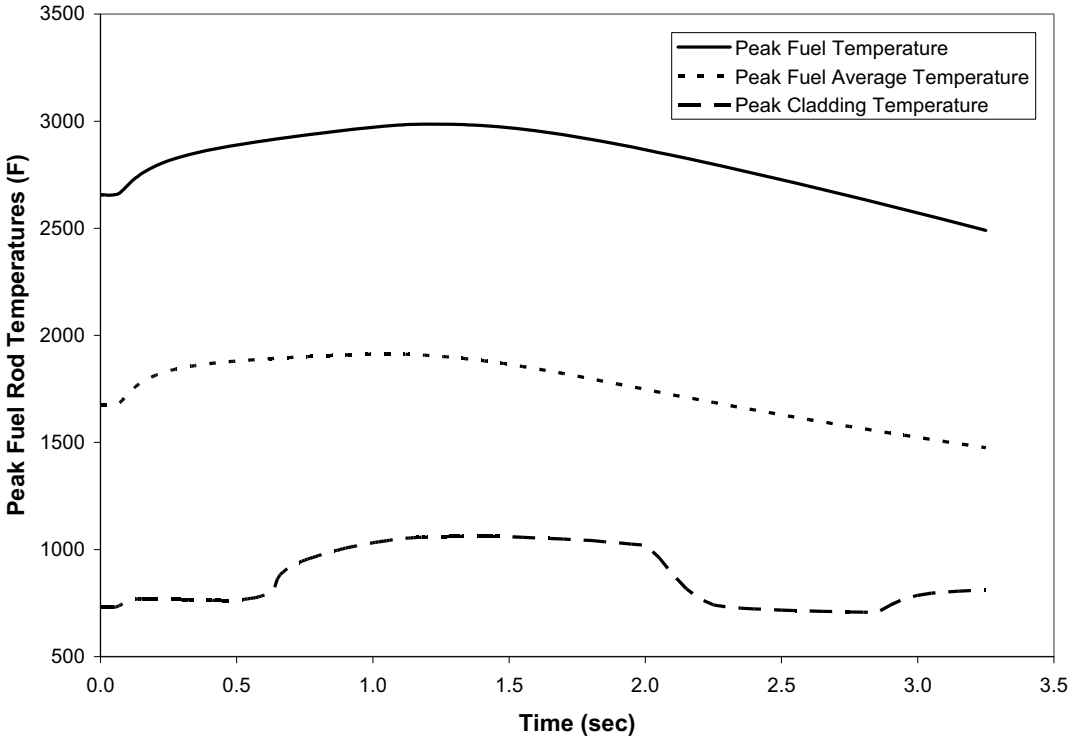

Figure 8-37 Peak Enthalpy Rise for EOC 60%

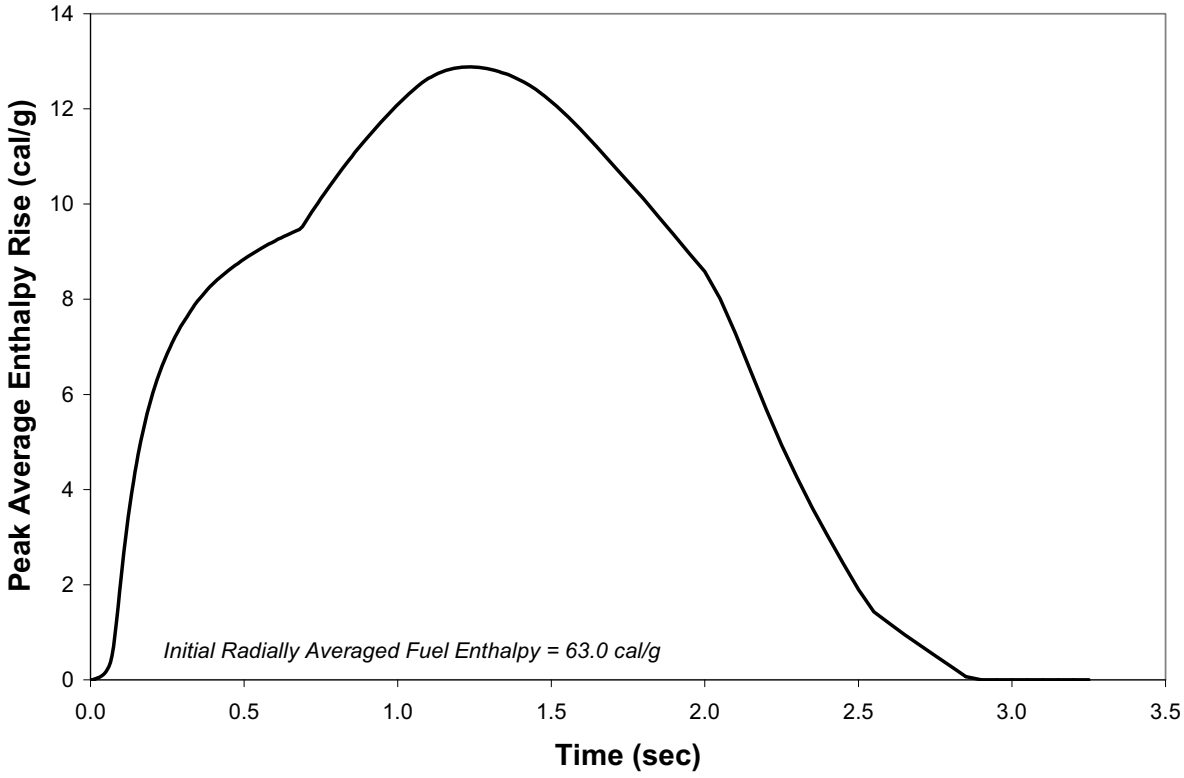

Figure 8-38 MDNBR for EOC HFP

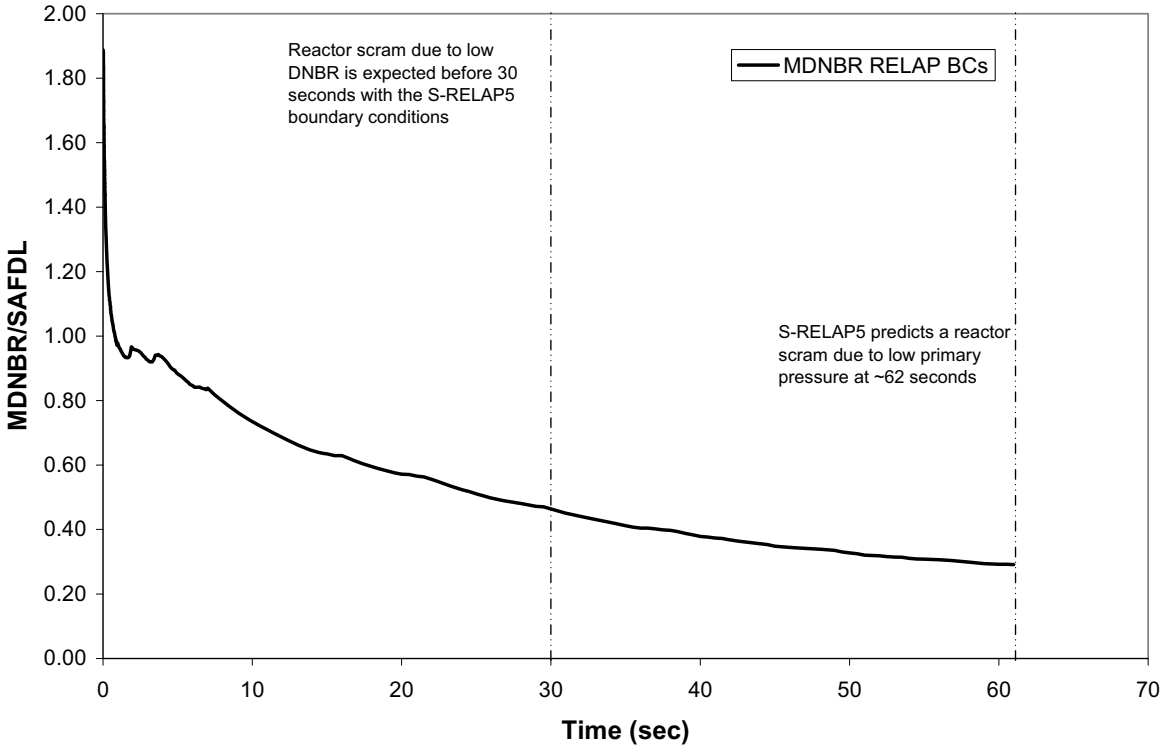

Figure 8-39 Fuel and Cladding Temperatures for EOC HFP

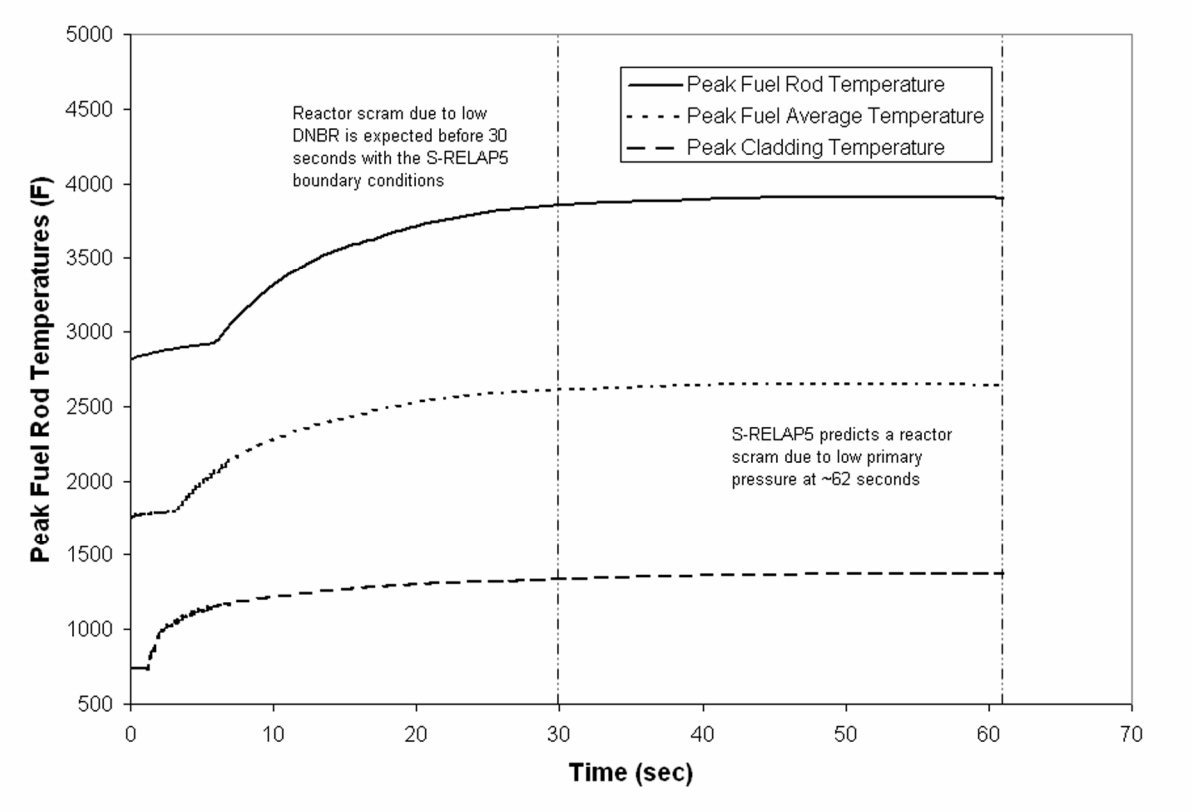

Figure 8-40 Peak Enthalpy Rise for EOC HFP

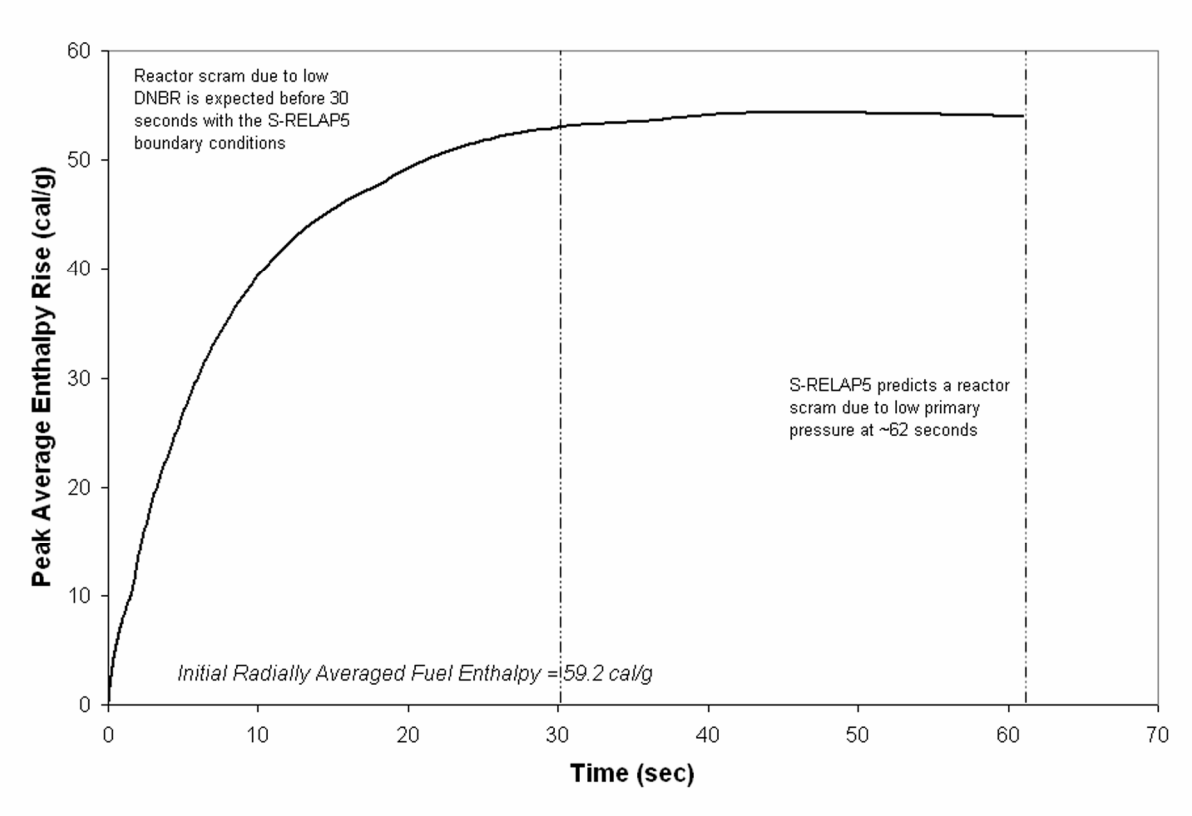

Figure 8-41 Static Ejected Rod Peak Correlated to Transient Peak

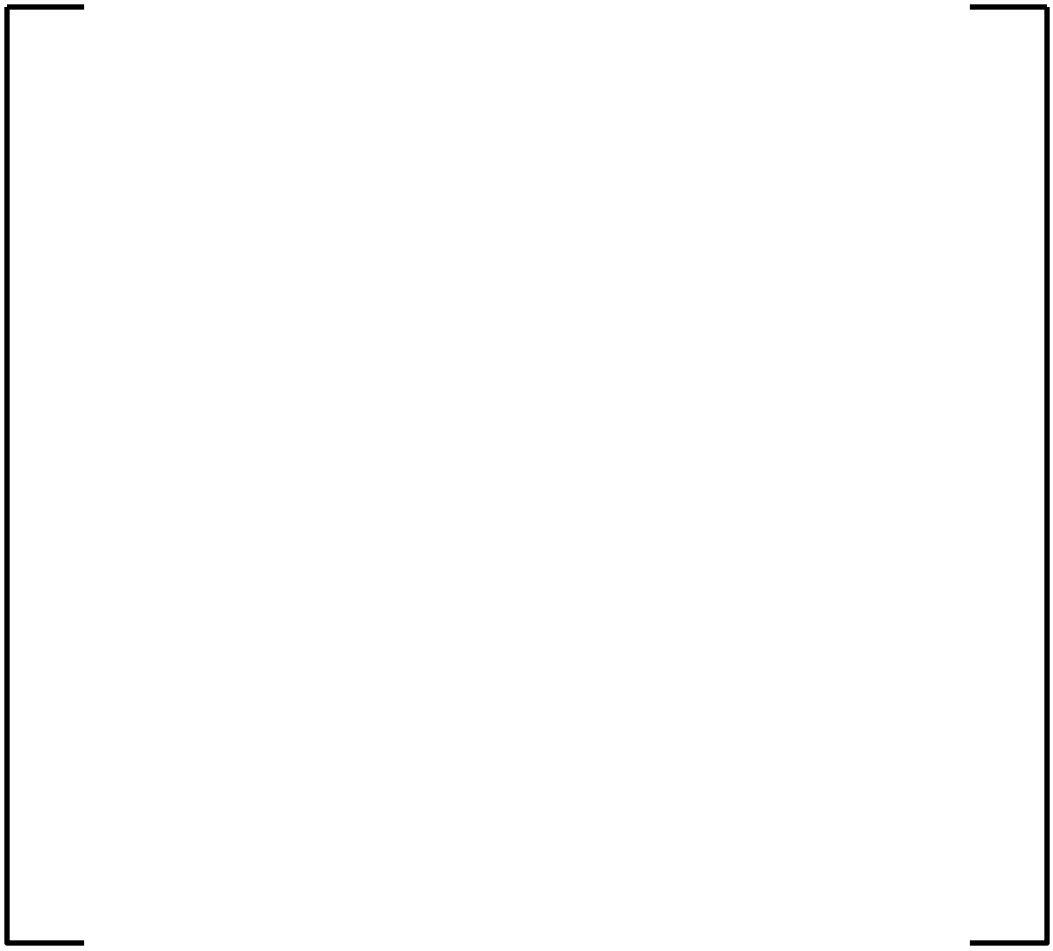

9.0 CONCLUSIONS AND CYCLE SPECIFIC CHECKS

This topical report provides a method and sample analysis to demonstrate acceptable results relative to the interim RIA criteria for the U.S. EPR. One of three options can be performed in order to meet any changes in cycle design requirements:

1. Portions of the example analysis can be repeated for each cycle.
2. The current record of analysis can be shown to be applicable to another core design.
3. A complete reanalysis.

Based on the analysis results of Section 8.0, a table to check for each new fuel cycle design can be composed of the limiting values. As concluded in Section 8.0, the limiting conditions occurred at either HZP or HFP. Therefore, only the HZP and HFP parameters need to be verified each cycle. Table 9-1 presents the checklist to validate the cycle specific verification of this sample problem. Table 9-2 presents the cycle 1 limiting values to compare to this sample problem.

Table 9-1 Ejected Rod Analysis Checklist

Parameter	Acceptable values	Cycle Specific Criteria			
		BOC		EOC	
		HZP	HFP	HZP	HFP
Maximum ejected rod worth, pcm	≤	433	64	634	97
β_{eff}	≥	0.0055	0.0055	0.0047	0.0047
MTC, pcm/°F	≤	2.16	0.01	-19.4	-28.47
DTC, pcm/°F	≤	-1.22	-0.96	-1.52	-1.28
Initial F_Q	≤	NA[a]	2.36	NA[a]	2.10
Static F_Q after ejection	≤	9.89	3.39	20.33	4.78
Maximum design $F_{\Delta H}$	≤	NA[a]	1.70	NA[a]	1.70
Static $F_{\Delta H}$ after ejection	≤	5.34	2.37	6.51	2.63
Equivalent nominal rods failed, %	≤	0	30	0	30
Trip setpoints	Not Affected[b]				

Notes:

[a] Not applicable since initial stored energy above the coolant temperature is zero.

[b] Any changes to the trips listed in Table 8-1 would have to be reviewed relative to their impact on this accident analysis.

Table 9-2 Cycle 1 Ejected Rod Parameters

Parameter	Acceptable values	Cycle 1 values			
		BOC[b]		EOC	
		HZP	HFP	HZP	HFP
Maximum ejected rod worth, pcm[a]	Yes	335	47	539	59
β_{eff}	Yes	0.0061	0.0061	0.0048	0.0048
MTC, pcm/°F	Yes	1.62	-3.38	-20.29	-29.73
DTC, pcm/°F	Yes	-1.35	-1.17	-1.63	-1.45
Initial F_Q	Yes	-	2.20	-	1.69
Static F_Q after ejection	Yes	6.66	2.68	17.76	3.33
Maximum design $F_{\Delta H}$	Yes	-	1.59	-	1.41
Static $F_{\Delta H}$ after ejection	Yes	3.08	1.68	5.01	1.86
Equivalent nominal rods failed, %	Yes	0	0.8	0	0.4
Trip setpoints	NV[c]				

Notes:

[a] Ejected rod worths are calculated with the offset skewed to LCO limits and the rods inserted to the Technical Specification Limit for the inserted banks.

[b] Composite of BOC and burnup at which the most positive MTC occurs if not BOC

[c] Not verified – plant information not available

10.0 REFERENCES

1. NUREG 800, Revision 3, “Standard Review Plan for the Review of Safety Analysis Reports for Nuclear Power Plants,” March 2007, ML070740002.

2. BAW-10231PA, Revision 1, “COPERNIC Fuel Rod Design Computer Code,” Framatome ANP, January 2004.

3. Letter, Ralph Landry, Acting Chief, Nuclear Performance and Code Review Branch, Division of Safety Systems, NRR, to Thomas Martin, Director, Division of Safety Systems, NRR, “Technical and Regulatory Basis for the Reactivity Initiated Accident Interim Acceptance Criteria and Guidance,” January 2007, ML070220400.

4. NUREG/CR-6742 LA-UR-99-6810, “Phenomenon Identification and Ranking Tables (PIRTs) for Rod Ejection Accidents in Pressurized Water Reactors Containing High Burnup Fuel,” Los Alamos National Laboratory, September 2001.

5. NUREG/CR-0497, TREE-1280, Revision 2, D. L. Hagman, G. A. Reymann, and R.E. Mason, MATPRO Version 11 (Revision 2), “A Handbook of Material Properties for Use in the Analysis of Light Water Reactor Fuel Rod Behavior,” August 1981.

6. BAW-10221PA, “NEMO-K a Kinetics Solution in NEMO,” September 1998.

7. BAW-10156A, Revision 1, “LYNXT Core Transient Thermal-Hydraulic Program,” B&W Fuel Company, August 1993.

8. EMF-2310PA Revision 1, “SRP Chapter 15 Non-LOCA Methodology for Pressurized Water Reactors,” May 2004.

9. NEACRP-L-335 (Revision 1), H. Finnemann and A. G. Galati, “NEACRP 3-D LWR Core Transient Benchmark,” Final Specifications, October 1991 (January 1992).

10. BNWL-1962, UC-32, “COBRA-IV-I: An Interim Version of COBRA for Thermal-Hydraulic Analysis of Rod Bundle Nuclear Fuel Elements and Cores,” Battelle Pacific Northwest Laboratories, March 1976.

11. BAW-10044, “TAFY – Fuel Pin Pressure and Gas Pressure Analysis,” Babcock & Wilcox, April 1972.

12. BAW-10087P, “TACO – Fuel Pin Performance Analysis,” Babcock & Wilcox, December 1975.

13. BAW-10141PA, “TACO2 – Fuel Pin Performance Analysis,” Babcock & Wilcox, June 1983.

14. BAW-10162PA, “TACO3 – Fuel Pin thermal Analysis Computer Code,” BW Fuel Company, October 1989.

15. BAW-10069A, Revision 1, “RADAR – Reactor Thermal and Hydraulic Analysis During Reactor Flow Coastdown,” Babcock & Wilcox, October 1974.

16. ANP-10263PA, Revision 0, “Codes and Methods Applicability Report for the U.S. EPR,” August 2007.

17. Letter J. H. Taylor to U.S. Nuclear Regulatory Commission, “Revised Measurement Uncertainty for Control Rod Worth Calculations,” JHT/96-01, January 3, 1996.

18. Letter J. H. Taylor to U.S. Nuclear Regulatory Commission, “Revised Measurement Uncertainty for Control Rod Worth Calculations,” JHT/95-124, December 20, 1995.

19. Letter J. H. Taylor to U.S. Nuclear Regulatory Commission, “Revised Measurement Uncertainty for Westinghouse 193 Plant Control Rod Worth Calculations,” JHT/97-20, April 11, 1997.

20. BAW-10150A, “Control Rod Assembly Ejection,” pp. 2-26, June 1986.

21. ANP-10269P, Revision 0, Supplement, “The ACH-2 CHF Correlation for the U.S. EPR, Topical Supplement,” August 2007.